Scholars' Mine

Masters Theses   Student Theses and Dissertations

Spring 2014

Bond performance of recycled aggregate concrete

Amanda Renee Steele

Follow this and additional works at: https://scholarsmine.mst.edu/masters_theses

Part of the Civil Engineering Commons

Department:

Recommended Citation

Steele, Amanda Renee, "Bond performance of recycled aggregate concrete" (2014). *Masters Theses*. 7278.
https://scholarsmine.mst.edu/masters_theses/7278

BOND PERFORMANCE OF RECYCLED AGGREGATE CONCRETE

by

AMANDA RENEE STEELE

A THESIS

Presented to the Faculty of the Graduate School of the

MISSOURI UNIVERSITY OF SCIENCE AND TECHNOLOGY

In Partial Fulfillment of the Requirements for the Degree

MASTER OF SCIENCE IN CIVIL ENGINEERING

2014

Approved by

Dr. Jeffery Volz, Advisor
Dr. Kamal Khayat
Dr. John J. Myers

ABSTRACT

In recent decades, engineers have sought a more sustainable method to dispose of concrete construction and demolition waste. One solution is to crush this waste concrete into a usable gradation for new concrete mixes. This not only reduces the amount of waste entering landfills but also alleviates the burden on existing sources of quality natural concrete aggregates. The objective of this study was to determine to effect of replacing coarse natural aggregates for recycled concrete aggregates (RCA) on the bond strength between deformed mild reinforcing steel and surrounding concrete. Two different RCA replacement levels were considered, 50% and 100%, and were compared to a standard Missouri Department of Transportation (MoDOT) mix design. All RCAs used were crushed from laboratory cured beams of the same MoDOT mix design containing 1 in. Potosi Dolomite crushed stone.

To evaluate bond strength, 18 direct pull-out specimens were tested with both #4 (No. 13) and #6 (No. 19) reinforcing bars and 9 full-scale beam specimens were tested with non-confined contact lap splices located at mid-span. The construction and test procedure of the direct pull-out specimens was based on RILEM 7-II-128. The full-scale beam splice specimens were based on a non-standard test procedure that is considered to be the most realistic stress state response for bond. Analysis of the test data indicates that replacing more than 50% of coarse natural aggregates results in diminished bond strength over concrete containing only virgin natural aggregates. This result suggests that the existing equation for development and splice length as reported in ACI 318 may require additional modification factors to account for the diminished bond strength associated with replacement of coarse virgin aggregates with RCA.

ACKNOWLEDGEMENTS

Above all, I would like to thank Dr. Jeffery Volz, my advisor and mentor through this long and challenging process. His counsel, patience, and most importantly, his kindness helped make this work as rewarding and successful as possible.

I would like to thank the Missouri Department of Transportation and National University Transportation Center at Missouri S&T for the financial support they provided for this project, as well as the Missouri University of Science & Technology for the investment of the Chancellor's Fellowship to aid in my studies.

I would also like to thank my committee members, Dr. Kamal Khayat and Dr. John Myers for reviewing this thesis and making suggestions for improvement.

I would like to thank Gary Abbot, Mahdi Arezoumandi, Ben Gliha, Jon Drury, Adam Smith, Dilbert Hampton, and Hesham Tuwair for their invaluable help constructing and testing my specimens. A special thanks to John Bullock for his assistance and advice throughout my specimen construction. This work was completed much more effectively and painlessly with support from such a great team.

Last but certainly not least, I would like to thank my fiancé Benjamin Weideman for his love and support through all of my undergraduate and graduate studies. His patience and understanding made the stressful times considerably more bearable and the celebratory times much more memorable.

TABLE OF CONTENTS

LIST OF FIGURES

Figure   Page

LIST OF TABLES

1. INTRODUCTION

1.1 BACKGROUND AND JUSTIFICATION

1.1.1   General. The construction of buildings, bridges, and roadways continues to increase in the twenty-first century, especially in areas with ever-growing populations. Existing structures and highways require repair or replacement as they reach the end of their service life or simply no longer satisfy their intended purpose due to the growing population. As modern construction continues, two pressing issues will become more apparent to societies: an increasing demand for construction materials, especially concrete and asphalt aggregates, and an increasing production of construction and demolition waste. Already, the Federal Highway Administration (FHWA) estimates that two billion tons of new aggregate are produced each year in the United States. This demand is anticipated to increase to two and a half billion tons each year by 2020. With such a high demand for new aggregates, the concern arises of the depletion of the current sources of natural aggregates and the availability of new sources. Similarly, the construction waste produced in the United States is expected to increase. From building demolition alone, the annual production of construction waste is estimated to be 123 million tons (FHWA 2012). Currently, this waste is most commonly disposed of in landfills.

To address both the concern of increasing demand for new aggregates and increasing production of waste, many states have begun to recognize that a more sustainable solution exists in recycling waste concrete for use as aggregate in new concrete, or recycled concrete aggregates (RCA). The solution helps address the question of how to sustain modern construction demands for aggregates as well as helps to reduce the amount of waste that enters already over-burdened landfills.

Many states have begun to implement recycled concrete aggregates in some ways in new construction. As shown in Figure 1.1 from the FHWA, most states have recognized the many uses of RCA as a raw material, such as for rip-rap, soil stabilization, pipe bedding, and even landscape materials. As shown in Figure 1.2, many states have gone a step further in integrating RCA into roadway systems for use as aggregate course

base material. However, as shown in Figure 1.3, only a small number of states have begun using RCA in Portland cement concrete for pavement construction. As shown in these figures, the state of Missouri does not currently integrate RCA in any function (FHWA). Currently, there are no accepted standards or guidelines in the United States for utilizing RCA in structural concrete.
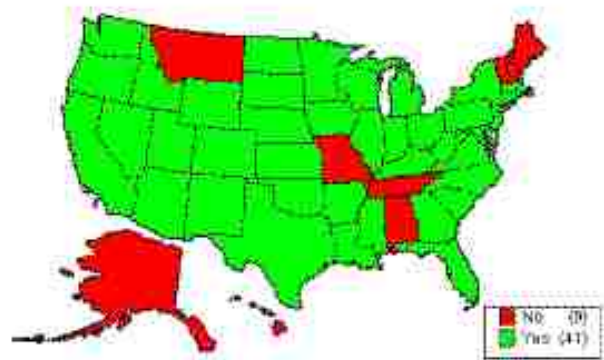
Figure 1.1 States using RCA as Aggregate (FHWA 2012)

Figure 1.2 States using RCA as Base Aggregate (FHWA 2012)

Figure 1.3 States using RCA in PC Concrete (FHWA 2012)

    1.1.2   Benefits of Recycled Aggregate Concrete. The use of recycled aggregate concrete (RAC) offers a sustainable solution for the continued growth of modern infrastructure. Primarily, RAC concrete diverts construction and demolition waste from the solid waste stream while easing the demand from non-renewable natural aggregate sources. Much research has been performed that shows up to 100% of the coarse aggregates in new concrete can be replaced with RCA.

    1.1.3   Concerns with Recycled Aggregate Concrete. RCAs are composed of both the original, or virgin, aggregate, as well as mortar which remains adhered to the surface of the aggregate. In the production of RCA, the removal of all this residual mortar would prove costly and detrimental to the integrity of the virgin aggregates within the concrete. Therefore, residual mortar is inevitable. Research has shown that this residual mortar causes high water absorption, low density, low specific gravity, and high porosity in RCAs compared to natural aggregates (Kou et al. 2012). These effects in the recycled aggregate can decrease hardened concrete properties of RAC. According to Abbas et al. (2008), the amount of residual mortar on the RCA can significantly affect the mechanical and durability properties of RAC. To reduce the negative impacts of this residual mortar, new mix design methods such as the equivalent mortar volume method can be used.

    Due to the variety of sources of RCA and the various functions, environment, and wear of the concrete structures and pavements from which the RCA can be obtained, characterizing this aggregate can be very difficult. Controlled studies must be performed to account for each of these variables on a regional basis, such as for each state's

department of transportation, so that the aggregates within the area can be adequately characterized.

1.2 OBJECTIVES AND SCOPE OF WORK

The main objective of this study was to determine the effect of replacing coarse virgin aggregates with RCA on concrete bond strength with deformed reinforcing steel bars. This experimental study consisted of comparing the bond performance of two RCA mixes designed at different replacement levels to a Missouri Department of Transportation (MoDOT) standard mix design at one strength level. Additionally, the effect of bar size on the bond strength of RCA concrete compared with virgin aggregate concrete was also evaluated. All RCAs used in this study contained state-approved 1 in. Potosi Dolomite coarse aggregate.

The following scope of work was implemented in an effort to reach these objectives: (1) review of the applicable literature; (2) develop a research plan; (3) design and construct test fixtures; (4) design and construct test specimens; (5) test specimens to failure and record applicable data; (6) analyze results and conduct comparisons between RAC and control mix designs; (7) develop conclusions and recommendations; (8) prepare this thesis in order to document the information obtained during this study.

1.3 RESEARCH PLAN

For this experimental program, the bond performance of RCA concrete designed at different replacement levels will be investigated and compared with a standard MoDOT mix design. The RCA mix design procedure to be investigated is the direct replacement method. This design method is a volumetric procedure that replaces a percentage of the virgin coarse aggregate directly with the RCA. For this bond study, the three replacement levels that will be considered are 0%, 50%, and 100%. The 0% replacement mix will serve as the control and will contain only virgin aggregates. For the 50% RCA mix, half of the total volume of coarse virgin aggregates will be substituted with RCA. For the 100% mix, the total volume of coarse virgin aggregates will consist of RCA. For all RCA mixes, the virgin aggregates used to make the RCA will be MoDOT approved 1" Potosi Dolomite. To control the amount of variables in this study, the RCA will be produced from beams that are cast and cured by the researchers in a controlled

laboratory environment. The crushing procedure and pre-crushed and post-crushed environmental conditions of the aggregates will be constant.

To investigate the bond performance, two bond test types will be performed: direct pull out tests and large scale beam splice tests. Direct pull out tests will be performed based on the RILEM 7-II-128 *RC6: Bond test for reinforcing steel. 1. Pull-out test* (RILEM, 1994). While direct pull out tests do not provide a realistic flexural type stress-state response in the specimen, they provide a basis of comparison among other direct pull out results and are commonly used for bond performance comparison. A total of 18 direct pull-out specimens were constructed and tested to bond failure using this test method. The full scale beam splice test will be based on a non-standardized procedure that has been developed in previous bond research. The beam splice test provides the most realistic response for bond performance in flexural stress state. A total of 9 full-scale beam splice specimens were constructed and tested to bond failure.

1.4 OUTLINE

This thesis consists of seven sections and four appendices. Section 1 contains a brief explanation of the current uses, benefits, and concerns of RAC as well as the objective and scope of work of this study.

Section 2 provides a discussion of the bond force transfer between concrete and embedded deformed steel bars, bond failure mechanisms, accepted tests for characterizing bond strength, and a review of the literature for RAC bond research.

Section 3 details the mix designs that were developed for this study as well as the test methods used to determine fresh and hardened concrete properties that were found at the time of testing bond specimens. Section 4 details the design, fabrication, test setup, and test procedure for the direct pull-out and full-scale beam splice specimens. Section 5 provides the recorded test data, the methodology used to normalize the data, normalized results, and a comparison among RCA replacement levels and across bar size.

Section 6 offers a discussion of a theoretical analysis of bond action and a comparison of analytical models to the experimental results obtained in this study. Section 7 summarizes the findings, conclusions, and recommendations from this study.

2. LITERATURE REVIEW

2.1 BOND CHARACTERISTICS

In reinforced concrete, the transfer of forces between deformed steel bars and the adjacent concrete occurs by three primary modes: 1) chemical adhesion between the bar and concrete, 2) friction forces, transverse forces, and relative slip, and 3) bearing of the ribs or deformations against the surrounding concrete. For deformed bars, adhesion is lost after the initial slip. This slip initiates bearing of the ribs against the surrounding concrete surface. Frictional forces along the surface of the bar remain small compared to these bearing forces, and bearing plays the biggest role in bond behavior. To balance the forces on the surface of the deformed bar, which are shown in Figure 2.1, compressive and shear stresses develop in the contacting concrete surfaces. These stresses develop into tensile stresses which in turn can lead to cracking of the concrete (ACI 408, 2003).
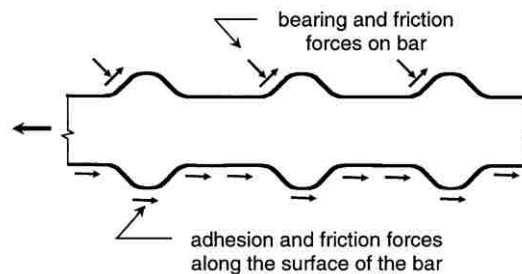
Figure 2.1 Bond Force Transfer Mechanisms (ACI 408, 2003)

Goto cracks can form as a result of the tension stresses induced by the compression forces at the bearing contact surfaces extending from the ribs. The formation of these cracks is shown in Figure 2.2. These cracks can result in a conical failure surface for bars in tension that extend outside of the concrete. However, Goto cracks do not play a significant role in bond anchorage or reinforcement development. (ACI 408, 2003)
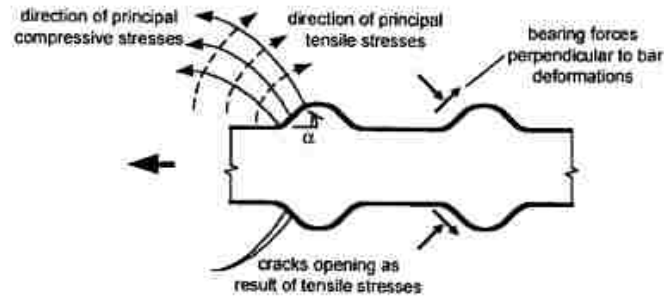
Figure 2.2 Formation of Goto Cracks (ACI 408, 2003)

Transverse cracks, form when the minimum concrete cover or bar spacing is small. The transverse cracks form as a result of hoop tensile stresses in the surrounding concrete induced by the bearing action of the ribs. With small cover, these cracks can reach the outside surface of the concrete and form splitting cracks as shown in Figure 2.3.
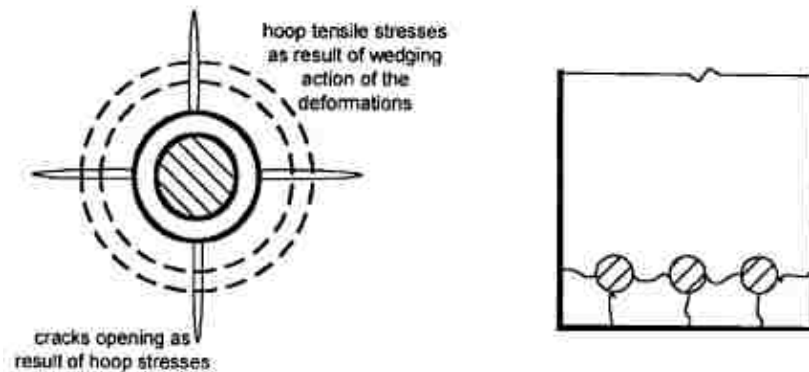
Figure 2.3 Formation of Hoop Stresses and Resulting Splitting Cracks (ACI 408, 2003)

When concrete cover and bar spacing is sufficiently large or enough transverse reinforcement is provided to prevent splitting failure, the bond failure may be a pull out type. This failure results in the shearing along the top surfaces of the reinforcing bar's ribs as shown in Figure 2.4. Most bond failures result as a combination of both concrete splitting and pull out type failure modes (ACI 408, 2003). It is also possible that if anchorage of the bar into the concrete is adequate or sufficient confinement is provided to

delay crack propagation, the steel bar may yield or strain harden prior to bond failure. Thus, bond failure only occurs when stresses in the steel do not exceed its tensile strength.
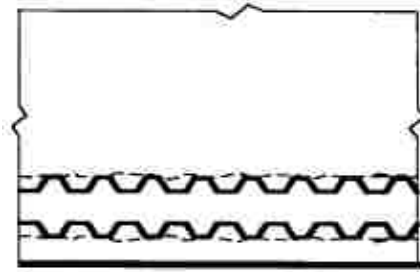
Figure 2.4 Pull-Out Failure (ACI 408, 2003)

Based on the above discussion, it is obvious that bond behavior is largely controlled by the following factors: mechanical properties of the surrounding concrete, concrete cover and bar spacing, presence or absence of confinement, surface condition of the bar, and the geometry of the bar (namely deformation shape, rib height, and bar diameter).

2.2 COMMON BOND TESTS

Many testing methods have been developed to measure bond strength between concrete and reinforcing steel bars. The configuration of each test method has an important role in the bond response. Four of the most common test configurations are pull-out specimens, beam-end specimens, beam anchorage specimens, and splice specimens (full beams). The direct pull-out test method is the most commonly used due to the ease of fabricating and testing of these specimens. However, this method produces the least realistic bond response of the four listed. As the bar of a pull-out specimen is loaded in tension, the surrounding concrete is in compression. In most practical applications of reinforced concrete, both the bar and the surrounding concrete experience tension. A concern with pull-out specimens is this additional confinement from the induced compression at the anchorage zone. Due to the unrealistic nature of the stress

state produced, pull-out specimens are not recommended as the only means of determining bond strength, but can serve as a useful comparison (ACI 408, 2003). A schematic of the pull-out test is shown in Figure 2.5.
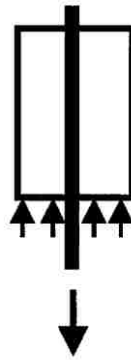
Figure 2.5 Schematic Direct Pull-Out Test (ACI 408, 2003)

The beam-end specimen, also known as the modified cantilever, more accurately represents reinforced concrete behavior. In this method, the bar and the surrounding concrete experience tension. This is achieved by loading the bar in tension and applying a compressive force a distance approximately equal to the embedded length of the bar away from the end of the bar. These specimens are relatively easy to fabricate and test, and offer bond strengths measurements more accurate to full-scale tests. A schematic of the beam-end test is shown in Figure 2.6.
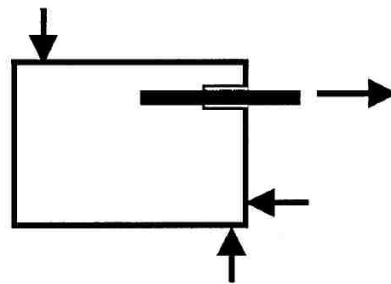
Figure 2.6 Schematic Beam-End Test (ACI 408, 2003)

Beam anchorage specimens are full-scale specimens with a configuration designed to simulate flexural cracks with a known bonded length. While these are specimens provide a realistic bond response, they can be challenging to fabricate (ACI 408, 2003). A schematic of the anchorage test is shown in Figure 2.7.
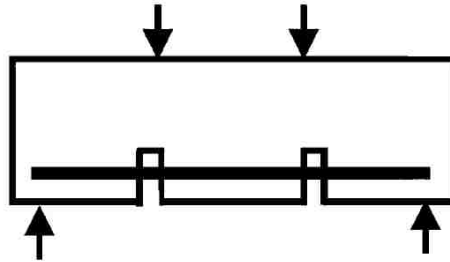
Figure 2.7 Schematic Beam-End Test (ACI 408, 2003)

Splice specimens are an alternative full-scale bond test. These splice beams are tested under four-point loading such that the splice is located in a constant moment region. Splice specimens are much easier to fabricate and will produce similar results as the anchorage specimens. Due to the simplicity of fabricating these specimens and the realistic bond response, splice specimens have provided the bulk of data used in developing current empirical design equations (ACI 408, 2003). A schematic of the beam splice test is shown in Figure 2.8.
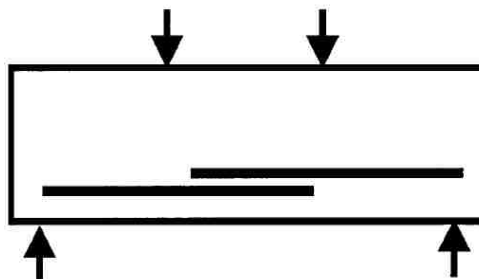
Figure 2.8 Schematic Beam-End Test (ACI 408, 2003)

2.3 RCA CONCRETE BOND RESEARCH

Much of the existing literature on recycled concrete aggregates (RCA) focuses on the mechanical and durability characteristics of concretes made with RCA. Few studies have been conducted to evaluate the structural performance of RCA concrete, and of those even fewer have concentrated on the bond characteristics of RCA concrete. In a study by Ajdukiewicz and Kliszczewicz (2002), pull-out specimens designed per RILEM recommendations were used to evaluate bond performance of 0% and 100% RCA replacement. The mix designs used in this study were developed by conventional direct replacement of natural aggregates with RCA. The RCAs used were taken from 6 structures demolished under the supervision of the researchers and with concrete strengths between 35-70 MPa. Five of the demolished structures were known to contain crushed granite coarse aggregate and one contained basalt. All structures demolished were between two to seven years old and the RCAs were crushed two or three months prior to use. They found that there is no significant difference between bond strength of deformed bars embedded in concrete with coarse RCA replacement and concrete containing only natural coarse aggregates. In this study, the greatest difference in bond strength was observed when smooth bars were used. There was a 20% decrease in bond strength when both coarse and fine aggregates were replaced with RCA, and an 8% decrease when natural sand and coarse RCA was used. (Ajdukiewicz and Kliszczewicz 2002) Typically, though, RCA fines are not recommended for use in new concretes.

Studies have shown that replacing natural sand with fine RCA will drastically increase the water demand and reduce the mix workability. Likewise, the drying shrinkage increases significantly from concrete made with coarse RCA only (20% to 50% more) to concretes made with both fine and coarse RCA (70% to 100% more). Further studies have shown that the mechanical properties are more negatively impacted with the addition of RCA fines. The decrease in compressive strength, tensile strength, and modulus of elasticity are much more pronounced when both fine and coarse RCA are present than when only coarse RCA is present (ACI 555R 2001).

Xiao and Falkner (2005) investigated the bond performance of concretes with 0%, 50%, and 100% replacement of coarse natural aggregates only with RCA using 36 direct pull-out specimens. The researchers obtained their RCAs from the runway of an airport in

Shanghai. The maximum particle size of the coarse natural aggregates in their RCAs was ½ in. (12.5 mm), and the material conformed to the Chinese standard GB50152-1992. The conclusions from this study were similar to those by Ajdukiewicz and Kliszczewicz (2002), namely that no difference was observed between the bond strength of deformed bars at 0% RCA replacement and 50% or 100% RCA replacement. When smooth bars were used, a maximum decrease in bond strength of 12% was observed in the RCA concrete (Xiao and Falkner 2005).

Generally, the mix design method used with RCA concrete has a significant impact on bond strength to mild steel reinforcing bars. Currently, there is no standard procedure for mix designing using RCA. The conventional method used in much of the current literature is a direct replacement of coarse aggregate with RCA. However, research has shown that the mortar attached to RCA negatively influences the mechanical and durability properties of RCA concrete (Shayan, 2003). To compensate for this residual mortar on RCA particles, Abbas (2008) has proposed a mix design procedure coined the "Equivalent Mortar Volume" (EMV) method. The key aspect of the EMV method is that the residual mortar of RCA is included in the total mortar volume of the mix, and the amount of new mortar and total amount of coarse aggregate are adjusted to account for this difference (Abbas, 2008).

Existing research has shown that bond strength of RCA designed by the conventional method is lower than bond strength of RCA designed by the EMV method. In 2008, Fathifazl utilized beam-end test specimens to evaluate bond performance under a more realistic stress state response with both conventional and EMV mix designs. He used RCAs from two different recycling plats- one in Montreal, Quebec and one in Vancouver, British Columbia. The RCAs from the Montreal plant contained crushed limestone as the original virgin aggregate whereas the RCAs from Vancouver contained predominantly well-rounded river-bed gravel. The parent material was a blend of various parent structures and roadways in the metropolitan areas. Using beam-end specimens with a Canadian standard No. 30 (d_b = 1.18 in. or 29.9mm) deformed reinforcing bars, Fathifazl found that the bond strength (normalized by the square root of compressive strength) of concrete specimens designed using conventional methods of coarse aggregate replacement were 24% lower than their companion natural aggregate specimens. He

observed similar bond strength reductions regardless of the original parent aggregate type. The study showed that bond strength of specimens designed using the EMV method were only 6% lower than their companion natural aggregate specimens. (Fathifazl, 2008)

In order to investigate the effect of bar size, Fathifazl compared the bond strengths of beam-end specimens containing either a Canadian standard No. 15 (d_b = 0.63 in. or 16.0mm) or No. 30 (d_b = 1.18 in. or 29.9mm) deformed bar. RCA made from two different sources and with different original virgin aggregate material were used. He found that, regardless of the original virgin aggregate material in the RCA and mix design method, the specimens containing No. 15 bars had higher bond strengths than those containing No. 30 bars. These findings are in consensus with ACI 408 that length to develop a reinforcing bar increases as bar diameter increases. This relationship is reflected in the development length equation presented in ACI 318. Furthermore, he found that when designed by the conventional method of direct replacement of natural aggregates for RCA, specimens containing No. 15 bars had 35% higher bond strengths than the specimens containing No. 30 bars. However, when designed by the EMV method, specimens containing No. 15 bars had bond strengths of at least 41% higher than those containing No. 30 bars (Fathifazl 2008).

In 2011, Butler, West, and Tighe evaluated bond performance using 100% direct replacement of coarse aggregates with RCA using 24 beam-end test specimens. Two RCA types were produced- one from the crushing of sidewalks, curbs, and gutter structures and one from crushing of a runway, apron, and terminal structures from the Pearson International Airport in Toronto, Canada. This study showed that natural aggregate beam-end specimens had bond strengths 9% to 21% higher than RCA beam-end specimens. Furthermore, they investigated a correlation between the RCA aggregate crushing value (ACV) and bond strength of concretes made with RCA. Using natural aggregates and two different sources of RCA, they found that as ACV increases, the bond strength decreases. For both RCA sources, an ACV of the RCA was 26% to 43% higher than natural aggregates indicating that the RCA is a weaker coarse aggregate than natural crushed stone. This relationship of decreasing bond strength with increasing ACV was linked to the influence of coarse aggregate crushing on fracture energy of concrete. Additionally, they observed a strong relationship between ACV and splitting tensile

strength, namely that as ACV increases, splitting tensile strength decreases (Butler et al. 2011).

Bond failures where splitting cracks control the peak load are governed by the tensile response of the concrete. The tensile response depends on the splitting tensile capacity and fracture energy, or capacity of the concrete to dissipate energy as a crack opens. As described in ACI 408R (2003), concrete with higher fracture energies provide improved bond capacities even if the concrete has similar tensile strengths.

3. MIX DESIGNS AND CONCRETE PROPERTIES

3.1 INTRODUCTION

The following section contains the procedures used to determine the fresh properties as well as the hardened mechanical properties of the concrete used in this study. A discussion of the mix designs used and their respective properties is also reported in this section.

3.2 CONCRETE PROPERTIES

3.2.1 Fresh Concrete Properties. For all three mixes used in this study the fresh concrete properties that were found were slump, unit weight, and air content. The slump test was performed in accordance with ASTM C 143 (2010) *Standard Test Methods for Slump of Hydraulic Cement Concrete*. The inside of a standard slump cone was wetted and placed on a damp surface. Concrete was added to the cone in three equal lifts and rodded 25 times each lift with the appropriately dimensioned steel rod. Excess concrete was struck off at the top of the cone using the rod, and any superfluous concrete was removed from around the base of the mold. The mold was lifted at a constant rate over five seconds, and the cone was inverted next to the slumped concrete. The slump measurement was taken from the rod placed over the top of the inverted cone to the center of the slumped concrete.

The unit weight of the concrete was determined in accordance with ASTM C 138 (2010) *Standard Test Method for Density (Unit Weight), Yield, and Air Content (Gravimetric) of Concrete*. A steel measure of known volume was weighed then filled with concrete in three equal lifts. Each lift was rodded 25 times and tapped with a rubber mallet to help consolidate the concrete. Once filled, a steel plate was placed flat on the top of the measure, covering approximately ¾ of the open area. The plate was pulled back across the covered area to screed off excess concrete. The plate was then placed flat in the same position and pushed forward to screed the rest of the open area of the measure. Next, the steel plate was tilted at an angle and used to screed the top surface of the measure until it was level and smooth. A wet sponge was used to wipe away excess concrete from the outside of the measure and along the top rim. The measure was then weighed, and the unit weight was determined.

The air content of the fresh concrete was determined in accordance with ASTM C 231 (2010) *Standard Test Method for Air Content of Freshly Mixed Concrete by the Pressure Method* using a type B pressure meter. After the unit weight was determined the same measure filled with concrete was used to determine air content. The pressure meter lid was wetted and secured over the top of the measure. The air chamber positioned on top of this lid was sealed off, and the appropriate initial pressure was added to the chamber. Next, water was gently injected into one petcock until it flowed without air bubbles from the opposite petcock ensuring the space between the lid and the surface of the concrete was filled with water. The stream of water was inspected for the presence of mortar, which would invalidate the test. The petcocks were then closed, and the air from the chamber was injected into the concrete-filled bottom measure while simultaneously tapping the measure with a rubber mallet. The air content was then recorded from the gauge on the pressure meter.

3.2.2 Compressive Strength of Concrete. The compressive strength, f_c, of the concrete was determined as per ASTM C39 (2011) *Standard Test Method for Compressive Strength of Cylindrical Concrete Specimens*. For each set of direct pull-out and beam splice specimens, accompanying cylinders were made to determine the compressive strength. The cylindrical molds used had a diameter of 4 in. (10.2 cm) and height of 8 in. (20.3 cm). These cylinders were left to cure in the same condition next to the bond test specimens. The compressive strength of the concrete was tested at 1, 3, 7, 14, 28, and 60 days as well as on the days of testing the bond specimens. Prior to testing, the cylinders were capped with a sulfur compound to give a uniform stress distribution during testing. The load rate was 565lb/sec (2.5kN/sec) as per the ASTM C39 standard. Figure 3.1 shows a capped cylinder in the loading machine. Three specimens were tested with the average representing one strength data point. The compressive strength of each mix design was determined from companion cylinders to the bond test specimens on the day of testing.

Figure 3.1 Compressive Strength Test

3.2.3   Modulus of Rupture of Concrete. The modulus of rupture, f_r, was determined according to ASTM C 78 (2010) Standard Test Method for Flexural Strength of Concrete. Small beams with dimensions 6 in. x 6 in. x 24 in. (15 cm x 15 cm x 60 cm) were cast to find the modulus of rupture. To test these beams, simple third point loading was used with a span length of 18 in. (45 cm). Upon reaching the peak load of the test, the modulus of rupture was calculated by Equation 3.1:

$$f_r = \frac{P*L}{b*d^2} \hspace{3cm} \text{(Eq. 3.1)}$$

where P is the peak load, L is the beam length, and b and d are the beam width and depth, respectively, measured at the fractured surface of the beam after failure. Three specimens were tested with the average representing one strength data point.

3.2.4   Modulus of Elasticity of Concrete. The modulus of elasticity, E_c, of the concrete was determined according to ASTM C 469 (2010) *Standard Test Method for Static Modulus of Elasticity and Poisson's Ratio of Concrete in Compression*. Cylinders with a 6 in. (15.2 cm) diameter and 12 in. (30.5 cm) height were used to determine the modulus of elasticity. The modulus of elasticity for each mix design was determined from companion cylinders to the bond test specimens on the day of testing.

3.2.5   Splitting Tensile Strength of Concrete. The splitting tensile strength, f_{tsp}, of the concrete was determined according to ASTM C496 (2011) *Standard Test Method for Splitting Tensile Strength of Cylindrical Concrete Specimens*. The splitting tensile strength was found on the day of bond specimen testing for each mix design. To find this strength, 6 in. x 12 in. (15.2 cm x 30.5 cm) cylinders were used. Upon reaching the peak load of this test, the splitting tensile strength was found by Equation 3.2:

$$f_{tsp} = \frac{2*P}{\pi*L*D} \qquad \text{(Eq. 3.2)}$$

where P is the peak load, L is the cylinder length, and D is the cylinder diameter. Figure 3.2 shows the failure mode from the splitting tensile test. Three specimens were tested with the average representing one strength data point. The splitting tensile strength of each mix design was determined from companion cylinders to the bond test specimens on the day of testing.

Figure 3.2 Splitting Tensile Failure Mode

3.2.6   Fracture Energy of Concrete. The fracture energy, G_f, was determined according to RILEM TC 50-FMC *Determination of the Fracture Energy of Mortar and Concrete by Means of Three-Point Bend Tests on Notched Beams*. Notched beams with dimensions 6 in. x 6 in. x 24 in. (15 cm x 15 cm x 60 cm) were cast in small batches for each mix design. Under three-point loading, the span was 18 in. (45 cm). The notch was cast into the concrete at midspan with a depth of 1.5 in. (4 cm) and width of 0.25 in. (0.6 cm). A gauge was applied at the notch to measure the crack mouth opening displacement, and displacement was measured at midspan by linear variable differential transformers (LVDTs). The fracture energy was calculated by dividing the total energy dissipated by the projected surface area of the crack as in Equation 3.3:

$$G_f = \frac{W}{bd - a_o} \qquad \text{(Eq. 3.3)}$$

Where *W* is the total energy dissipated, *b* and *d* are the beam width and depth respectively, and a_o is the depth of the notch. Three specimens were tested with the average representing one fracture energy data point.

3.3 RAC MIX DESIGNS

For this study, three mix designs were produced and evaluated for bond performance. A MoDOT Class B air-entrained mix design was used as a baseline for reference throughout the study. The specified cement content in this mix was 535 lb., the water-to-cement ratio was 0.40, the target slump was 6 in., and the design air content was 6%. The specified amount of fine aggregate as a volume of total aggregates was 40%. For this mix, the typical dosage range of the MoDOT-approved air entrainer MB-AE 90 was 0.25-4.0 fl.oz./100 lb. of cement (0.16-2.61 mL/kg of cement). The typical dosage of the Type A water reducer Glenium 7500 was 5.0 - 8.0 fl.oz./100 lb of cement (0.33-5.22 mL/kg of cement). Two RCC mixes were produced as modified Class B mix designs. The direct replacement method of RCA for coarse aggregate was used to design the RCA mixes. Two RCA replacement levels were considered: 50% and 100% volumetric replacement.

3.3.1 Pre-Recycled Concrete Mix Design. In order to control the number of variables in this experimental study, the recycled aggregates were produced by the researchers in a controlled laboratory environment. Unreinforced concrete beams were cast in five separate pours, and fresh and hardened concrete properties were determined from companion small-scale specimens from each pour. An equal volume of concrete was produced in each pour. The mix design used for the RCA production was the same Class B mix design used for the control in this study. MoDOT's specifications for this mix and the oven-dry design batch weights are provided in Section 3.3.2.

To better understand the aggregate properties of the RCA, the concrete properties including air content, unit weight, compressive strength, splitting tensile strength, modulus of rupture, and modulus of elasticity were determined for each pour that the RCA parent beams were cast. The fresh concrete properties are shown below in Table 3.1. The air content for two pours could not be determined due to faulty equipment. The hardened concrete properties are shown in Tables 3.2 through 3.5. The hardened properties were determined at the day of crushing, some 60 days after the parent beams were originally cast. For these hardened properties, an overall average value is presented. This value was assumed to be the average value for all of the concrete used to create the RCA since each pour contributed an equal volume to the total concrete crushed.

Table 3.1 Fresh Concrete Properties of Pre-Recycled Concrete

Pour	Slump (in.)	Air (%)
1	8	-
2	7	5.75
3	6	-
4	8	7
5	6	5.5

Conversion: 1 in. = 2.54 cm

Table 3.2 Compressive Strength Results of Pre-Recycled Concrete

Pour	Specimen	Compressive Strength, psi	Average Compressive Strength, psi	Overall Average Compressive Strength, psi
1	1	6571	6420	5390
1	2	6501	6420	5390
1	3	6173	6420	5390
2	1	4045	4270	5390
2	2	4363	4270	5390
2	3	4392	4270	5390
3	1	5472	5350	5390
3	2	5311	5350	5390
3	3	5277	5350	5390
4	1	4780	5290	5390
4	2	5553	5290	5390
4	3	5547	5290	5390
5	1	5690	5600	5390
5	2	5619	5600	5390
5	3	5484	5600	5390

Conversion: 1 psi = 6.9 kPa

Table 3.3 Splitting Tensile Strength Results of Pre-Recycled Concrete

Pour	Specimen	Tensile Strength (psi)	Average Tensile Strength (psi)	Overall Average Tensile Strength (psi)
1	1	564	585	520
1	2	611	585	520
2	1	554	515	520
2	2	478	515	520
3	1	555	525	520
3	2	494	525	520
4	1	520	515	520
4	2	507	515	520
5	1	592	465	520
5	2	342	465	520

Conversion: 1 psi = 6.9 kPa

Table 3.4 Modulus of Rupture Results of Pre-Recycled Concrete

Pour	Specimen	MOR (psi)	Average MOR (psi)	Overall Average MOR (psi)
1	1	716	745	
	2	775		
2	1	572	505	
	2	438		
3	1	538	565	570
	2	593		
4	1	532	500	
	2	471		
5	1	582	535	
	2	488		

Conversion: 1 psi = 6.9 kPa

Table 3.5 Modulus of Elasticity Results of Pre-Recycled Concrete

Pour	MOE (psi)	Overall Average MOE (psi)
1	6,000,000	
2	5,100,000	
3	5,700,000	5,520,000
4	5,150,000	
5	5,650,000	

Conversion: 1 psi = 6.9 kPa

3.3.2   Control Mix Design and Concrete Properties. A MoDOT Class B air-entrained mix was used for the control mix in this study. The target strength was 4000 psi (27.58 MPa). The MoDOT mix specifications are summarized in Table 3.6, and the oven-dry design batch weights are shown in Table 3.7. The fresh properties of the concrete were determined after the addition of the chemical admixtures on the day of casting the bond test specimens. The slump was 8 in. (20.3 cm), the air content was 13%, and the unit weight was 144.4 lb/yd^3 (2313 kg/m^3).

The compressive strength, slitting tensile strength, and modulus of elasticity of the mix were determined from companion cylinders that were cast from the same concrete batch as the bond test specimens. Figure 3.3 shows the compressive strength

gain over time. At 90 days, the compressive strength was 4650 psi (32.06 MPa), just over the target strength. On the day of testing, the compressive strength was 4000 psi (27.58 MPa). The splitting tensile strength on the day of testing the bond specimens was 397 psi (2.74 MPa). The results are shown in Table 3.8. Likewise, the modulus of elasticity of the concrete found on the day of testing the bond specimens was 4,300,000 psi (29.65 GPa).

Table 3.6 Control Mix Design Specifications

Cementitious Amount, lb/yd^3	535
w/c Ratio	0.4
Amount of Fine Aggregate (by volume), %	40
Design Air Content, %	6.0
Target Slump, in.	6.0

Conversion: 1 lb./yd^3 = 0.59 kg/m^3
          1 in. = 2.54 cm

Table 3.7 Control Design Mix Proportions, Oven-Dry Basis

Cement	535 lb/yd^3
Water	214.0 lb/yd^3
Coarse Aggregate	1958.2 lb/yd^3
Fine Aggregate	1252.7 lb/yd^3
Air Entrainer MB-AE 90	1 fl.ozs/cwt
Water Reducer Glenium 7500	6 fl.ozs/cwt

Conversion: 1 lb./yd^3 = 0.59 kg/m^3
           1 oz. = 29.6 ml
           1 lb. = 0.45 kg

Figure 3.3 Control Mix Strength Gain with Time
Conversion: 1 psi = 6.9 kPa

Table 3.8 Control Splitting Tensile Strength Results

Specimen	Splitting Tensile Strength (psi)	Average Splitting Tensile Strength (psi)
Control-1	369	
Control-2	423	397
Control-3	397	

Conversion: 1 psi = 6.9 kPa

3.3.3   50% RCA Mix Design and Concrete Properties. The first mix
incorporating RCA was a 50% direct replacement design. Half of the total volume of
coarse aggregate in the control MoDOT Class B mix was directly substituted with the
laboratory-produced RCA. In order to maintain consistency with the control specimens,
the MoDOT Class B mix specifications were used to design the 50% direct replacement
mix. The achieved 28-day strength of this mix during trial batching was 5500 psi (37.92
MPa), so this was used for the design of bond test specimens.

The mix specifications are summarized in Table 3.9, and the oven-dry design
batch weights are shown in Table 3.10. The fresh properties of the concrete were

determined after the addition of the chemical admixtures on the day of casting the bond test specimens. The slump was 6.5 in. (16.5 cm), the air content was 8%, and the unit weight was 139.8 lb/yd^3 (2239 kg/m^3).

The compressive strength, slitting tensile strength, and modulus of elasticity of the mix were determined from companion cylinders that were cast from the same concrete batch as the bond test specimens. Figure 3.4 shows the compressive strength gain over time. At 60 days, the compressive strength was 3800 psi (26.20 MPa). On the day of testing, the compressive strength was 3560 psi (24.54 MPa). The splitting tensile strength on the day of testing the bond specimens was 344 psi (2.37 MPa). The results are shown in Table 3.11. Likewise, the modulus of elasticity of the concrete on the day of testing the bond specimens was 3,750,000 psi (25.86 GPa).

Table 3.9 RCA-50 Mix Design Specifications

Cementitious Amount, lb/yd^3	535
w/c Ratio	0.4
Amount of Fine Aggregate (by volume), %	40
Design Air Content, %	6.0
Target Slump, in.	6.0

Conversion: 1 lb./yd^3 = 0.59 kg/m^3
          1 in. = 2.54 cm

Table 3.10 RCA-50 Design Mix Proportions, Oven-Dry Basis

Cement	535 lb/yd^3
Water	214.0 lb/yd^3
Coarse Natural Aggregate	979.1 lb/yd^3
Coarse Recycled Aggregate	845.9 lb/yd^3
Fine Aggregate	1252.7 lb/yd^3
Air Entrainer MB-AE 90	1 fl.ozs/cwt
Water Reducer Glenium 7500	4 fl.ozs/cwt

Conversion: 1 lb./yd^3 = 0.59 kg/m^3
          1 oz. = 29.6 ml
          1 lb. = 0.45 kg

Figure 3.4 RCA-50 Mix Strength Gain with Time
Conversion: 1 psi = 6.9 kPa

Table 3.11 RAC-50 Splitting Tensile Strength Results

Specimen	Splitting Tensile Strength (psi)	Average Splitting Tensile Strength (psi)
RCA-50-1	341	344
RCA-50-2	347	

Conversion: 1 psi = 6.9 kPa

3.3.4   100% RCA Mix Design and Concrete Properties. The second mix incorporating RCA was a 100% direct replacement design. The total volume of coarse aggregate in the control MoDOT Class B mix was directly substituted with the laboratory-produced RCA. In order to maintain consistency with the control specimens, the MoDOT Class B mix specifications were used to design the 100% direct replacement mix. However, during laboratory trial batching, it was noticed from the slump test that the mixes lacked cohesion. To remediate this lack of cohesion, the mix was modified by increasing the amount of fine aggregate volume by 5% of total aggregates. This change

notably improved the cohesion of the mix. The achieved 28-day strength of this mix during trial batching was 5500 psi (37.92 MPa), so this was used for the design of bond test specimens.

The mix specifications are summarized in Table 3.12, and the oven-dry design batch weights are shown in Table 3.13. The fresh properties of the concrete were determined after the addition of the chemical admixtures on the day of casting the bond test specimens. The slump was 8.5 in. (21.6 cm), the air content was 7%, and the unit weight was 137.2 lb/yd^3 (2198 kg/m^3).

The compressive strength, slitting tensile strength, and modulus of elasticity of the mix were determined from companion cylinders that were cast from the same concrete batch as the bond test specimens. Figure 3.5 shows the compressive strength gain over time. At 60 days, the compressive strength was 5300 psi (36.54 MPa). On the day of testing, the compressive strength was 4840 psi (33.37 MPa). The splitting tensile strength found on the day of testing the bond specimens was 320 psi (2.21 MPa). The results are shown in Table 3.14. Likewise, the modulus of elasticity of the concrete found on the day of testing the bond specimens was 4,000,000 psi (27.58 GPa).

Table 3.12 RAC-100 Mix Design Specifications

Cementitious Amount, lb/yd^3	535
w/c Ratio	0.36
Amount of Fine Aggregate (by volume), %	45
Design Air Content, %	6.0
Target Slump, in.	6.0

Conversion: 1 lb./yd^3 = 0.59 kg/m^3
1 in. = 2.54 cm

Table 3.13 RCA-100 Design Mix Proportions, Oven-Dry Basis

Cement	535 lb/yd^3
Water	192.6 lb/yd^3
Coarse Aggregate	1650.5 lb/yd^3
Fine Aggregate	1441.6 lb/yd^3
Air Entrainer MB-AE 90	1 fl.ozs/cwt
Water Reducer Glenium 7500	6 fl.ozs/cwt

Conversion: 1 lb./yd^3 = 0.59 kg/m^3
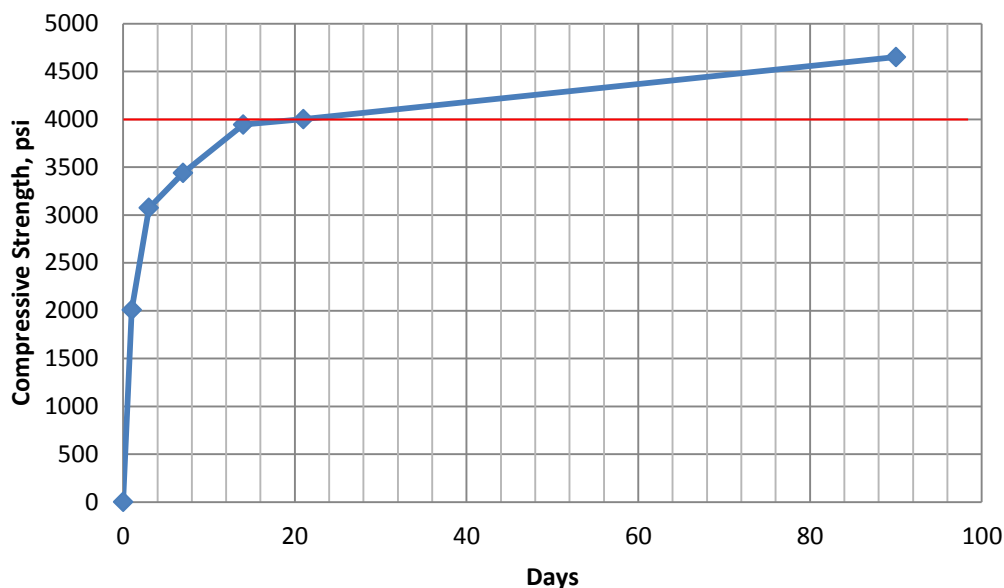   1 oz. = 29.6 ml
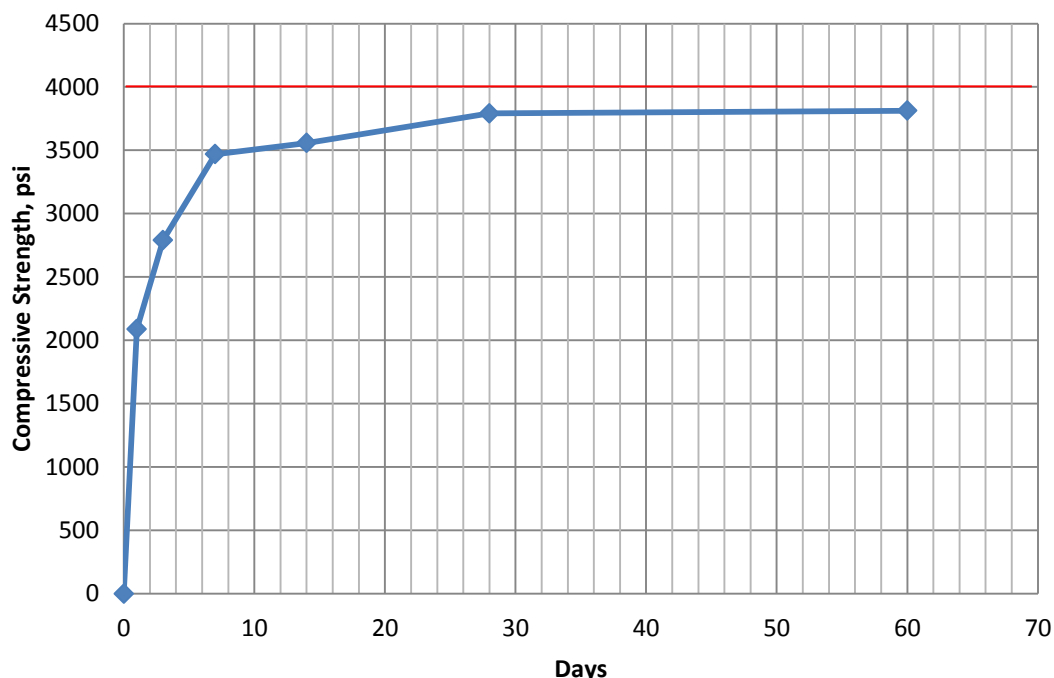   1 lb. = 0.45 kg
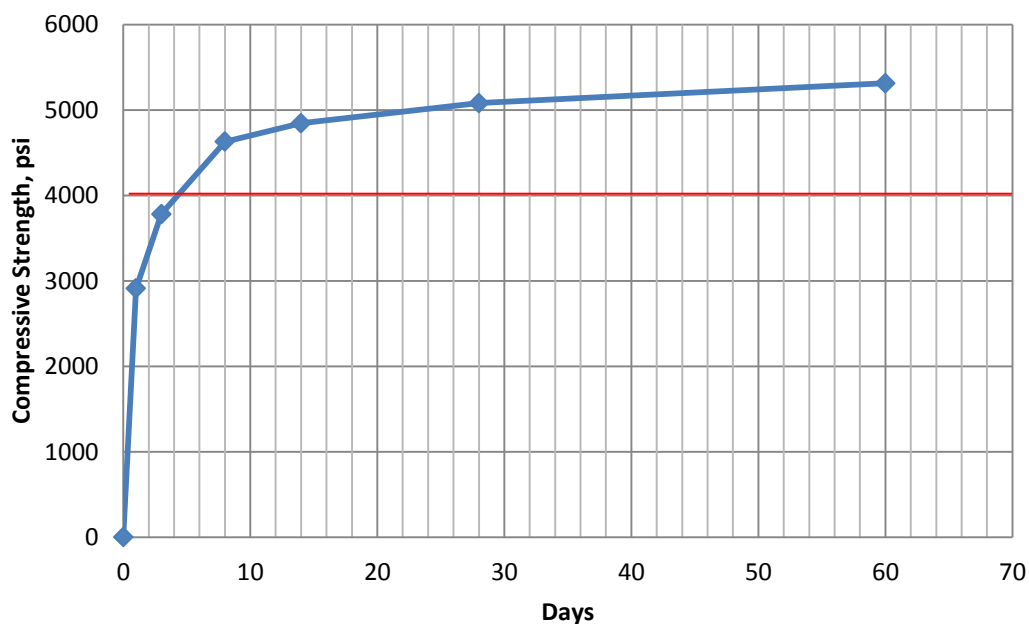
Figure 3.5 RCA-100 Mix Strength Gain with Time
Conversion: 1 psi = 6.9 kPa

Table 3.14 RAC-100 Splitting Tensile Strength Results

Specimen	Splitting Tensile Strength (psi)	Average Splitting Tensile Strength (psi)
RCA-100-1	320	
RCA-100-2	320	320
RCA-100-3	319	

Conversion: 1 psi = 6.9 kPa

3.4 CONCRETE MECHANICAL PROPERTIES

3.4.1   Modulus of Rupture Results. The modulus of rupture, f_r, of the VAC and 100% RCA mixes is shown in Table 3.15 along with the corresponding compressive strengths on the day of testing. The modulus of rupture for each mix was determined from small batches, and companion cylinders were cast to find the compressive strength. In order to compare the test results across mix designs, the moduli of rupture were normalized by dividing the test value by the square root of the concrete compressive strength. This method of normalization is based on the accepted relationship between modulus of rupture and compressive strength as presented in ACI 318R (2011):

$$f_r = 7.5\lambda\sqrt{f_c'} \qquad\qquad \text{(Eq. 3.4)}$$

where λ is a correction factor for lightweight concrete.

Table 3.15 Modulus of Rupture Results

Mix	f_c (psi)	f_r (psi)	Normalized f_r	COV	Average Normalized f_r
VAC	5416	501	6.81	9.3%	6.39
	4959	420	5.96		
RCA-100	4546	339	5.03	8.5%	5.69
	4417	391	5.88		
	4944	400	5.69		
	4350	407	6.17		

Conversion: 1 psi = 6.9 kPa

3.4.2   Modulus of Elasticity Results. The average modulus of elasticity, E_c, of the VAC, 50% RCA, and 100% RCA mixes is shown in Table 3.16 along with the corresponding compressive strengths on the day of testing. The modulus of elasticity of each mix was determined from companion cylinders cast on the same day as the beam splice specimens. To compare the results across mix designs, the moduli of elasticity were normalized by dividing the test value by the square root of the concrete compressive

strength. This method of normalization is based on the accepted relationship between modulus of elasticity and compressive strength as presented in ACI 318R (2011):

$$E_c = w_c^{1.5} 33 \sqrt{f_c'} \qquad \text{(Eq. 3.5)}$$

where w_c is the unit weight of the concrete.

Table 3.16 Modulus of Elasticity Results

Mix	f_c (psi)	Average MOE (ksi)	Average Normalized MOE
VAC	4000	4300	67.99
RCA-50	3560	3750	62.85
RCA-100	4840	4000	57.50

Conversion: 1 psi = 6.9 kPa

3.4.3   Splitting Tensile Strength Results. The average splitting tensile strength, f_{tsp}, of the VAC, 50% RCA, and 100% RCA mixes is shown in Table 3.17 along with corresponding compressive strengths on the day of testing. The splitting tensile strength of each mix was determined from companion cylinders cast on the same day as the beam splice specimens. To compare the results across mix designs, the splitting tensile strengths were normalized by dividing the test value by $f_c^{2/3}$. This method of normalization is based on the relationship between splitting tensile strength and compressive strength as presented in CEB-FIP (1990):

$$f_{tsp} = 1.57 f_c^{2/3} \qquad \text{(Eq. 3.6)}$$

Table 3.17 Splitting Tensile Strength Results

Mix	f_c (psi)	Average f_{tsp} (psi)	Average Normalized f_{tsp}
VAC	4000	397	1.58
RCA-50	3560	325	1.39
RCA-100	4840	320	1.12

Conversion: 1 psi = 6.9 kPa

3.4.4   Fracture Energy Results. The average fracture energy, G_f, of the VAC, 50% RCA, and 100% RCA mixes is shown in Table 3.18 along with the corresponding compressive strengths on the day of testing. The fracture energy for each mix was determined from small batches, and companion cylinders were cast to find the compressive strength. To compare the results across mix designs, the fracture energies were normalized by dividing the test value by $f_c^{.0.7}$. This method of normalization is based on the relationship between fracture energy and compressive strength as presented in CEB-FIP (1990):

$$G_f = G_{fo} \left(\frac{f_c}{f_{cmo}} \right)^{0.7} \qquad \text{(Eq. 3.7)}$$

where G_{fo} is a constant base value fracture energy dependent on the maximum aggregate size and f_{cmo} is a constant equal to 1450 psi (10 MPa).

Table 3.18 Fracture Energy Results

Mix	f_c (psi)	Average G_f (lbf/ft)	Average Normalized G_f
VAC	5394	20.9	0.0510
RCA-50	6598	20.8	0.0440
RCA-100	4945	15.3	0.0397

Conversion: 1 psi = 6.9 kPa

1 lbf/ft = 6.9 N/m

3.4.5   Comparison of Mechanical Properties. Figure 3.6 shows a graphical comparison of the mechanical properties of the three mixes. All properties are negatively impacted with increasing replacement of coarse natural aggregates with RCA. The most drastic decreases were seen in splitting tensile strength and fracture energy. The splitting tensile strength decreased 12% and 29% for 50% RCA replacement and 100% RCA replacement, respectively. The fracture energy decreased 14% and 22% for 50% RCA

replacement and 100% RCA replacement, respectively. The reduced tensile response of the concrete is likely due to the presence of two interfacial transition zones (ITZ) in concrete containing RCAs. The two ITZs include the bond between the original virgin aggregates and the residual adhered mortar as well as between the new virgin aggregates and fresh mortar. Additionally, the demolition and crushing processes introduce the potential for internal transverse cracks and micro-cracking in RCAs. With more planes of weakness, the ability to resist tensile forces is weakened in concrete containing these RCAs.

In bond failures where splitting cracks control, the peak load is governed by the tensile response of the concrete which depends on its splitting tensile capacity and fracture energy. Thus, as shown in the deteriorated splitting tensile strength and fracture energy of high volume RCA concrete, it is expected that the bond carrying capacity will be negatively impacted.
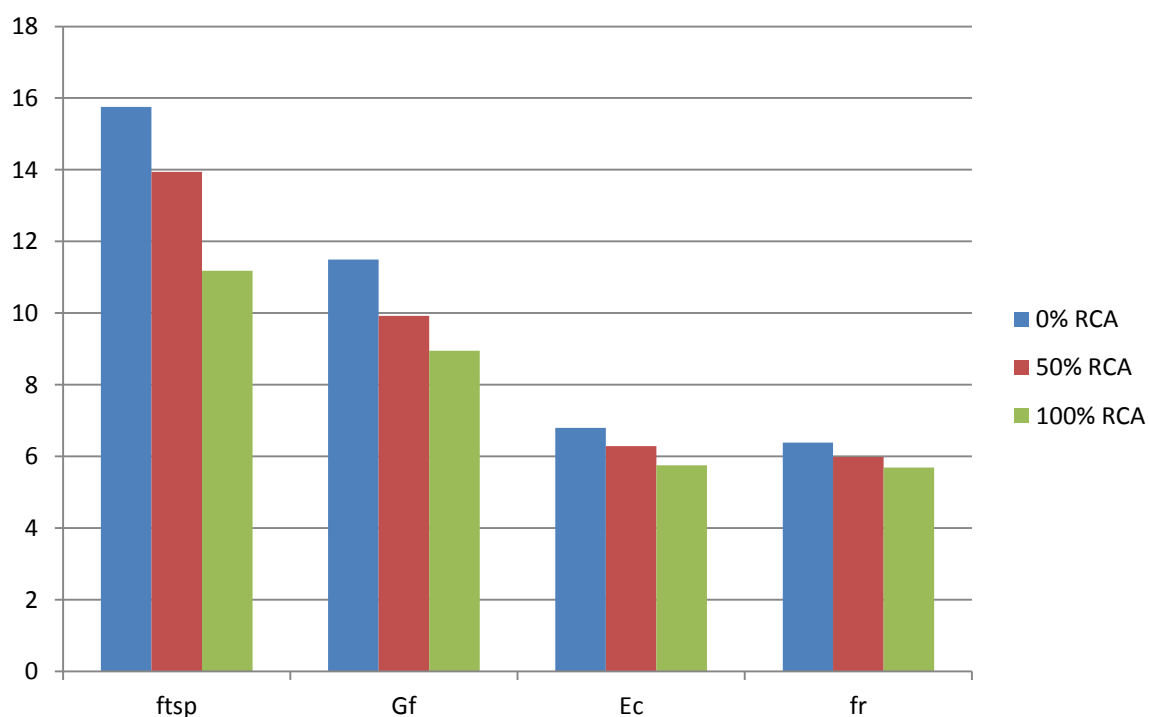
Figure 3.6 Comparison of Normalized Mechanical Properties
Note: Normalized values of $f_{tsp}*10$ and E_c*10^{-1}

4. EXPERIMENTAL PROGRAM

4.1 INTRODUCTION

To evaluate the bond performance of RAC, both direct pull-out and full-scale beam splice specimens were used. RILEM 7-II-128 *RC6: Bond test for reinforcing steel* was used to develop the direct pull-out type specimens and test method. Likewise, recommendations from ACI 408R-03 *Bond and Development of Straight Reinforcing Bars in Tension* as well as procedures reported in previous research of bond performance were used to develop the full-scale beam splice specimens and test method.

4.2 RCA PRODUCTION

The RCA used throughout the study was produced in the laboratory environment. This step precluded variables such as varying levels of chloride and organic contamination, varying and/or unknown sources of virgin aggregates, and different levels of residual mortar deterioration of the recycled aggregates. By using this laboratory-produced RCA, the amount of residual mortar on the aggregates was a "worst-case" condition with a very high content by volume.

In order to make the RCA, the parent concrete beams were cast and cured in the laboratory. Thirty 1 ft. x1.5 ft. x 5 ft. (0.30 m x 0.46 m x 1.52 m) and twenty 1 ft. x1.5 ft. x 7 ft. (0.30 m x 0.46 m x 2.13 m) un-reinforced beams were cast in a total of five separate pours. Short beams were produced to improve the ease of transportation to the crushing site. To build the formwork for these beams, 10 ft. (3.05 m) and 14 ft. (4.27 m) steel and wood forms were used with a plywood divider in the middle to create the smaller beams. Polyvinyl chloride (PVC) tubes were inserted at two locations through the middle of each formwork such that a steel rod could be temporarily placed through the beams after the formwork was removed and used to lift the beams onto a truck bed. This step was done to eliminate the need to use steel hooks which might have damaged the crushing equipment. Figure 4.1 shows the prepared formwork for the parent concrete beams.

Once all these beams were cast and allowed to reach a minimum compressive strength of 4000psi (27.58MPa), they were transported to the crushing site. For this study, the rock crushers at Capitol Quarries of Jefferson City, Missouri were used to

crush down the parent concrete beams to the desired MoDOT gradation D distribution. A mobile crushing plant located in Rolla, MO was used. This plant is shown in Figure 4.2. Steel jaw crushers were used, and the rock was processed through both the primary and secondary crushers.

Figure 4.1 Formwork for Casting Pre-Recycled Concrete

4.3 DIRECT PULL-OUT SPECIMENS

4.3.1 Direct Pull-Out Specimen Design. RILEM 7-II-128 *RC6: Bond test for reinforcing steel* describes the pull-out specimen as a steel reinforcing bar embedded in a concrete cube with a volume of $10d_s$ by $10d_s$ by $10d_s$, where d_s is the bar diameter. A direct tensile load is applied to the end of the steel bar until the bonded region fails. During testing, both the slip of the embedded bar and applied load are measured. The test specification calls for a bonded length of $5d_s$ and an un-bonded length of $5d_s$ at the end closest to the applied load. Some changes were made to RILEM recommended test specimen design based on results from previous research (Wolfe, 2011).

The direct pull out specimen used in this experimental program was a reinforcing steel bar embedded in a cylindrical volume of concrete with a diameter of 12 in. (30.5

cm). This deviation from the RILEM standard was made to reduce the potential for a splitting failure by maintaining a constant, large concrete cover for the reinforcing bar. The bonded length was $5d_s$ and the un-bonded length was $5d_s$ as per the RILEM testing standard. This un-bonded length is necessary in the design of the direct pull-out specimens to prevent a conical failure surface from forming within the concrete volume at the location of bearing (ACI 408, 2003).

In this testing program, both ASTM A615-09, Grade 60 #4 (No. 13) and #6 (No. 19) deformed steel bars were used in direct pull out specimens. The total length of each bar measured 40 in. (101.6 cm). A length of 3/8 in. (.95 cm) remained exposed at the end of the bonded portion to facilitate the measure of slip during testing using a linear voltage differential transformer (LVDT). The bonded and un-bonded lengths were 2.5 in. (6.4 cm) for the #4 (No.13) direct pull-out specimens and 3.75 in. (9.5 cm) for the #6 (No. 19) direct pull out specimens. A schematic of the #4 (No. 13) and #6 (No. 19) specimens are shown in Figures 4.2 and 4.3, respectively.
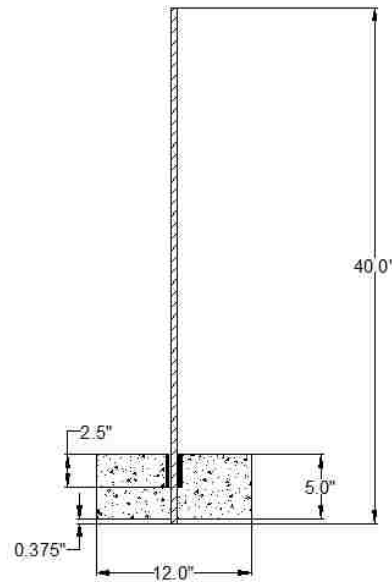
Figure 4.2 Schematic of #4 (No. 13) Bar Direct Pull-Out Specimen
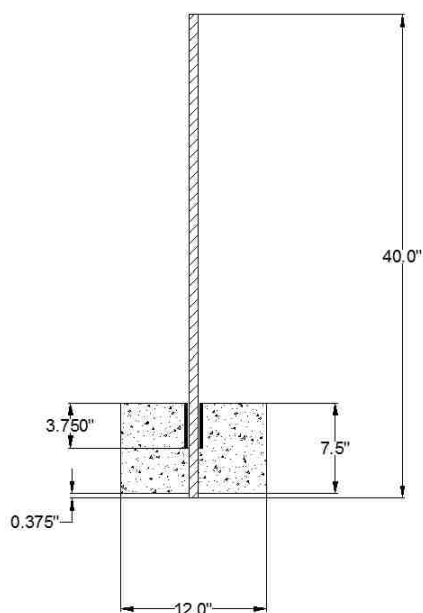
Figure 4.3 Schematic of #6 (No. 19) Bar Direct Pull-Out Specimen

     4.3.2   Direct Pull-Out Specimen Fabrication. The molds for the direct pull out specimens were constructed from segments of 12 in. (30.5 cm) diameter cardboard tube concrete forms. Strips measuring 5 in. (12.7 cm) and 7.5 in. (19.1 cm) in length were cut for the #4 (No. 13) bar and #6 (No. 19) bar specimens, respectively. The bases of the molds were constructed from 3/8in. (.95cm) plywood cut to 14 in. x 14 in. (35.6 cm x 35.6 cm) squares. The 3/8 in. (0.95 cm) base thickness was chosen to allow a 3/8 in. (0.95 cm) length exposed at the end of the bonded portion to facilitate the measure of slip at the unloaded end during testing. A hole was drilled in the center of the base pieces 1/16 in. (0.16 cm) larger than the nominal diameter of the bar in order for the 3/8 in. (0.95 cm) length of the bar to remain exposed. The cardboard segments of cardboard tube were then aligned along the base pieces with the drilled-out hole at the center. A bead of waterproof, adhesive silicon was applied at the junction of the plywood base and cardboard segment in order to attach the pieces of the mold and to prevent cement paste from leaking during the casting and curing of the specimens.

    Both the #4 (No.13) and #6 (No. 19) steel reinforcing bars were sectioned into 40 in. (101.6cm) long segments for the pull out specimens. PVC pipes were used to form the

bond breaker within the concrete cylinder. For the #4 (No. 13) bars, PVC pipe with an inner diameter of 3/4 in. (1.91cm) was used, and for the #6 (No. 19) bars, PVC pipe with an inner diameter of 1 in. (2.54cm) was used. The PVC pipe segments were cut 1/4 in. (0.64cm) longer than the required un-bonded length. This step was done so that this 1/4 in. (0.64cm) length would remain beyond the concrete cylinder on the bearing surface. This extra length was used to help ensure that concrete did not inadvertently fall between the PVC bond breaker and steel bar during casting and finishing of the specimens.

To attach the bond breaker to the bars, a single layer of bubble wrap was taped around the portion to remain un-bonded. This wrap helped to align the PVC concentrically with the steel bar and to also help keep concrete from filling the space within the bond breaker. The segments of PVC were slid over the bubble wrap, and a small bead of waterproof silicone was carefully applied around the top and bottom of the bond breaker to prevent concrete infiltration.

The top pieces of the direct pull out molds were made from 3/8 in. plywood cut to 14 in. x 14 in. (35.6 cm x 35.6 cm) squares. A hole measuring 1/16 in. (0.16 cm) larger than the outside diameter of the PVC pipe was drilled at the center of each top piece. Prior to casting the specimens, the reinforcing bars were placed into the completed forms and leveled to ensure they were plumb with the cylindrical mold base. An outline of the cylindrical base was sketched on the bottom side of the top piece when the steel bar was shown to be plumb through the use of levels. Three wood blocks were then screwed onto the bottom of the top piece of plywood tangentially along the outline of the cardboard tubing to snugly secure the top in place.

To cast the specimens, the steel bar was first inserted into the hole in the bottom of the mold. The bar was held perpendicular as concrete was filled to the top of the mold. A vibrator was used to lightly consolidate the concrete as needed, and the surface of the concrete was finished with a trowel. Once finished, the top piece of the mold was gently slid down over the bar and fitted around the extruded PVC bond breaker. The pull out specimens and the companion compression and splitting tensile specimens were left to cure until the specified peak strength was reached prior to testing. The cardboard and plywood components of the molds were removed on the day of testing. The completed pull-out specimens curing in their molds are shown in Figure 4.4.

Figure 4.4 Completed Direct Pull-Out Specimens in Molds

4.3.3   Direct Pull-Out Specimen Test Set-Up. A 200 kip-capacity (890kN) loading frame manufactured by Tinius Olson was used to test the direct pull out specimens. After the specimens were de-molded, they were inverted and positioned through the top platform of the load frame as shown in Figure 4.5. A steel bearing plate was used, and a neoprene pad was placed directly between the concrete surface and steel plate to ensure uniform bearing on the concrete. The steel bar was fed through grips on the middle platform of the testing frame. A smaller steel plate was placed on the top of the concrete cylinder and an LVDT was clamped to a magnetic stand at the top of the specimen. The head of the LVDT was placed on the 3/8 in. (0.95 cm) exposed end of the steel bar to measure the slip during testing. The LVDT set-up is shown in Figure 4.6.
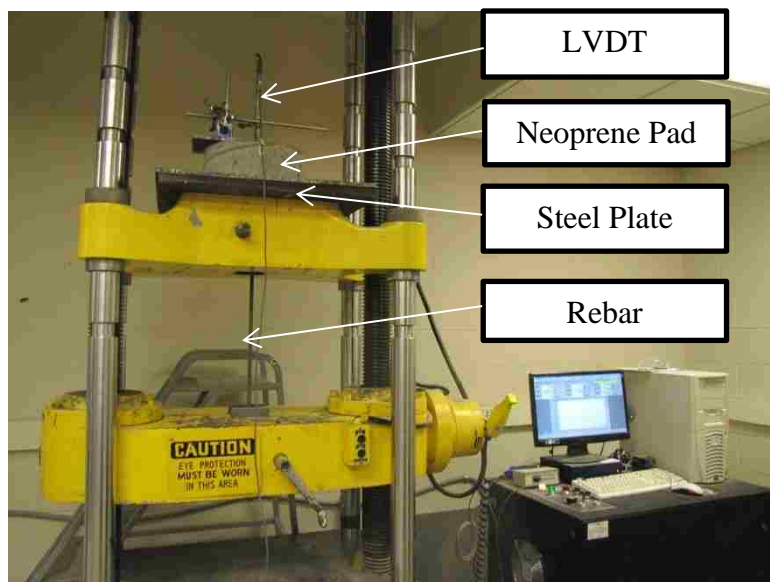
Figure 4.5 Test Set-Up for Direct Pull-Out Specimen

Figure 4.6 LVDT Set-Up for Direct Pull-Out Specimen

4.3.4   **Direct Pull-Out Specimen Test Procedure.** The computer software controlling the Tinius Olson was programmed to apply a displacement controlled load rate of 0.10 in. (0.3 cm) per minute. A preload of approximately 100 lb. (0.44kN) was applied to the rebar by manually moving the middle platform. This was done to help the middle fixture properly grip the steel bar. After this preload was applied, the test was initiated. A distinct peak in the load versus slip output plot was watched for during testing. After this peak was detected, the test was continued while the load began to decrease with increasing slip. The test was allowed to run this way in order to determine if there was any additional bond capacity and to be sure that the captured peak load was a true bond failure.

4.4 BEAM SPLICE SPECIMENS

4.4.1   **Beam Splice Specimen Design.** The beam splice test used in this experimental program is a non-ASTM testing procedure for full scale beams. The design and fabrication of the specimens was based on previous research of bond performance (Looney, 2012 and Wolfe, 2011). The beams used in this study were 10 ft. (3.05m) long with a cross section of 12 in. x 18 in. (0.30m x 0.46m). The longitudinal reinforcement consisted of three ASTM A615-09, Grade 60 #6 (No. 19) deformed steel bars, which were contact lap-spliced at the midspan of the beams. The splice length used for these beams was a reduced value of the development length equation recommended in ACI 318-11 "Building Code Requirements for Structural Concrete", shown as Equation 4.1. Based on previous research by Looney (2012), 70% of this calculated development length was used for the beam splice specimen design. Looney found that this reduction was sufficient to avoid yielding of the bar in a flexural failure mode and to ensure a bond failure mechanism. The equation for development length is:

$$l_d = \left[\frac{3}{40} \frac{f_y}{\lambda \sqrt{f_c'}} \frac{\Psi_t \Psi_e \Psi_s}{\left(\frac{c_b + K_{tr}}{d_b} \right)} \right] * d_b \qquad \text{(Eq. 4.1)}$$

where, l_d = development length
                f_y = specified yield strength of reinforcement
                λ = lightweight concrete modification factor

f'$_c$ = specified compressive strength of concrete
Ψ_t = reinforcement location modification factor
Ψ_e = reinforcement coating modification factor
Ψ_s = reinforcement size modification factor
c_b = smallest of distance from center of a bar to nearest concrete surface or
one-half the center-to-center bar spacing
K_{tr} = transverse reinforcement index
d_b = nominal diameter of the reinforcing bar

A standard hook was specified at the ends of each longitudinal reinforcing bar to achieve sufficient development. As per ACI 318-11, this hook included a 90-degree bend with the minimum recommended bend diameter of 4.5 in.(11.4cm) and an extension of $12d_b$ at the free end of the bar (ACI 318, 2011).

Transverse reinforcement against shear failure consisted of #3 (No. 10), ASTM A615-09, Grade 60, U-shaped stirrups. To ensure that a shear failure would not occur before bond failure, a stirrup spacing less than the ACI 318-11 maximum stirrup spacing was used. The stirrups were not placed within the lap spliced region in order to avoid the interaction of confinement of the concrete within the splice zone. Figures 4.7 and 4.8 detail the cross-sectional and plan views of the beam splice specimens, respectively. As shown in the schematic below, 180-degree hooks were used at the free ends of the U-stirrups. To help stabilize and align the cages, #4 (No. 13) bars were used as top bars and placed inside of these hooks.
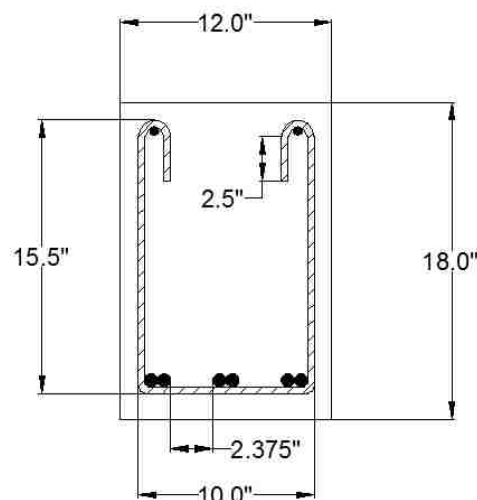
Figure 4.7 Schematic of Beam Splice Specimen Profile
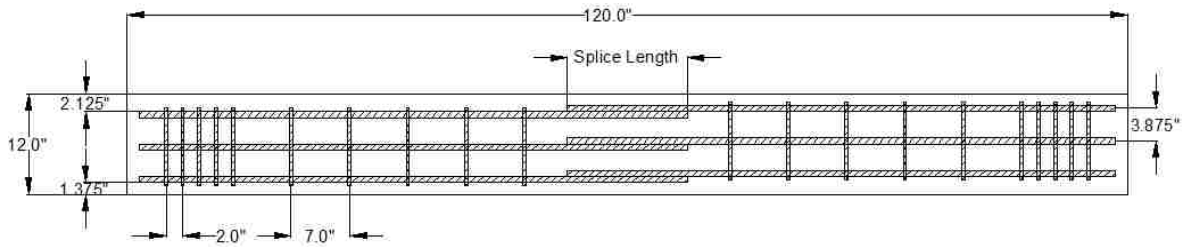
Figure 4.8 Schematic of Beam Splice Specimen Plan

4.4.2   Beam Splice Specimen Fabrication. The reinforcing bars were sectioned and bent to the appropriate lengths. Before the cages were assembled, a wire brush was used to clear the rust and mill scale at the ends of the longitudinal bars that were to be spliced. This was done to reduce test variability by reducing the influence of the rust and mill scale on the bond performance. Saw-horses were then used to lay out the bottom reinforcement. Stirrups were placed along the longitudinal bars at the appropriate locations and the top bars were laid in the stirrup hooks. Levels were used to ensure that the stirrups were plumb with the longitudinal reinforcement, and then wire ties were used to connect every joint of the cages. To ensure appropriate concrete cover on the sides of the cages, two very short pieces of #8 (No. 25) bars, about 1in. (2.54 cm) in diameter, were tied to the outside to serve as spacers. Likewise, 1.5 in (3.81 cm) steel chairs were tied to the bottom of the cages in order to provide sufficient cover.

Upon completion of the steel cages, strain gauges were installed at both ends of the contact lap splice to measure strain in the steel during testing. Before the strain gages were attached to the steel, the location along the bar was prepared by grinding a smooth surface, cleaning the area with an acid, and then neutralizing the area. Figure 4.9 shows the spliced region with installed strain gauges, and Figure 4.10 shows the finished cages.

Figure 4.9 Spliced Length with Attached Strain Gauges

Figure 4.10 Completed Cage for Beam Splice Specimen

Steel-framed forms were used to construct the beam splice specimens. The walls of these forms were constructed of wood and were held together by steel wedge bolts and wire ties. The forms measured 14ft. (4.27m) in length, but in order to reduce this length to the required 10ft. (3.05m) wood block-outs were constructed. After the forms were assembled, form release oil was applied to the walls of the forms to facilitate de-molding of the beams. The finished cages were then placed inside of the forms, and hooks were

welded onto the top bars to allow for ease of transportation of the beams after curing. Figure 4.11 shows the completed cages inside the concrete forms.

Figure 4.11 Steel Cages in Forms

The mix design was sent to the local Rolla Ready Mix plant, and the concrete was delivered to the lab. A small amount of the water was withheld from each mix design during delivery so that the water content could be slightly adjusted at the lab. Upon arrival of the truck, the slump of the concrete was performed in order to verify that the mix was correct prior to the addition of the chemical admixtures. Once this check was performed, the air entraining dose and high range water reducer were added along with the additional water required to bring the water-to-cement ratio up to the required mix design. The concrete was allowed to mix at higher speed to produce the desired mix. Once this mixing was complete, the slump and air content were measured to ensure the mix behaved as anticipated. Once this was verified, fresh concrete was placed into an overhead crane bucket which was used to fill the concrete forms. The filling of the forms is shown in Figure 4.12. Simultaneously, a wheelbarrow was filled with fresh concrete and used to cast the companion splitting tensile and compression cylinders.

Figure 4.12 Casting of Beam Splice Specimens

The concrete was consolidated in layers in the beam forms. Once the forms were filled, wood blocks were used to screed the surface of the beams. Finishing towels were then used to smooth and level the beam top surface. Care was taken to avoid damage to the strain gauge wires that extended from the middle edge of the concrete beams.

The following day, the beams were removed from the forms after a compression test confirmed that the concrete had developed sufficient strength to be lifted after 24 hours. Before the day of testing, the beams were prepared by lines being drawn at the locations of the supports and load points. Additionally, an aluminum angle was anchored into the concrete on the side of the beam at the midspan so that the deflection there could be monitored.

4.4.3   Beam Splice Specimen Test Set-Up. Third-point loading was used in order to create a constant, maximum moment in the middle third of the beam, helping to induce bond failure at the splice location at midspan. Figure 4.13 shows a schematic of the third-point loading condition used to test the beam splice specimens. Through the use of jacks and wheeled-platforms, the beam was position onto roller supports beneath two 140 kip-capacity (623kN) hydraulic actuators in the load test frame shown below in Figure 4.14. Care was taken to ensure that the beam was positioned along the center line

of the test frame. Spreader beams were used to transfer the applied load from the actuators to the concrete test beam. Rollers were placed on top of the beam at the location of the third points. Well-sorted masonry sand was placed beneath these rollers and leveled to prevent any roughness along the top of the concrete beam from causing gaps beneath the base of the rollers. The actuators were lowered, and the bottom spreader beam was lined up along the center of the test specimen through the use of levels and T-squares. A 4 ft. (1.22 m) long mirror was kept nearby so that the rupture at the bottom of the beam could be safely inspected upon failure.

The LVDT was attached to a stand next to the beam. The pin of the LVDT was placed on the aluminum angle that had been previously anchored at the midspan of the beam so that midspan deflection could be measured and recorded. This set-up is shown in Figure 4.15. The LVDT along with all six strain gauges were connected to data acquisition channels.
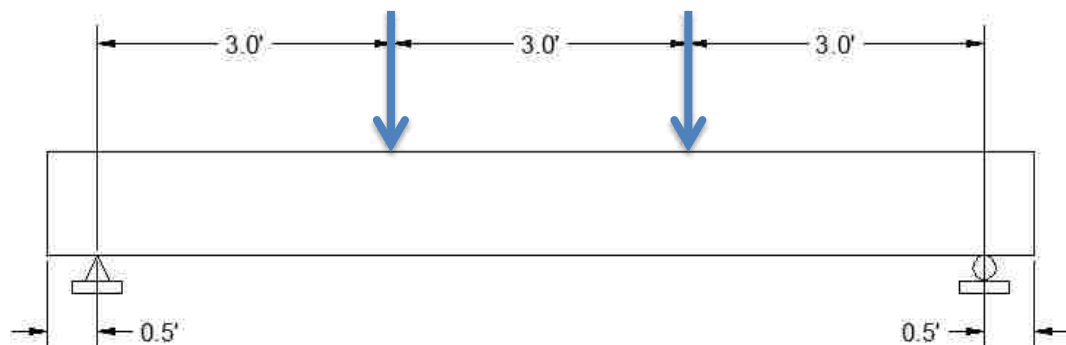
Figure 4.13 Schematic of Beam Splice Loading

Figure 4.14 Beam Splice Specimens in Testing Load Frame

Figure 4.15 LVDT Set-Up for Beam Splice Test

4.4.4 Beam Splice Specimen Test Procedure. The data acquisition system was initiated to record data from the strain gauges and LVDT as well as the applied load from the actuators. The test was performed on a displacement-controlled basis; the load was applied in a series of loading steps where each step corresponded to a midspan deflection of 0.02 in. (0.05 cm). After each applied step, the crack patterns were traced in order to track the crack propagation.

The beam was loaded until failure occurred. This bond failure was marked by a very sudden rupture in the concrete along the bottom of the beam in the spliced region. Often, pieces of the concrete cover in the spliced region fell from the beam. This rupture was accompanied by a rapid and drastic drop-off in the load and increase in midspan deflection. Once this failure occurred, testing was completed and data collection was terminated.

5. TEST RESULTS AND EVALUATIONS

5.1 RAC DIRECT PULL-OUT TEST RESULTS

The direct pull-out specimens were constructed to provide a relative measure of performance among the three mix designs. Both RCA mix designs were compared with the MoDOT Class B control mix. For this experimental program, a total of 18 pull-out specimens were tested. To investigate the effect of bar size on the relative bond performance, three specimens were constructed with #4 (No. 13) bars and three with #6 (No. 19) bars for each mix design. The testing matrix is shown below in Table 5.1.

Table 5.1 Testing Matrix for Direct Pull-Out Specimens

Mix	Reinforcing Bar Size	Number of Specimens
VAC	#4 (No. 13)	3
	#6 (No. 19)	3
RAC-50	#4 (No. 13)	3
	#6 (No. 19)	3
RAC-100	#4 (No. 13)	3
	#6 (No. 19)	3

Throughout the testing of these specimens, the slip of the bar and the applied load were recorded. When all testing was completed, the maximum applied load was determined for each pull-out specimen, and an average maximum value was found. The maximum bond stress was found by dividing the peak load carried by the bonded surface area of the bar. Table 5.2 shows the results from the testing. Within each of the specimen names, VAC represents virgin aggregate concrete (the control), RAC50 represents recycled aggregate concrete designed with 50% RCA replacement, and RAC100 represents recycled aggregate concrete designed with 100% RCA replacement. The letters PO signify that these were pull-out specimens, and the number 4 or 6 indicates what bar size was used in the specimen. The final number in the specimen name indicates which of the three tests that specimen was identified as.

The coefficient of variation (COV) of each set of data is also given in Table 5.2. For each test set, the variation is relatively low; the maximum within all of the collected test data is 7.3%. These low COV values indicate consistency in the results and reliability in the test as a measure of relative bond performance. Plots of the peak bond stresses for VAC, RAC-50, and RAC-100 specimens are shown in Figures 5.1, 5.2, and 5.3, respectively.

Table 5.2 Pull-Out Test Results

Mix	Bar Size	Specimen	Max. Applied Load (lb)	Bond Stress (psi)	Average Bond Stress (psi)	Bond Stress COV
VAC	#4(No. 13)	VAC-PO4-1	10344	2634	2730	5.3%
		VAC-PO4-2	10435	2657		
		VAC-PO4-3	11379	2898		
	#6 (No. 19)	VAC-PO6-1	27172	3075	2965	3.3%
		VAC-PO6-2	25869	2928		
		VAC-PO6-3	25563	2893		
RAC-50	#4(No. 13)	RAC50-PO4-1	12760	3249	3183	6.0%
		RAC50-PO4-2	13083	3332		
		RAC50-PO4-3	11657	2968		
	#6 (No. 19)	RAC50-PO6-1	31109	3521	3432	5.4%
		RAC50-PO6-2	28430	3218		
		RAC50-PO6-3	31440	3558		
RAC-100	#4(No. 13)	RAC100-PO4-1	13968	3557	3281	7.3%
		RAC100-PO4-2	12236	3116		
		RAC100-PO4-3	12451	3171		
	#6 (No. 19)	RAC100-PO6-1	30302	3429	3384	1.2%
		RAC100-PO6-2	29597	3350		
		RAC100-PO6-3	29804	3373		

Conversion: 1 lb. = 4.45 N
Conversion: 1 psi = 6.9 kPa
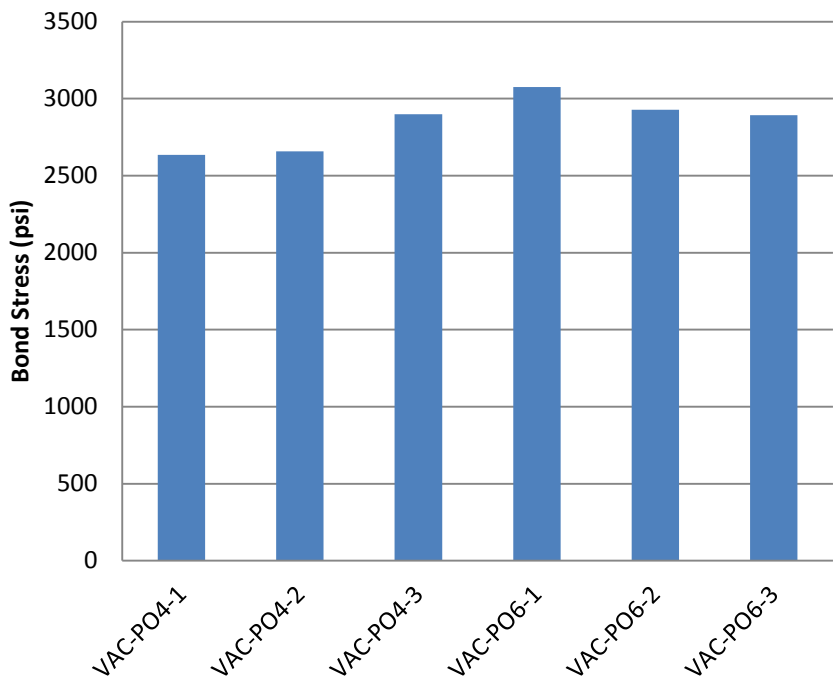
Figure 5.1 Peak Bond Stresses for VAC Pull-Out Specimens
Conversion: 1 psi = 6.9 kPa
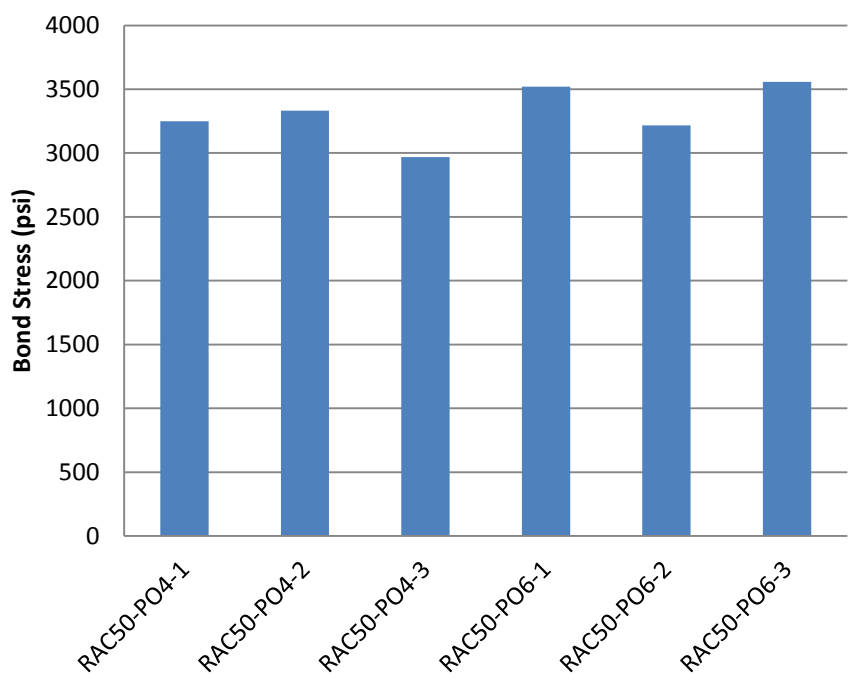
Figure 5.2 Peak Bond Stresses for RAC-50 Pull-Out Specimens
Conversion: 1 psi = 6.9 kPa
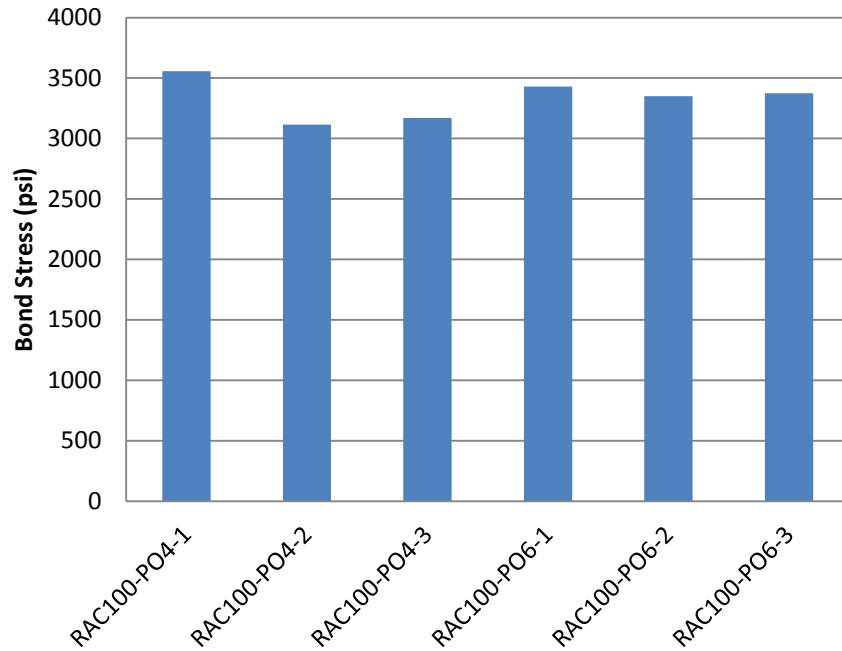
Figure 5.3 Peak Bond Stresses for RAC-100 Pull-Out Specimens
Conversion: 1 psi = 6.9 kPa

For each tested specimen, the bar slip was plotted against the applied load. The plots for most of these specimens indicated that a pull-out failure did occur, as evidenced in the gradual shedding of load after the peak. A typical load-slip plot is shown in Figure 5.4 from specimen RAC50-PO4-2. The load-slip plots for all tested direct pull-out specimens are included in Appendix A.
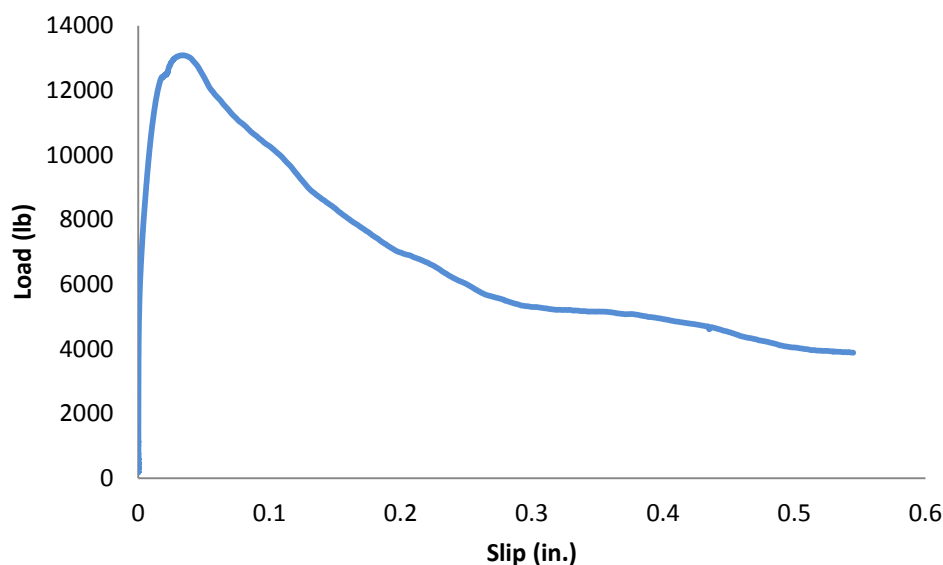
Figure 5.4 Typical Plot of Slip versus Applied Load
Conversion: 1 in. = 25.4 mm
1 lb. = 4.45 N

5.2 BEAM SPLICE TEST RESULTS

Beam splice specimens were included in this experimental program to provide a test method to evaluate bond performance under a realistic flexural stress-state response. Three beam splice specimens were constructed for each mix design in this study as shown in the test matrix in Table 5.3. Both RCA mixes were compared to the performance of the control specimens. The beams were all constructed with a splice in the longitudinal reinforcement located at midspan.

Throughout the testing of the beam splice specimens, the midspan deflection, applied total load, and strain in the steel were recorded. When all testing was complete, the maximum applied load (peak load) of each beam was determined. Additionally, the maximum strain in the steel was taken as the average of the maximum strains in each of the strain gauges. Then, using the modulus of elasticity of the steel as determined in the tension testing of the reinforcing bars, the average maximum stress in the steel was determined. This value was compared with the yield stress of the steel found in tension testing of the bars to ensure that the steel did not yield during beam splice testing. The experimentally determined yield stress of the steel was found to be 74.9ksi. Upon

comparing the maximum stress in the steel to the yield stress, it was observed that none of the specimens experienced steel yield prior to bond rupture failure.

Table 5.4 shows the results from the beam splice testing. Within each of the specimen names, VAC represents virgin aggregate concrete (the control), RAC50 represents recycled aggregate concrete designed with 50% RCA replacement, and RAC100 represents recycled aggregate concrete designed with 100% RCA replacement. The final number in the specimen name indicates which of the three tests that specimen was identified as. The coefficient of variation (COV) of both the peak load carried and the peak stress developed in the longitudinal reinforcement of each set of data is also given in Table 5.4. For each test set, the variation is relatively low; the maximum within all of the collected test data is 7.8%. These low COV values indicate consistency in the results and reliability in the test as a measure of bond performance. Plots of the maximum applied loads for VAC, RAC-50, and RAC-100 specimens are shown in Figures 5.5, 5.6, and 5.7, respectively. Likewise, plots of the maximum developed stresses for VAC, RAC-50, and RAC-100 specimens are shown in Figures 5.8, 5.9, and 5.10, respectively.

Table 5.3 Testing Matrix for Beam Splice Specimens

Mix	Bottom Reinforcement	Top Reinforcement	Number of Beams
Control	3 #6	2 #4	3
RAC-50	3 #6	2 #4	3
RAC-100	3 #6	2 #4	3

Table 5.4 Beam Splice Test Results

Mix	Specimen	Peak Load (kips)	Peak Load COV	Steel Stress at Failure (ksi)	Peak Stress COV
VAC	VAC-1	62.0		63.0	
	VAC-2	67.3	4.2%	70.8	7.6%
	VAC-3	65.9		61.6	
RAC-50	RAC50-1	54.4		56.5	
	RAC50-2	48.8	5.7%	55.2	1.7%
	RAC50-3	50.1		54.8	
RAC-100	RAC100-1	48.8		47.3	
	RAC100-2	50.7	7.3%	49.9	7.8%
	RAC100-3	56.1		55.1	

Conversion: 1 kip = 4.45 kN
Conversion: 1 ksi = 6.9 MPa
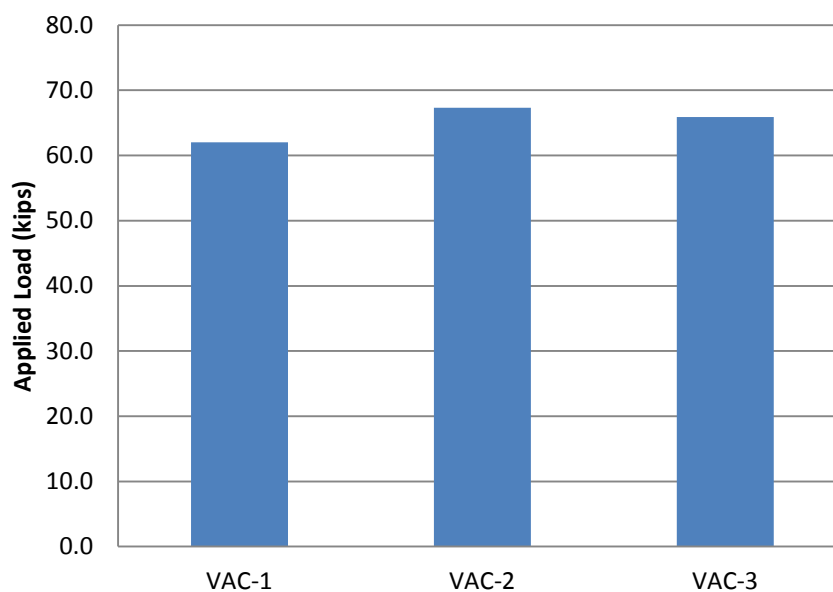
Figure 5.5 Peak Loads for VAC Beam Splice Specimens
Conversion: 1 kip = 4.45 kN
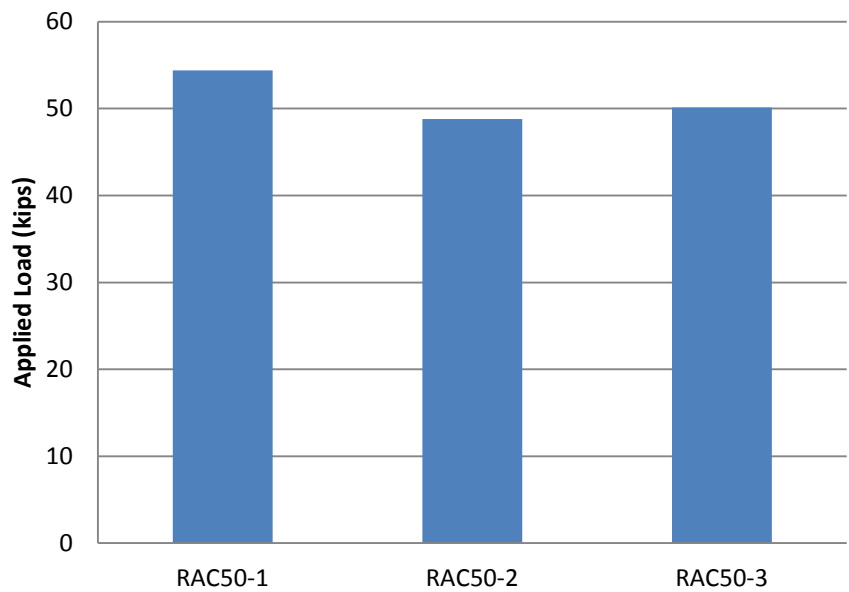
Figure 5.6 Peak Loads for RCA-50 Beam Splice Specimens
Conversion: 1 kip = 4.45 kN
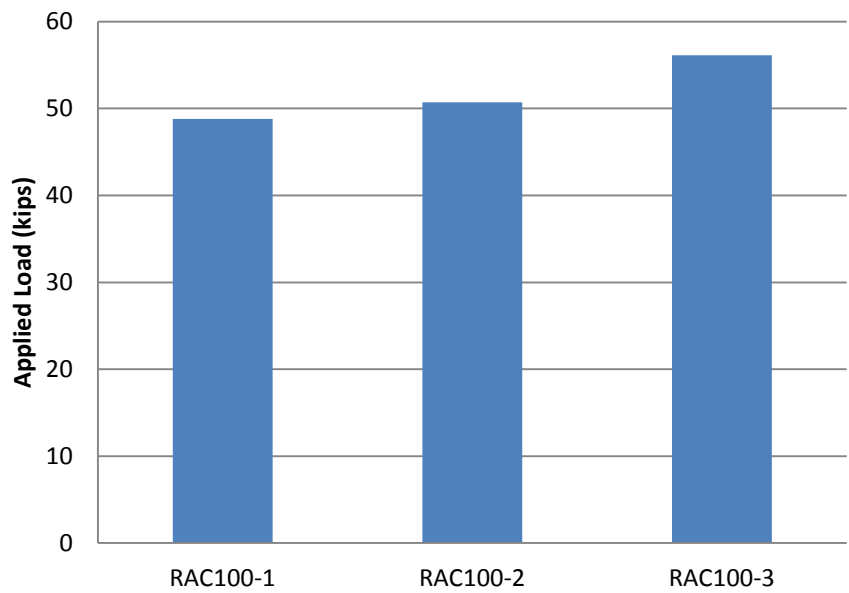
Figure 5.7 Peak Loads for RCA-100 Beam Splice Specimens
Conversion: 1 kip = 4.45 kN
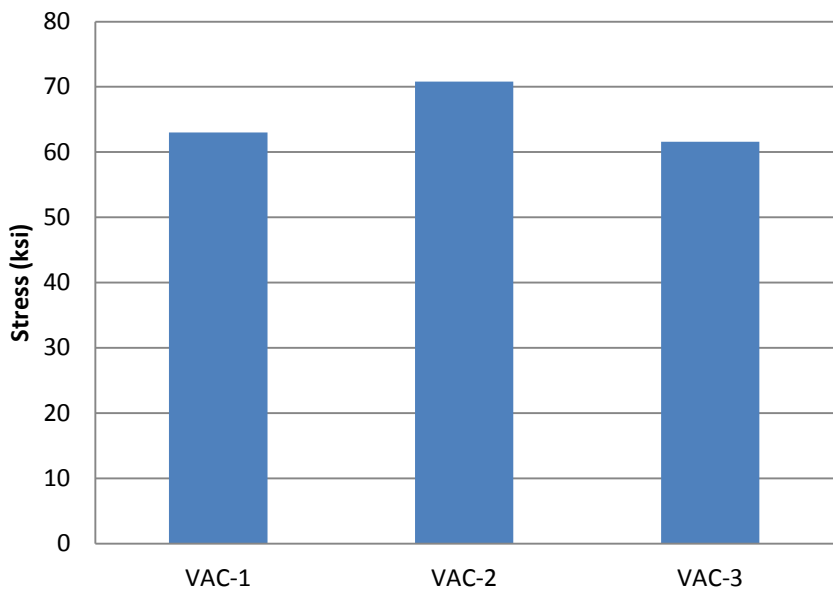
Figure 5.8 Peak Stresses for VCA Beam Splice Specimens
Conversion: 1 ksi = 6.9 MPa
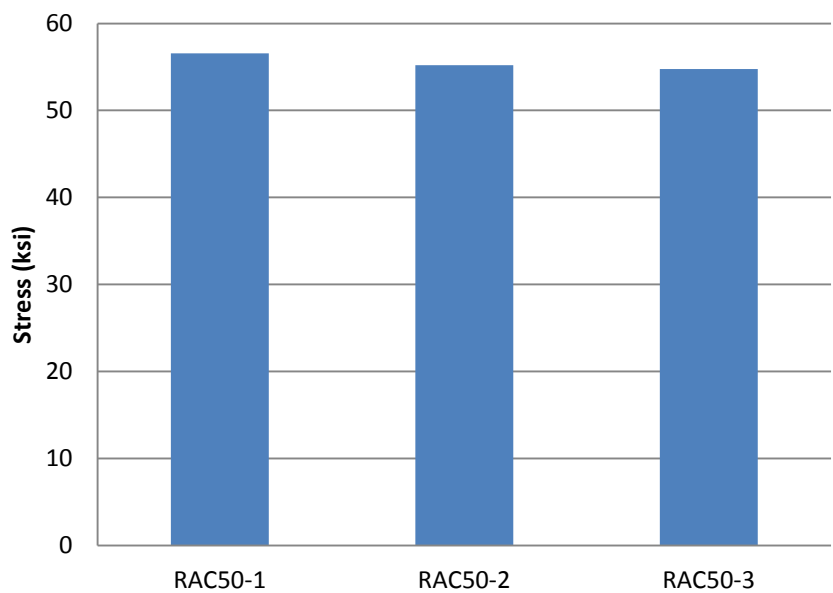
Figure 5.9 Peak Stresses for RCA-50 Beam Splice Specimens
Conversion: 1 ksi = 6.9 MPa
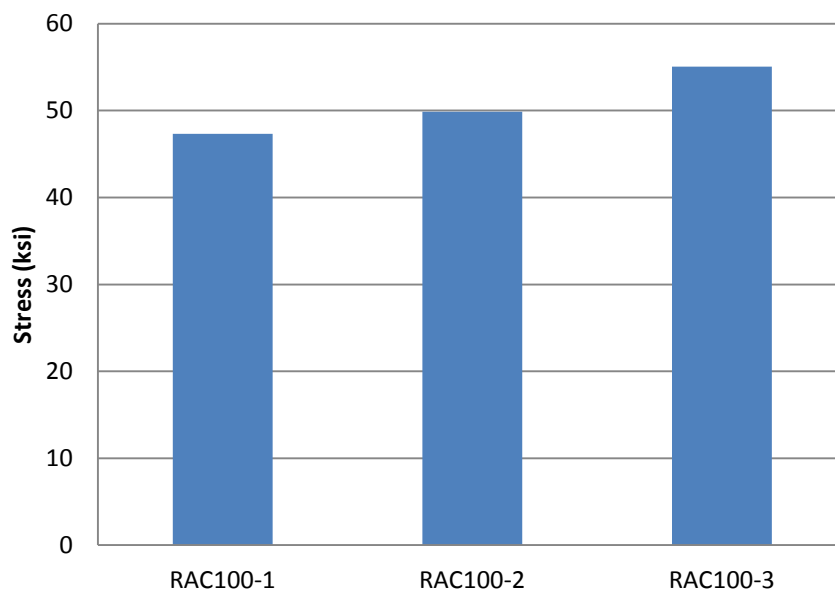
Figure 5.10 Peak Stresses for RCA-100 Beam Splice Specimens
Conversion: 1 ksi = 6.9 MPa

In order to better evaluate and compare the response of the beam splice specimens, the deflection and steel strain data were plotted against the total applied load for each beam. A typical plot of load versus deflection is shown in Figure 5.11, and a typical plot of load versus strain is shown in Figure 5.12. The plots shown are from specimen VAC-3. Both plots indicate that flexural cracking began to occur in specimen VAC-3 around 15kips (66.7kN), as evidenced by the change in slope of the plots at this load. From the constant linear-elastic nature of the load versus strain and load versus deflection plots of the specimens, it was again verified that the steel did not reach yield in any of the test specimens. The load versus deflection and load versus strain plots for each of the tested specimens are included in Appendix B.

At their failure loads, all specimens experienced a bond rupture type of failure. This failure type was indicated by the abrupt audible and visible signs of splitting crack development at the peak load. A typical crack pattern at failure is shown from specimen RAC50-1 in Figure 5.13. The corresponding bottom view at midspan of specimen RAC50-1 is shown in Figure 5.14. In both pictures, the splitting cracks at the spliced longitudinal reinforcement are evident. In some beam splice tests, the splitting cracks were so pronounced that the concrete cover within the spliced region spalled off of the

specimen. Images of crack patterns of all tested specimens at failure are shown in Appendix C.
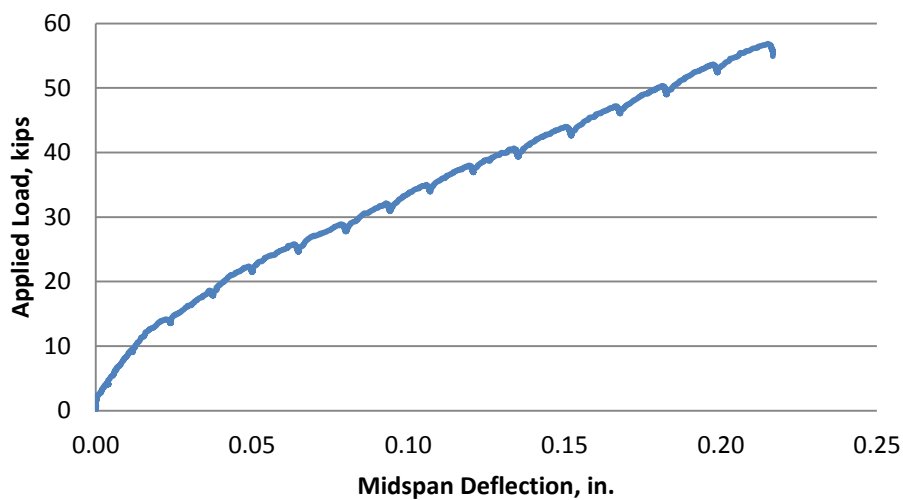
Figure 5.11 Typical Load versus Deflection Plot (VAC-3)
Conversion: 1 in. = 25.4 mm
1 kip = 4.45 kN
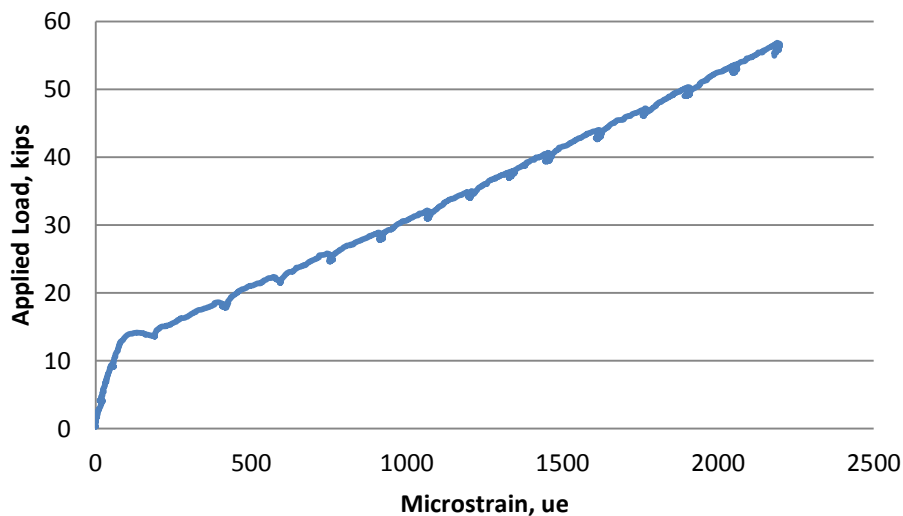
Figure 5.12 Typical Load versus Strain Plot (VAC-3)
Conversion: 1 kip = 4.45 kN

Figure 5.13 Beam Splice Crack Propagation at Failure (RAC50-1)

Figure 5.14 Beam Splice Specimen Bottom View at Failure (RAC50-1)

5.3 REINFORCING BAR TENSION TEST RESULTS

In order to determine the ultimate stress, yield stress, and modulus of elasticity of the reinforcing bars used in the beam splice specimens, tension tests were performed in accordance with ASTM E8-09 *Standard Test Methods for Tension Testing of Metallic Materials* (ASTM E9-09). This test was performed on three 30 in. (76.2 cm) lengths of #6 reinforcing bars. Each specimen was clamped at each end in a 200 kip (890kN)

capacity load frame and loaded until rupture. Throughout testing, both strain and load were recorded. For each specimen, the yield stress of the bar was determined from the 0.5% strain offset of the stress versus strain plot. The modulus of elasticity was also determined for each bar using both the 0.5% offset stress and strain value and the stress and strain value at 40% of the yield stress. Table 5.5 shows the results of the #6 reinforcing bar tension test.

Table 5.5 #6 Reinforcing Bar Tension Test Results

Specimen	Yield Stress (ksi)	Average Yield Stress (ksi)	Modulus of Elasticity (ksi)	Average Modulus of Elasticity (ksi)
1	74.84		28,114	
2	75.14	74.85	29,814	27,992
3	74.58		26,048	

Conversion: 1 ksi = 6.9 MPa

5.4 ANALYSIS OF RESULTS

5.4.1 Methodology. In order to directly compare the test results across mix designs, the data was normalized to account for the different test day strengths of the concrete. For the beam splice specimens, the data was also normalized to account for the design strength of the beams. Two different normalization techniques were used to compare the results. The first normalization technique was based on the development length equations provided in ACI 318-11 (ACI 318, 2011), shown in Equation 5.1, and AASHTO LRFD-07 (AASHTO, 2007), shown in Equation 5.2. Both development length equations are indirectly proportional to the square root of the concrete compressive strength. Thus, in order to normalize the results with varying compressive strengths, peak bond stresses in the direct pull-out tests were divided by the square root of the corresponding compressive strength as shown in Equation 5.3. Furthermore, to account for the different design strengths of the concrete used in developing the splice length of the beam splice specimens, the results from these tests were normalized by multiplying the peak stresses by the square root of the design concrete strength. Thus, the developed

stress in the steel was multiplied by the square root of the ratio of design strength to actual test-day strength as shown in Equation 5.4.

$$l_d = \left[\frac{3}{40} \frac{f_y}{\lambda \sqrt{f_c'}} \frac{\Psi_t \Psi_e \Psi_s}{\left(\frac{c_b + K_{tr}}{d_b} \right)} \right] * d_b \qquad \text{(Eq. 5.1)}$$

where, l_d = development length
           f_y = specified yield strength of reinforcement
           λ = lightweight concrete modification factor
           f_c' = specified compressive strength of concrete
           Ψ_t = reinforcement location modification factor
           Ψ_e = reinforcement coating modification factor
           Ψ_s = reinforcement size modification factor
           c_b = smallest of distance from center of a bar to nearest concrete surface or one-half the center-to-center bar spacing
           K_{tr} = transverse reinforcement index
           d_b = nominal diameter of the reinforcing bar

$$l_{db} = \frac{1.25 \, A_b \, f_y}{\sqrt{f_c'}} \geq 0.4 \, d_b \, f_y \qquad \text{(Eq. 5.2)}$$

where, l_{db} = tension development length
           A_b = area of the reinforcing bar
           f_y = specified yield strength of reinforcement
           f_c' = specified compressive strength of concrete
           d_b = the nominal diameter of the reinforcing bar

$$Normalized \; Stress = \frac{Failure \; Stress}{\sqrt{Test-Day \; Concrete \; Strength}} \qquad \text{(Eq. 5.3)}$$

$$Normalized \; Stress = Failure \; Stress * \sqrt{\frac{Design \; Concrete \; Strength}{Test-Day \; Concrete \; Strength}} \qquad \text{(Eq. 5.4)}$$

The second normalization technique is a fourth root normalization as recommended by ACI 408R (2003) and Zuo and Darwin (2000). Zuo and Darwin observed from a large international database of beam splice specimens that $f_c'^{1/4}$ best represents the effect of concrete strength on development and splice length. This observation was based on 171 beam specimens with bottom-cast bars not confined by

transverse reinforcement (Zuo and Darwin 2000). Using this relationship with bond strength and concrete compressive strength, the peak bond stresses of direct pull-out specimens were divided by the fourth root of the test-day concrete compressive strength as shown in Equation 5.5. Similarly, the peak stress developed in the beam splice specimens was normalized by the fourth root of the ratio of the design concrete compressive strength and the realized test-day strength as shown in Equation 5.6.

$$Normalized\ Stress = \frac{Failure\ Stress}{\sqrt[4]{Test-Day\ Concrete\ Strength}} \qquad (Eq.\ 5.5)$$

$$Normalized\ Stress = Failure\ Stress * \sqrt[4]{\frac{Design\ Concrete\ Strength}{Test-Day\ Concrete\ Strength}} \qquad (Eq.\ 5.6)$$

For the VAC control beam splice specimens, the design strength used was 4000 psi (27.58 MPa). For the RCA-50 and RCA-100 beam splice specimens, the design strength was 5500 psi (37.92 MPa). These design strengths were determined from trial batching of the mix designs prior to beam splice specimen construction. On test day, the actual concrete compressive strengths were determined from companion cylinder specimens, and the resulting values are shown in Tables 5.6.

Table 5.6 Beam Splice Test Day Compressive Strengths

Cylinder Break	VAC	RCA-50	RCA-100
1	4012	3666	4861
2	4166	3436	4750
3	3823	3571	4919
Average	**4000**	**3558**	**4843**
COV	4.3%	3.2%	1.8%

Conversion: 1 psi = 6.9 kPa

5.4.2 Analysis and Interpretation of Direct Pull-Out Results. The
normalized results from the direct pull-out tests are shown in Table 5.7 below. The table
shows the test-day compressive strength used to normalize the peak bond stress prior to
pull-out failure for each set of specimens. For the #4 (No. 13) specimens, the average
square root and fourth root normalized results for each RCA replacement level are shown
in Figures 5.15 and 5.16, respectively. For the #6 (No. 19) specimens, the average square
root and fourth root normalized results for each RCA replacement level are shown in
Figures 5.17 and 5.18, respectively. Boxplots indicating the spread of the data for each
normalization technique are shown in Figures 5.19 and 5.20 for the #4 (No.13) specimens
and Figures 5.21 and 5.22 for the #6 (No.19) specimens.

A comparison of the average square root normalized data for the #4 (No.13)
specimens indicates that there was essentially no change in peak bond stress between the
VAC and RAC-50 specimens. However, there was a 6.0% increase in the RAC-100 over
the VAC specimens. Using the average fourth root normalized data for the #4 (No.13)
specimens, there was a slight increase in peak bond stress between the control and both
RCA replacement levels. The bond stress increased 7.9% in RAC-50 specimens and
12.9% in the RAC-100 specimens.

A comparison of the average square root normalized data for the #6 (No.19)
specimens indicates that there was a 1% decrease in peak bond stress in the RAC-50
specimens over the controls. However, there was a very slight increase in peak bond
stress of 0.5% in the RAC-100 specimens over the VAC specimens. Using the average
fourth root normalized data for the #6 (No. 19) specimens, there was a slight increase in
peak bond stress between the control and both RCA replacement levels. In both RAC-50
and RAC-100 specimens, the average peak bond stress was 7.1% higher than the control.

A parametric statistical analysis was performed on the normalized peak bond
stresses between both RCA replacement levels and the control specimens for both
normalization techniques. A student's t-test between two-sample assuming unequal
variances and a 95% confidence interval was utilized. An analysis of the square root
normalized bond stresses in the #4 (No. 13) pull-out specimens showed that both the 50%
and 100% RCA specimens were statistically the same as the control #4 (No.13)
specimens. Likewise, an analysis of the fourth root normalized bond stresses in the #4

(No. 13) pull-out specimens showed that both the 50% and 100% RCA specimens were statistically the same as the control #4 (No.13) specimens. This analysis helps verify that the slight percent increase in bond stress was within the test variability. An analysis of the square root normalized bond stresses in the #6 (No. 19) pull-out specimens showed that both the 50% and 100% RCA specimens were statistically the same as the control #6 (No.13) specimens. Likewise, an analysis of the fourth root normalized bond stresses in the #6 (No. 13) pull-out specimens showed that the 50% RCA specimens were statistically the same as the control #6 (No.13) specimens. However, the student's t-test shows that the percent increase between the 100% RCA specimens and the controls is statistically significant.

Because the data sets were small, a non-parametric analysis was also performed to verify the student's t-test. The Mann-Whitney test was utilized to compare the normalized peak bond stresses between both RCA pull-out sets and the control set with a 95% confidence interval. Analyzing the square root normalized peak bond stresses, this test showed that there was no significant difference from the control in either the 50% RCA specimens or 100% RCA specimens for both #4 (No.13) and #6 (No.19) bars. Likewise, analyzing the fourth root normalized peak bond stresses, this test showed that there was no significant difference from the control in either the 50% RCA specimens or 100% RCA specimens for both #4 (No.13) and #6 (No.19) bars. This analysis reveals that while there was a slight increase in peak bond stress, this increase was not significantly large. A summary of these statistical analyses are provided in Appendix D.

Table 5.7 Normalized Bond Stresses for Pull-Out Specimens

Mix	Bar Size	Specimen	Max. Applied Load (lb)	Bond Stress (psi)	Test Day Strength (psi)	Normalized Bond Stress (Square Root)	Average of Normalized Bond Stress (Square Root)	Normalized Bond Stress (Fourth Root)	Average of Normalized Bond Stress (Fourth Root)
VAC	#4 (No. 13)	VAC-PO4-1	10344	2634	4000	42	43	331	343
		VAC-PO4-2	10435	2657		42		334	
		VAC-PO4-3	11379	2898		46		364	
	#6 (No. 19)	VAC-PO6-1	27172	3075		49	47	387	373
		VAC-PO6-2	25869	2928		46		368	
		VAC-PO6-3	25563	2893		46		364	
RAC-50	#4 (No. 13)	RAC50-PO4-1	12760	3249	5460	44	43	378	370
		RAC50-PO4-2	13083	3332		45		388	
		RAC50-PO4-3	11657	2968		40		345	
	#6 (No. 19)	RAC50-PO6-1	31109	3521		48	46	410	399
		RAC50-PO6-2	28430	3218		44		374	
		RAC50-PO6-3	31440	3558		48		414	
RAC-100	#4 (No. 13)	RAC100-PO4-1	13968	3557	5147	50	46	420	387
		RAC100-PO4-2	12236	3116		43		368	
		RAC100-PO4-3	12451	3171		44		374	
	#6 (No. 19)	RAC100-PO6-1	30302	3429		48	47	405	400
		RAC100-PO6-2	29597	3350		47		395	
		RAC100-PO6-3	29804	3373		47		398	

Conversion: 1 psi = 6.9 kPa

Figure 5.15 Average #4 Pull-Out Bond Stresses by Square Root Normalization
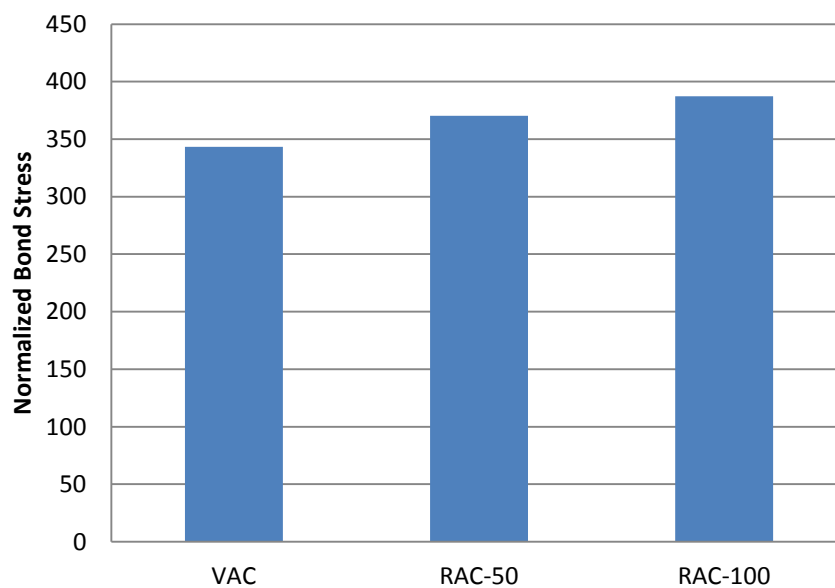
Figure 5.16 Average #4 Pull-Out Bond Stresses by Fourth Root Normalization
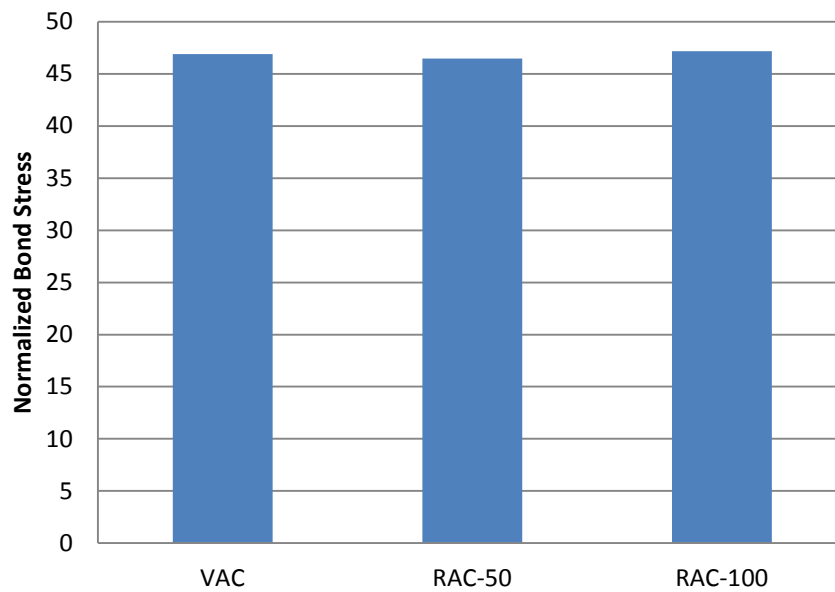
Figure 5.17 Average #6 Pull-Out Bond Stresses by Square Root Normalization
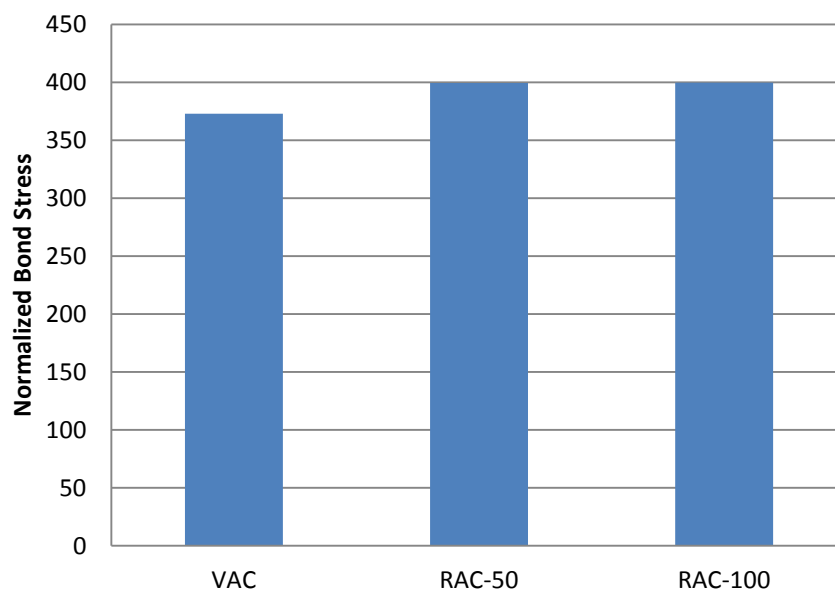
Figure 5.18 Average #6 Pull-Out Bond Stresses by Fourth Root Normalization

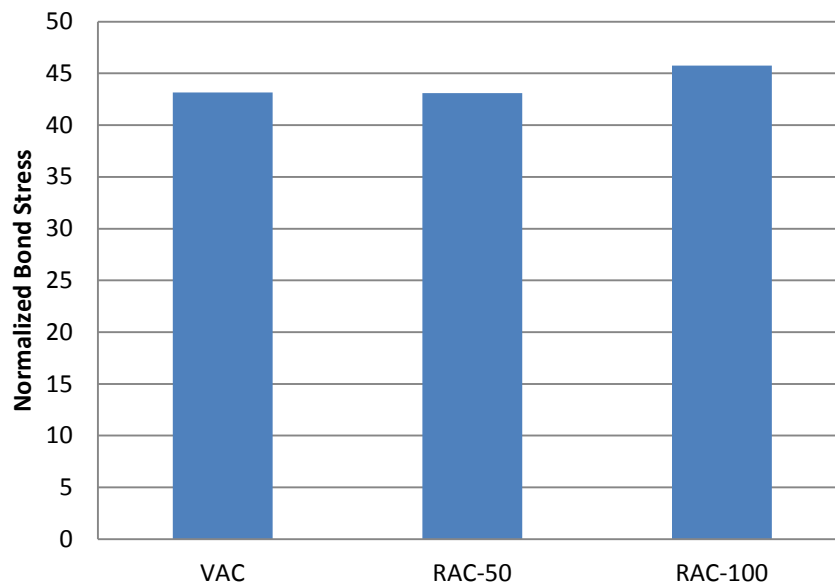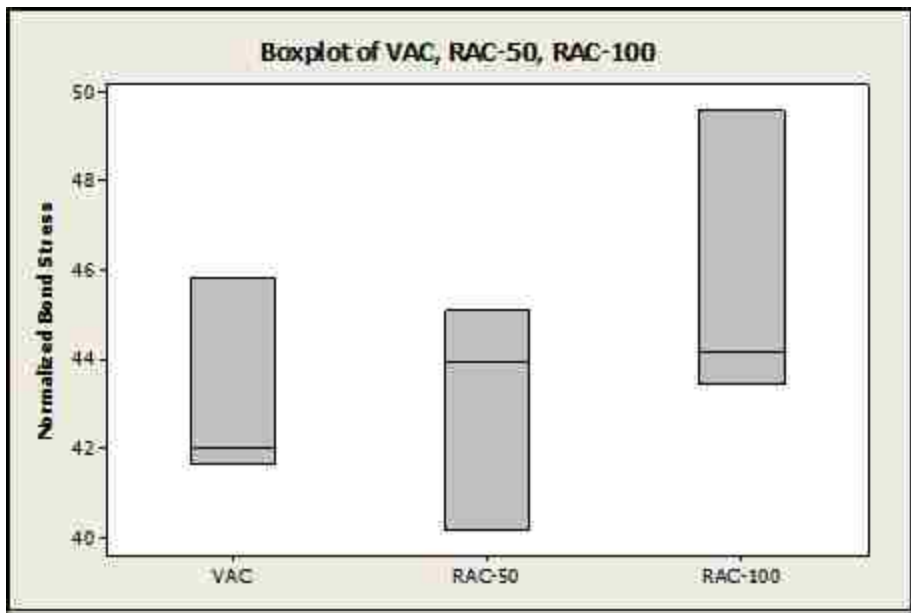**Figure 5.19 Boxplot of #4 Pull-Out Bond Stresses by Square Root Normalization**
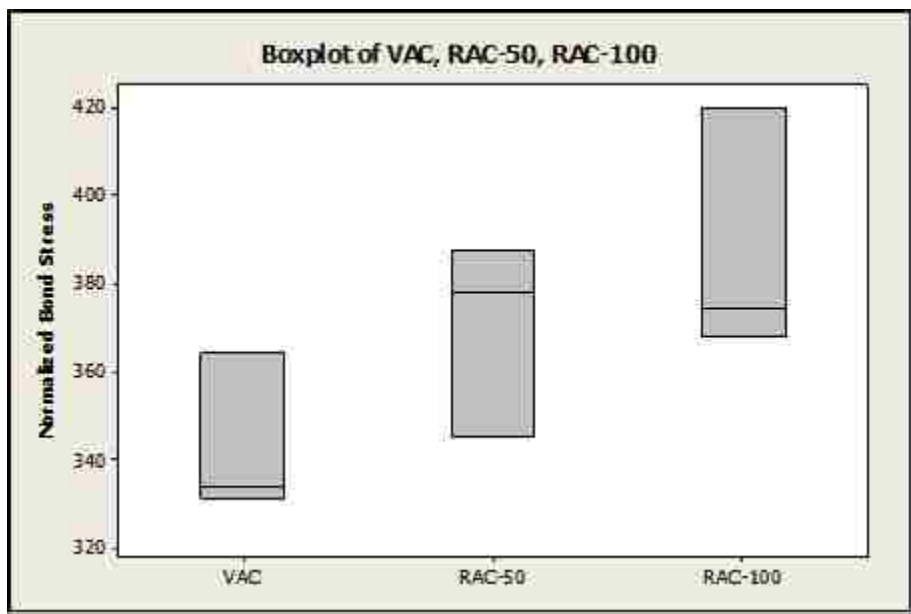
Figure 5.20 Boxplot of #4 Pull-Out Bond Stresses by Fourth Root Normalization
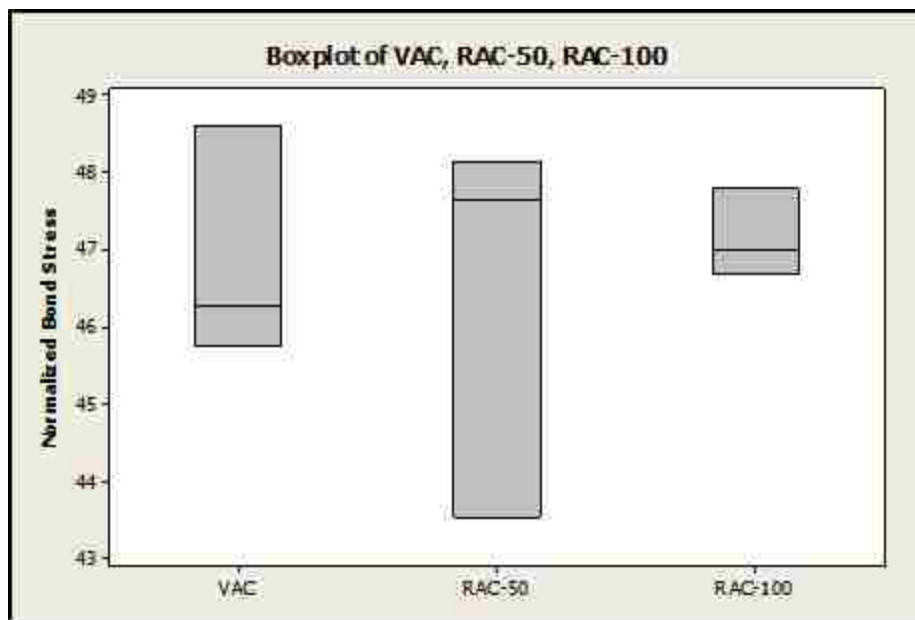
Figure 5.21 Boxplot of #6 Pull-Out Bond Stresses by Square Root Normalization
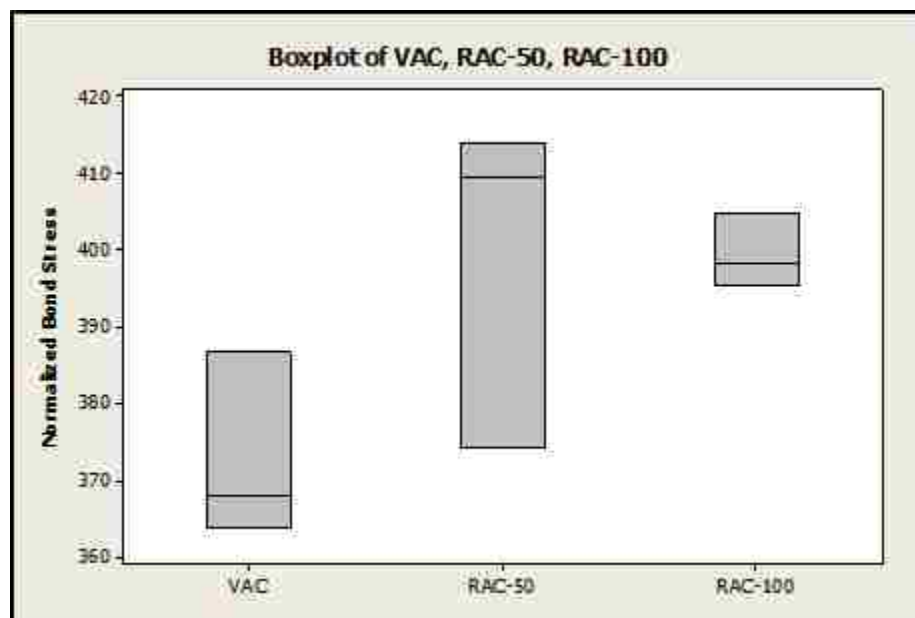
Figure 5.22 Boxplot of #6 Pull-Out Bond Stresses by Fourth Root Normalization

To evaluate the effect of bar size, the average normalized peak bond stresses were compared between the #4 (No. 13) and #6 (No. 19) specimens. In all RCA replacement levels, the #6 (No. 19) specimens exhibited higher bond stresses than the #4 (No. 13) specimens. However, as RCA replacement increases, the percent difference between decreased. The percent difference between #4 (No. 13) and #6 (No. 19) was 8.6%, 7.8%, and 3.1% for the VAC, RAC-50, and RAC-100, respectively. This comparison is shown in Figure 5.23 for the square root normalized bond stresses and in Figure 5.24 for the fourth root normalized bond stresses.
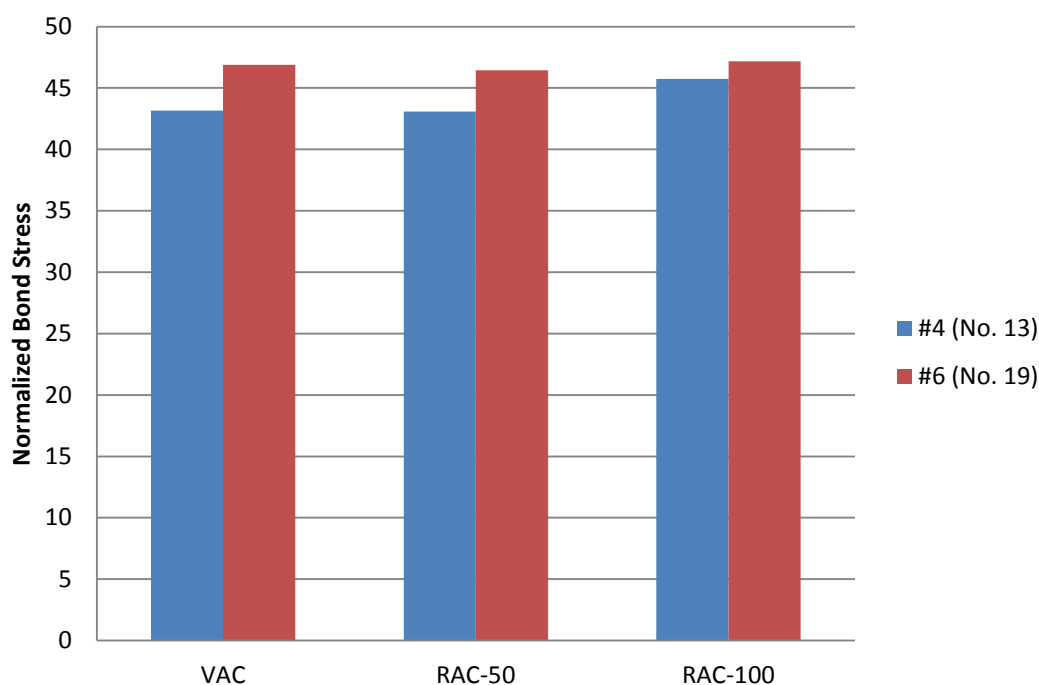
Figure 5.23 Comparison of #4 (No.13) and #6 (No. 19) square root normalized pull-out results
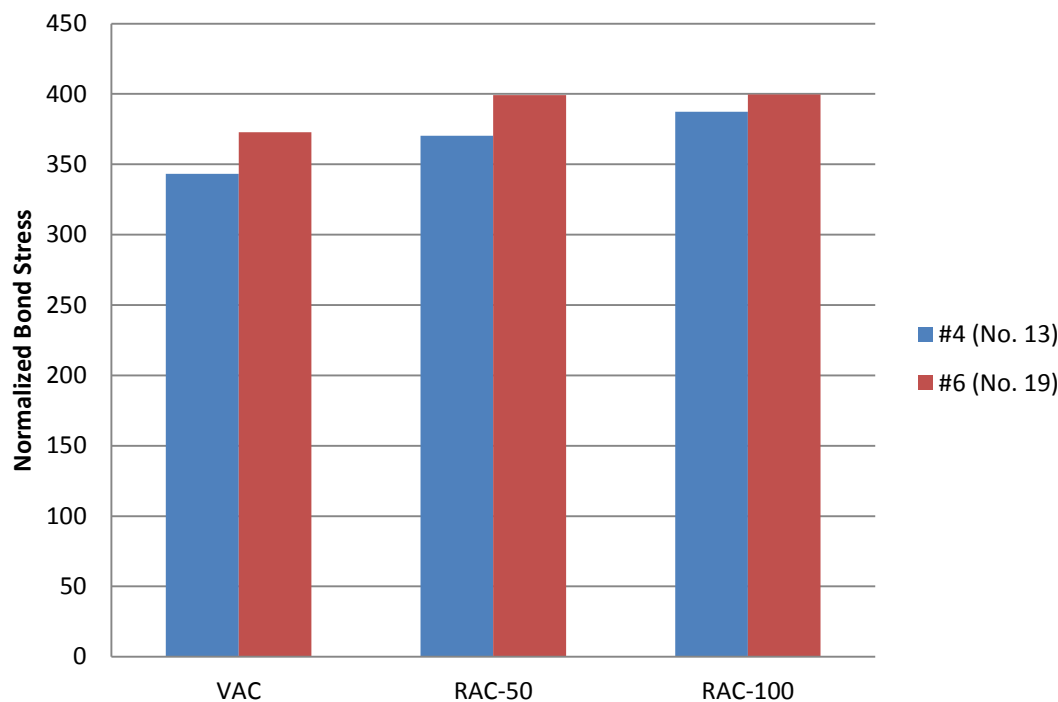
Figure 5.24 Comparison of #4 (No.13) and #6 (No. 19) fourth root normalized pull-out results

5.4.3   Analysis and Interpretation of Beam Splice Results. The normalized results from the beam splice tests are shown in Table 5.8. The table shows the test day compressive strength for each set of beams as well as the design strength of the beams. These values were used to normalize the peak stresses developed in the beams prior to bond rupture. The average square root normalized stresses for each set of beams are also plotted in Figure 5.25. A boxplot indicating the spread of the square root normalized beam splice results is provided in Figure 5.26. Likewise, the average fourth root normalized stresses for each set of beam are plotted in Figure 5.27, and a boxplot indicating the spread of the data is shown in Figure 5.28.

A comparison of the square root normalized results indicates that 50% RCA beams had a slight increase in developed stress in the steel of 5.9% over the VCA control. However, the 100% RCA beams had a decrease in stress of 16.9% over the VCA control. A comparison of the fourth root normalized results shows that generally, both RCA beam

sets had a lower stress in the steel. The 50% RCA beams decreased by 5.0%, and the 100% RCA beams decreased by 19.5%.

A parametric statistical analysis was performed on the normalized peak stresses between both RCA mix beams and the control beams for both normalization techniques. A student's t-test between two-sample assuming unequal variances and a 95% confidence interval was utilized. For the square root normalized results, the t-test showed that the 50% RCA beam results are statistically the same as the control beam results. However, the same student's t-test showed that the 100% RCA beam results are different from the control beams under square root normalization. This statistical analysis verifies that the slight percent increase between the 50% RCA beams and the control beams is well within the test variability, whereas the 100% RCA beams exhibited diminished bond strength over the control beams. For the fourth root normalization, the t-test likewise showed that the 50% RCA beam results are statistically the same as the control beam results, and the 100% RCA beam results are different from the control beams. This statistical analysis verifies that the percent difference between the 50% RCA beams and control beams is within the test variability, whereas the 100% RCA beams exhibited diminished bond strength over the control beams. A summary of this parametric statistical analysis is provided in Appendix D.

Given that the data set for each set of beams was small, a non-parametric statistical analysis was performed to validate the student's t-test. The Mann-Whitney test was utilized to compare the normalized peak stresses between both RCA beam sets and the control beam set with a 95% confidence interval. This test verified the results from the student's t-test that there was no difference between the 50% RCA and the control beams under both normalization techniques. However, the test showed that the difference between the 100% RCA and control beams under both normalization techniques was just barely insignificant. A summary of this non-parametric statistical analysis is provided in Appendix D.

Table 5.8 Normalized Developed Stresses for Beam Splice Specimens

Mix	Specimen	Design Strength (psi)	Test Day Strength (psi)	Peak Stress (ksi)	Square Root Normalized Stress (ksi)	Average of Square Root Normalized Stress (ksi)	Fourth Root Normalized Stress (ksi)	Average of Fourth Root Normalized Stress (ksi)
VAC	VAC-1	4000	4000	63.0	63.01	65.13	63.01	65.13
	VAC-2			70.8	70.79		70.79	
	VAC-3			61.6	61.58		61.58	
RAC-50	RAC50-1	5500	3560	56.5	70.28	68.98	63.04	61.87
	RAC50-2			55.2	68.61		61.54	
	RAC50-3			54.8	68.05		61.04	
RAC-100	RAC100-1	5500	4840	47.3	50.46	54.10	48.87	52.40
	RAC100-2			49.9	53.14		51.47	
	RAC100-3			55.1	58.69		56.85	

Conversion: 1 psi = 6.9 kPa
1 ksi = 6.9 MPa
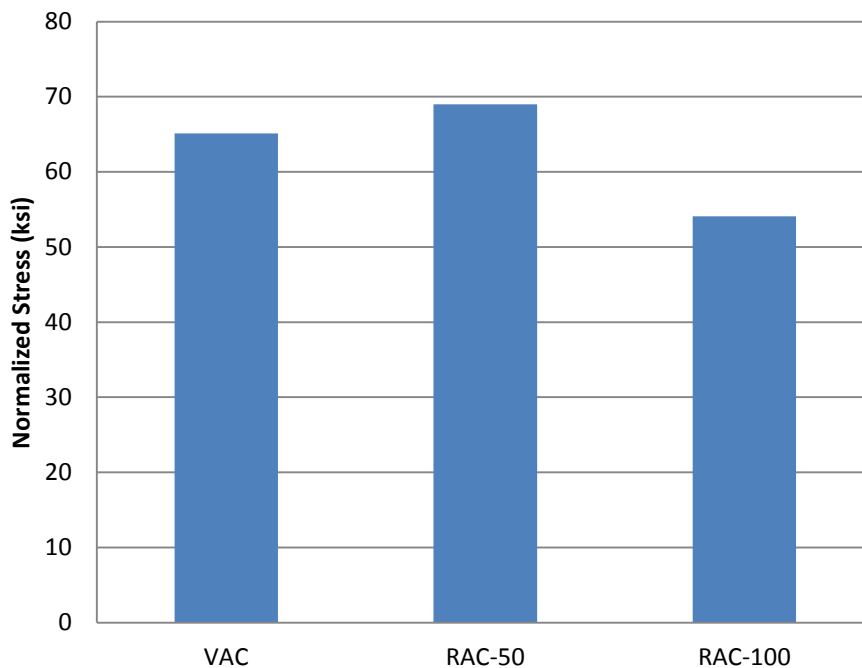
Figure 5.25 Average Beam Splice Peak Stresses by Square Root Normalization
Conversion: 1 ksi = 6.9 MPa
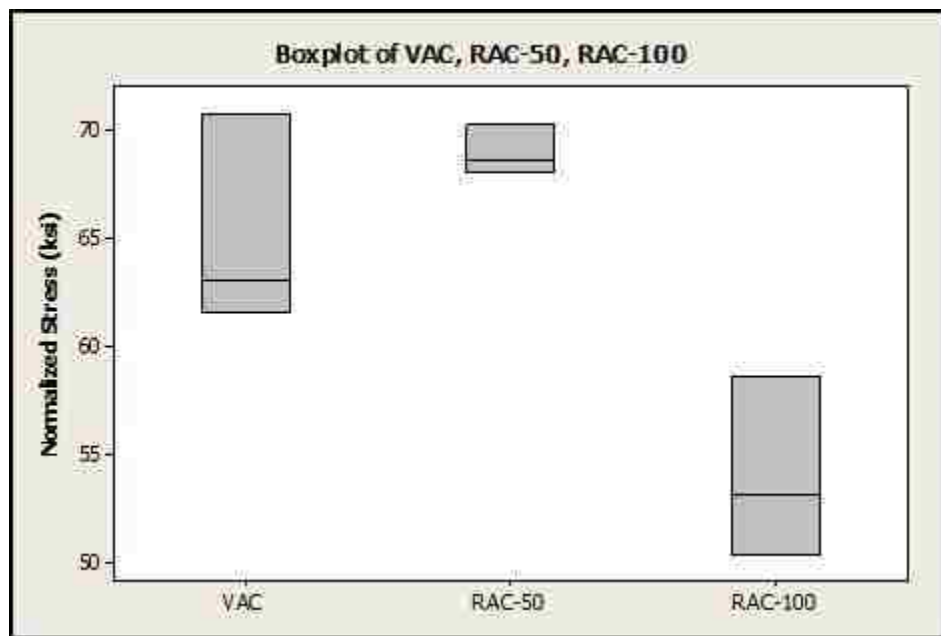
Figure 5.26 Boxplot of Peak Stresses by Square Root Normalization
Conversion: 1 ksi = 6.9 MPa
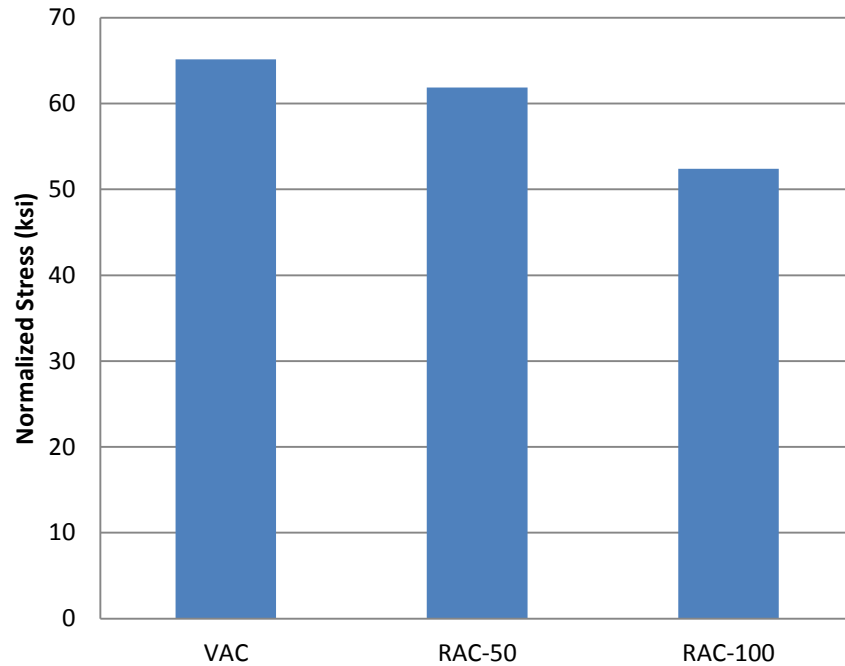
Figure 5.27 Average Beam Splice Peak Stresses by Fourth Root Normalization
Conversion: 1 ksi = 6.9 MPa
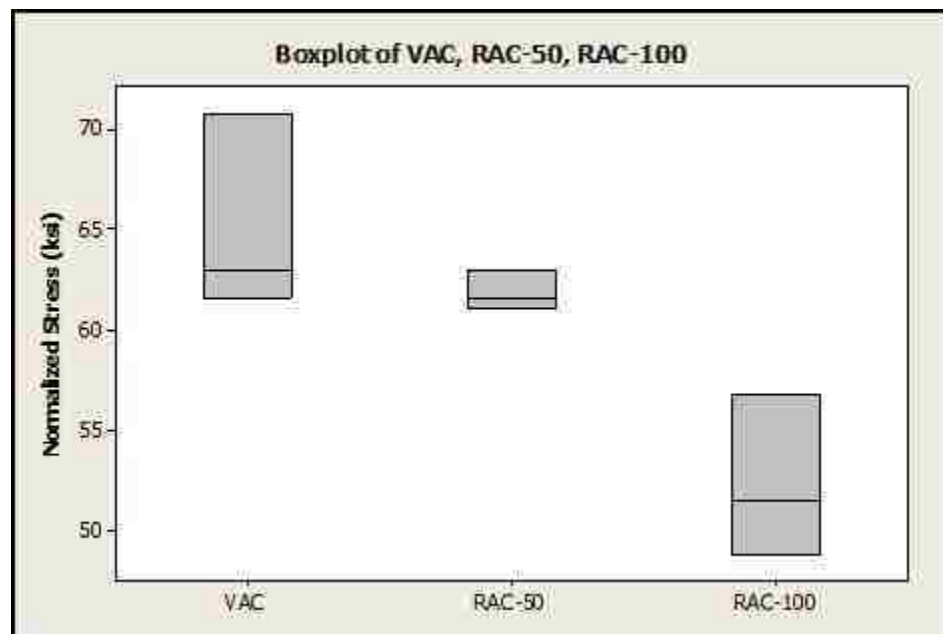
Figure 5.28 Boxplot of Peak Stresses by Fourth Root Normalization
Conversion: 1 ksi = 6.9 MPa

The stress developed in the longitudinal steel was compared to the theoretical values from moment-curvature calculations of the section. This was done in order to further evaluate the validity of the test results and to evaluate the applicability of stress-strain relationships to the 50% and 100% RCA mixes. To calculate the theoretical stress in the longitudinal reinforcement, the moment-curvature program *Response-2000* (Bentz and Collins 2000) was used to evaluate the section under the peak applied moment observed in the specimens. These applied moments were calculated from the average peak loads carried by the beams. Two different stress-strain models were used to describe the concrete. The first was Hognestad's stress-strain relationship, which is recommended by ACI 408R (2003). The second was Popovic, Thorenfeldt and Collins' stress-strain relationship. Table 5.9 shows the summary of measured and theoretically calculated stress values.

Table 5.9 also shows the ratio of measured to theoretically calculated stress. This ratio provides an indication of how well the measured values were predicted by the theoretical models. The theoretical values slightly underestimated the measured results, as indicated by the ratio values slightly over unity. Despite this small underestimation, the measured stresses were fairly accurately predicted. This analysis indicates that both Hognestad's stress-strain relationship as well as the Popovic, Thorenfeldt and Collins' stress-strain relationship for concrete may be acceptable for use with concrete containing up to 100% RCA replacement for coarse aggregates.

Table 5.9 Comparison of Measured to Theoretical Stress in Beam Splice Specimens
Table reports stress values in ksi
Conversion: 1 ksi = 6.9 MPa

Mix	Specimen	Measured[a]	Average Measured[a]	M-ϕ[b]	Average M-ϕ[b]	$f_{s(measured)}/f_{s(M-\phi)}$[b]	M-ϕ[c]	Average M-ϕ[c]	$f_{s(measured)}/f_{s(M-\phi)}$[c]
VAC	VAC-1	63.01		58.5			58.5		
	VAC-2	70.79	65.13	63.6	61.53	1.06	63.5	61.37	1.06
	VAC-3	61.58		62.5			62.1		
RAC-50	RAC50-1	56.54		51.7			51.5		
	RAC50-2	55.20	55.50	46.4	48.57	1.14	46.3	48.40	1.15
	RAC50-3	54.75		47.6			47.4		
RAC-100	RAC100-1	47.33		45.8			45.8		
	RAC100-2	49.85	50.75	47.5	48.60	1.04	47.6	49.17	1.03
	RAC100-3	55.06		52.5			54.1		

[a] Strain (average from strain gages) multiplied by modulus of elasticity

[b] Hognestad stress-strain model (ACI 408R-03 recommended method)

[c] Popovic, Thorenfeldt, & Collins stress-strain model

The beam splice results were compared to the bond strength prediction equations summarized in ACI 408R 2003. This was done in order to evaluate if the trend of decreasing bond strength with increasing replacement with RCA could be observed under the normalization techniques used in all of these formulae. Further, this analysis was performed to evaluate how closely RCA concrete bond behavior could be predicted by these equations developed for conventional concrete. The prediction ratios were calculated as the measured bond stress over the calculated bond stress. The measured stresses in the steel were normalized as per the technique adopted by each descriptive equation. These ratios are provided in Table 5.10. A graphical representation is provided in Figure 5.29.

As shown in Figure 5.29, the bond stress generally decreases as the amount of RCA increases. Furthermore, all equations underestimate the bond strength for both VAC and RAC-50 on average, whereas RAC-100 is not as conservatively predicted. The equation ACI 318 2011 for development and splice length of straight reinforcement in tension is based on the equations provided by Orangun, Jirsa, and Breen (1977). For all three levels of RCA replacement, their technique was the most conservative as it most underestimated average bond strengths.

Table 5.10 Prediction Ratios for Beam Splice Results

Specimen	Orangun, Jirsa, & Breen (1977)	Darwin et al. (1992)	Zuo & Darwin (2000)	Esfahani & Rangan (1998)	ACI 408 (2003)
VAC-1	1.40	1.34	1.33	1.27	1.31
VAC-2	1.57	1.50	1.49	1.43	1.48
VAC-3	1.37	1.31	1.30	1.24	1.28
Average	1.45	1.38	1.37	1.31	1.36
RAC50-1	1.49	1.36	1.34	1.29	1.33
RAC50-2	1.45	1.33	1.31	1.26	1.30
RAC50-3	1.44	1.32	1.30	1.25	1.29
Average	1.46	1.33	1.32	1.27	1.30
RAC100-1	1.07	1.05	1.04	0.99	1.03
RAC100-2	1.12	1.11	1.10	1.04	1.08
RAC100-3	1.24	1.23	1.21	1.15	1.20
Average	1.14	1.13	1.12	1.06	1.10
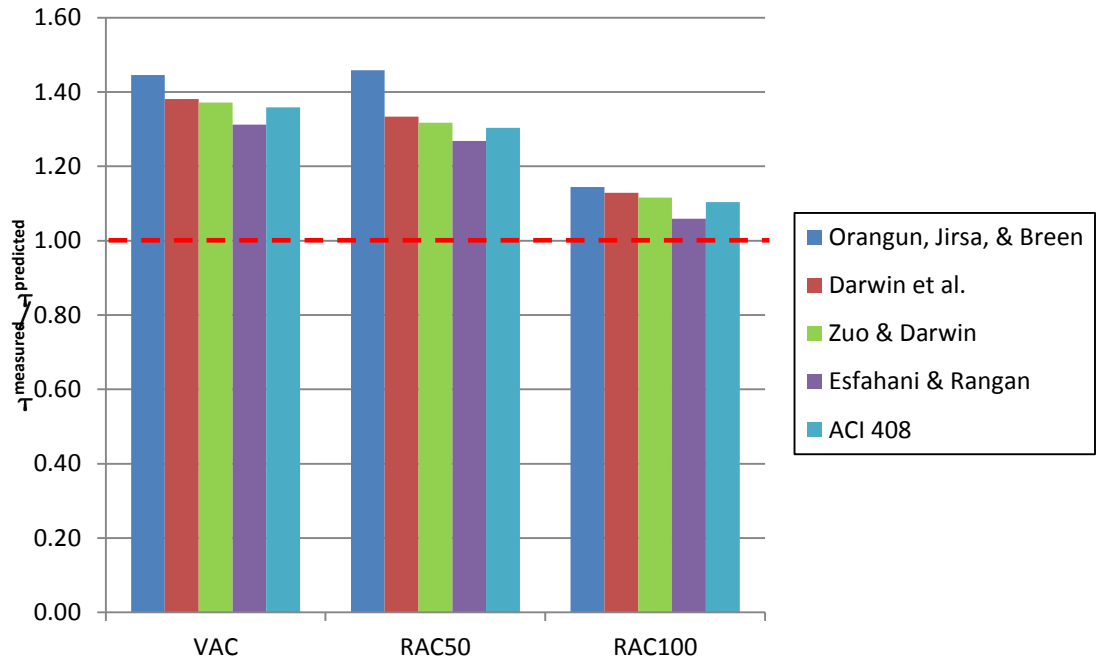
Figure 5.29 Comparison of Prediction Ratios for Beam Splice Results

The beam splice results were compared to the bond database 10-2001 provided by ACI Committee 408 (ACI 408R, 2003) in Figure 5.30. The plot below shows those beam splice tests results from similar bond specimens with bottom-cast bars and no transverse confinement in the spliced region. This comparison helps validate the test method from this study as falling within the range of data provided by previous bond researchers. For a given compressive strength of concrete, the beam splice results fit well within the scatter of the data. However, due to the large scatter of this historical bond data, it is difficult to draw a conclusion about the trend of bond strength with concrete compressive strength.
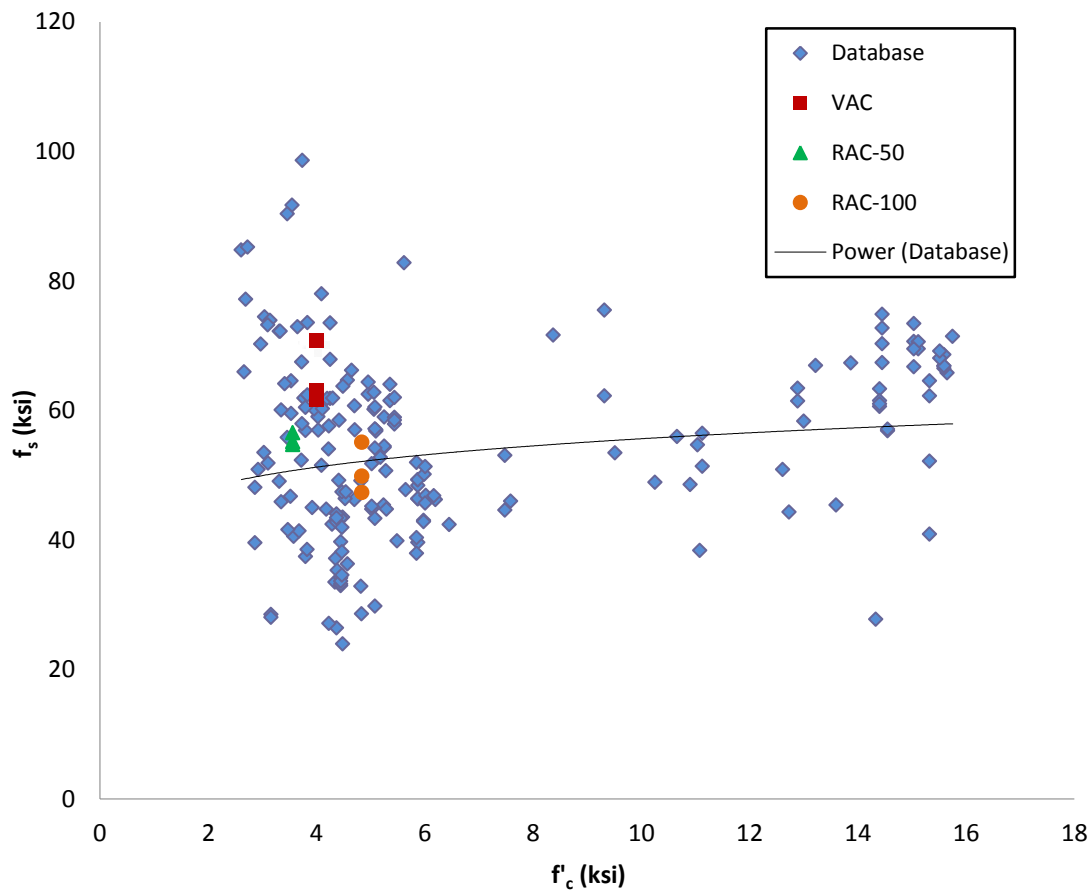
Figure 5.30 Comparison of Beam Splice Results to Database
Conversion: 1 ksi = 6.9 MPa

6. THEORETICAL ANALYSIS

6.1 BOND ACTION IN GENERAL

As previously mentioned, in reinforced concrete, the transfer of forces between deformed steel bars and the adjacent concrete occurs by three primary modes: 1) chemical adhesion between the bar and concrete, 2) friction forces, transverse forces, and relative slip, and 3) bearing of the ribs or deformations against the surrounding concrete, or mechanical interaction between the concrete and the steel. For deformed steel bars, bond stress is primarily transferred through this mechanical interaction. Lutz and Gergeley (1967) showed that ribs with a face angle between 40 and 90 degrees have a sufficient amount of friction between the rib face and surrounding concrete to prevent relative movement at this interface. This feature means that the mechanical action of the deformed bars occurs primarily through crushing of the concrete in front of the ribs and not through wedging action between the ribs. The crushed concrete at the face of the ribs results in effective face angles of between 30 and 40 degrees.

When the bond forces act at an angle α between the concrete and the bar axis, the bond forces can be resolved into both radial and tangential components. The bond stress in the tangential direction is expressed as change in steel stress over an infinitesimal length dx, and is defined as τ in Equation 6.1. The radial component of the bond stress is then defined as $\tau\tan\alpha$.

$$\tau = \frac{A_s}{\pi d_s} * \frac{d\sigma_s}{dx} \qquad \text{(Eq. 6.1)}$$

The radial component of the bond force induces tensile hoop stresses in the surrounding concrete cover as shown in Figure 6.1. This action essentially causes the concrete surrounding the deformed steel bar to behave like a thick-walled cylinder with a thickness equal to the minimum dimension of the concrete cover and an internal pressure equal to the radial bond stress, $\tau\tan\alpha$. When the tension rings are stressed to rupture, the cover splits, forming longitudinal cracks. Tepfers first described this bond action in three stages: uncracked elastic stage, partially cracked elastic stage, and plastic stage (1977).
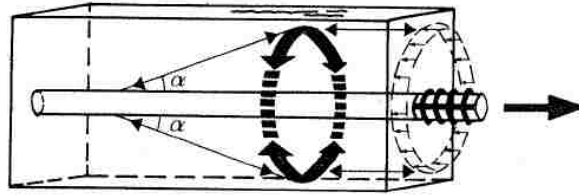
Figure 6.1 Schematic of Tensile Hoop Stresses Balancing Radial Stresses, (Tepfers 1977)

6.2 THREE STAGES OF BOND ACTION

     6.2.1 Uncracked Elastic Stage. In Tepfers (1977) analytical solution for the bond stresses, the geometry of the bar was considered as a smooth bar. The deformations appeared in the ultimate magnitude and slope of the bond stresses. He regarded the concrete surrounding the reinforcing bar as a thick-walled cylinder in order to calculate the hoop, σ_t, and radial, σ_r, stresses that developed in the concrete cover using Timoshenko's solution for the stresses in a thick-walled cylinder subjected to internal pressure, given by Equations 6.2 and 6.3 and as shown in Figure 6.2 (1956):

$$\sigma_t = \frac{P_i r_i^2}{r_o^2 - r_i^2}\left[1 + \frac{r_o^2}{r^2}\right] \qquad\qquad \text{(Eq. 6.2)}$$

$$\sigma_r = \frac{P_i r_i^2}{r_o^2 - r_i^2}\left[1 - \frac{r_o^2}{r^2}\right] \qquad\qquad \text{(Eq. 6.3)}$$
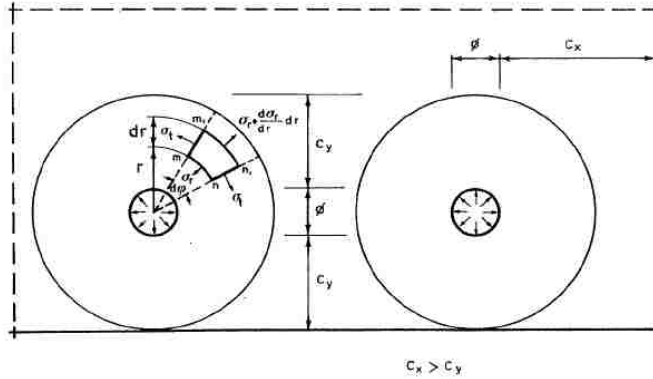
Figure 6.2 Idealized Concrete Cylinder with Minimum Concrete Cover as Maximum Dimension (Tepfers 1977)

P_i is internal pressure, r_i is the inside radius of the cylinder, and r_o is the outside radius of the cylinder. In the case of a reinforcing bar embedded in a concrete cylinder, P_i is the radial bond stress $\tau\tan\alpha$, r_i is the radius of the bar, $0.5*d_s$, and r_o is the smallest dimension for the concrete cover, c_y. Substituting these terms into the stress equations for a thick-walled cylinder gives Equations 6.4 and 6.5:

$$\sigma_t = \frac{\left(\frac{d_s}{2}\right)^2 \tau\tan\alpha}{\left(c_y+\frac{d_s}{2}\right)^2 - \left(\frac{d_s}{2}\right)^2}\left[1 + \frac{\left(c_y+\frac{d_s}{2}\right)^2}{r^2}\right] \qquad (Eq.\ 6.4)$$

$$\sigma_r = \frac{\left(\frac{d_s}{2}\right)^2 \tau\tan\alpha}{\left(c_y+\frac{d_s}{2}\right)^2 - \left(\frac{d_s}{2}\right)^2}\left[1 - \frac{\left(c_y+\frac{d_s}{2}\right)^2}{r^2}\right] \qquad (Eq.\ 6.5)$$

If the concrete cylinder behaves perfectly elastically, the ultimate load that the bonded bar can carry before the manifestation of longitudinal splitting cracks is when the maximum tension hoop stress exceeds the splitting tensile strength of the concrete, f_{tsp}. Inspection of the equation for hoop stress, σ_t, shows that the maximum tensile stress in the elastic uncracked stage will occur at the surface of the bar, $r = 0.5*d_s$. Substituting, the maximum tensile bond hoop stress at this stage is given by Equation 6.6.

$$\sigma_{t,max} = \frac{\tau\tan\alpha\left[\left(c_y+\frac{d_s}{2}\right)^2+\left(\frac{d_s}{2}\right)^2\right]}{\left(c_y+\frac{d_s}{2}\right)^2-\left(\frac{d_s}{2}\right)^2} \qquad \text{(Eq. 6.6)}$$

6.2.2 Uncracked Plastic Stage. If the concrete behaves perfectly plastically, bond rupture will not occur until the hoop stresses at every point in the model concrete cylinder reach the ultimate tensile strength of the concrete. In this case the highest possible bond stress can be achieved before longitudinal splitting cracks appear. The stress distribution across the cylinder is shown in Figure 6.3. Considering equilibrium, the hoop stress can be written as:

$$c_y\sigma_t = d_s\tau\tan\alpha$$

$$\sigma_t = \frac{d_s}{2c_y}\tau\tan\alpha \qquad \text{(Eq. 6.7)}$$
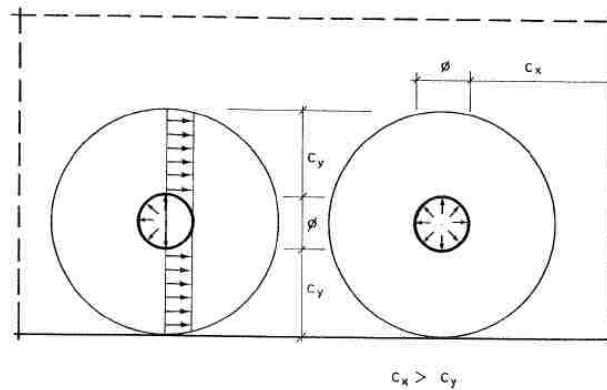
Figure 6.3 Stress Distribution at Plastic Stage (Tepfers 1977)

6.2.3 Partially Cracked Elastic Stage. If the concrete is considered to have no plasticity, an internal crack will first appear when the tensile hoop stress exceeds the splitting tensile strength of the concrete. However, the longitudinal splitting cracks through the concrete cover will not develop until the bond carrying capacity is reached. Thus, the concrete cylinder contains internal cracks where the hoop stresses have reached the ultimate tensile stress as shown in Figure 6.4. Now, the internal radial pressure,

τtanα, must be transferred through the cracked section of the concrete to the uncracked elastic concrete cylinder. This transformation is expressed as:

$$P_1 \pi d_s = P_2 \pi 2e$$

$$P_2 = \frac{d_s}{2e} \tau \tan\alpha \qquad \text{(Eq. 6. 8)}$$
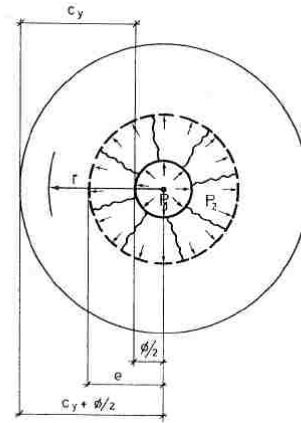
Figure 6.4 Stress Distribution at Partially Cracked Elastic Stage (Tepfers, 1977)

In the above equation, P_1 is the radial bond pressure due to the steel bar, τtanα, d_s is the reinforcing bar diameter, *e* is the radius to the depth of the internal cracks, and P_2 is the radial pressure at the crack depth. The corresponding hoop stress distribution can be expressed as:

$$\sigma_t = \frac{e^2 \frac{d_s}{2e} \tau \tan\alpha}{\left(c_y + \frac{d_s}{2}\right)^2 - e^2} \left[1 + \frac{\left(c_y + \frac{d_s}{2}\right)^2}{r^2}\right] \qquad \text{(Eq. 6.9)}$$

The maximum stress in the partially cracked elastic stage will occur at the interface between the cracked and uncracked concrete, at a depth *e*. Solving for the hoop stress at this location gives:

$$\sigma_{t,max} = \frac{d_s}{2e}\tau\tan\alpha\frac{\left(c_y+\frac{d_s}{2}\right)^2+e^2}{\left(c_y+\frac{d_s}{2}\right)^2-e^2} \qquad \text{(Eq. 6.10)}$$

Recognizing that $\sigma_{t,max}$ is f_{tsp}, this hoop stress can be rewritten as:

$$\frac{f_{tsp}}{\tau\tan\alpha} = \frac{d_s}{2e}\frac{\left(c_y+\frac{d_s}{2}\right)^2+e^2}{\left(c_y+\frac{d_s}{2}\right)^2-e^2} \qquad \text{(Eq. 6.11)}$$

$$where, \quad \frac{d_s}{2} \le e \le \left(c_y + \frac{d_s}{2}\right)$$

To find the optimum depth e which yields the maximum value for $f_{tsp}/\tau\tan\alpha$, the above equation is differentiated with respect to e. Equating this derivative to zero and solving for the roots of e, Tepfers showed that the only real root within the limits of the bar radius and concrete cover is:

$$e = 0.486\left(c_y + \frac{d_s}{2}\right) \qquad \text{(Eq. 6.12)}$$

Then the optimum crack depth, e-0.5*d_s can be written as:

$$e - \frac{d_s}{2} = 0.486\left(c_y + \frac{d_s}{2}\right) - \frac{d_s}{2} = 0.486c_y - 0.257d_s \qquad \text{(Eq. 6.13)}$$

Thus, the minimum concrete cover at which point the internal crack will immediately split through the cover can be expressed as:

$$0.486c_y - 0.257d_s = 0$$
$$c_y = 0.529d_s \qquad \text{(Eq. 6.14)}$$

Substituting the equation for optimum depth into the maximum tensile stress at the partially cracked elastic stage gives:

$$\sigma_{t,max} = \frac{1.664d_s\tau\tan\alpha}{\left(c_y+\frac{d_s}{2}\right)} \qquad \text{(Eq. 6.15)}$$

6.2.4   Comparison of the Three Stages.   Assuming that the angle α between the bond forces and the axis of the longitudinal reinforcing bar is the same at the elastic, plastic, and partially cracked elastic stages, the bond force carrying capacity is compared as a function of concrete cover in Figure 6.5.
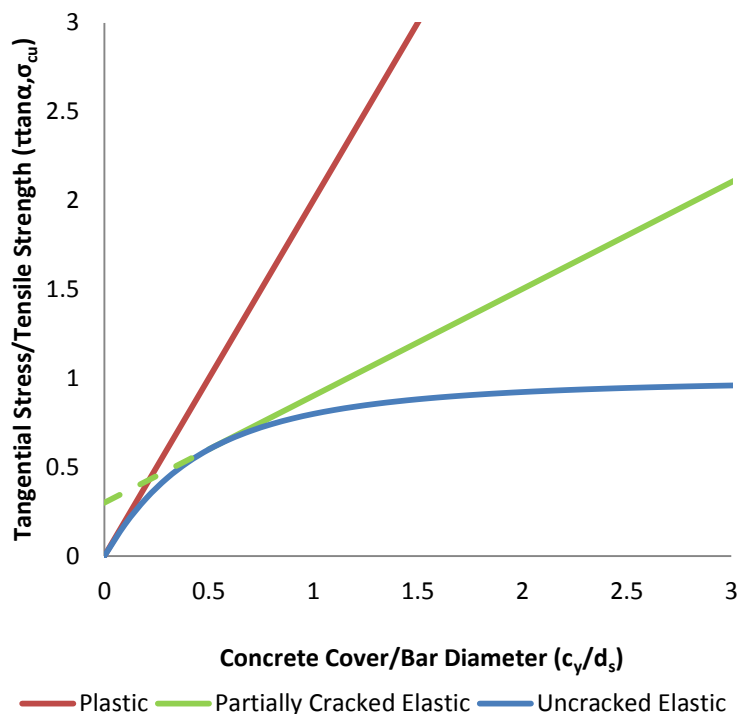
Figure 6.5 Plot of Bond-Carrying Capacity as a Function of Concrete Cover

In the uncracked elastic stage, ultimate load-carrying capacity occurs when the maximum tensile stress in the concrete ring exceeds the tensile strength of the concrete. This maximum tensile stress first appears at the inner surface of the concrete cylinder, or the reinforcing bar and concrete interface. In the plastic stage, tensile hoop stresses across the entire cylindrical section are allowed to reach the tensile strength of the concrete prior to the occurrence of ultimate load-carrying capacity. In the partially cracked elastic stage, the ultimate tensile hoop stress occurs when the bond force carrying capacity of the concrete cylinder is exhausted. It can be reasonably expected that the concrete will not behave perfectly plastically. Thus, this curve serves as an upper limit for the bond load-

carrying capacity. Because Tepfers' derivation for the partially cracked elastic stage did not consider the plastic deformations of the concrete, the load carrying-capacity is expected to be somewhat higher than predicted at this stage. Thus, a partially cracked elasto-plastic model is expected to plot between the plastic and partially cracked elastic stages.

6.3 SOFTENING BEHAVIOR OF CONCRETE

In the fracture mechanics approach, the stress-deformation curve for a uniaxial test of concrete is comprised of a strain part and a crack opening part as shown in Figure 6.6. In the strain part, there are both reversible and irreversible strains. However, the irreversible strains are small in comparison and are negligible. Thus the strain part can be described as purely linear elastic and the non-linearities are contained in the cracking of the concrete. Reinhardt (1984) proposed a simple power function to describe this behavior in Equation 6.16:

$$\frac{\sigma}{f_t} = 1 - \left(\frac{\delta}{\delta_o}\right)^k$$

$$\delta = \delta_o \left(1 - \frac{\sigma}{f_t}\right)^{\frac{1}{k}} \qquad \text{(Eq. 6.16)}$$
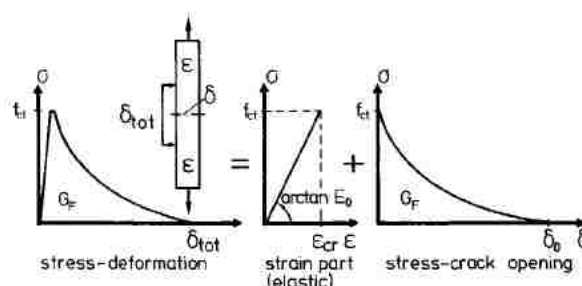
Figure 6.6 Stress-Deformation of Concrete Uniaxial Test in Two Parts (Reinhardt 1984)

In the above equation, k is a material constant, δ_o is the crack opening after which stress can no longer be transferred (also a material constant), and f_t is the tensile strength

of the concrete. The area under the complete stress-deformation curve is the total fracture energy, expressed as:

$$G_f = f_t \delta_o \frac{k}{1+k} \qquad \text{(Eq. 6.17)}$$

Van der Veen (1990) derived a simple model for describing the hoop stress distribution over the idealized thick-walled concrete cylinder that takes the concrete softening behavior after cracking into account as shown in Figure 6.7. His solution is described herein. Using Tepfers Equation 6.10 to describe the uncracked tangential stresses, he first considered the deformations in the cracked portion. Recognizing the total tangential deformation consists of an elastic part and the crack opening from n cracks, he derived the following expression:

$$\delta_{total} = \varepsilon_t 2\pi r + n\delta_o \left(1 - \frac{\sigma_t}{f_t}\right)^{\frac{1}{k}} \qquad \text{(Eq. 6.18)}$$
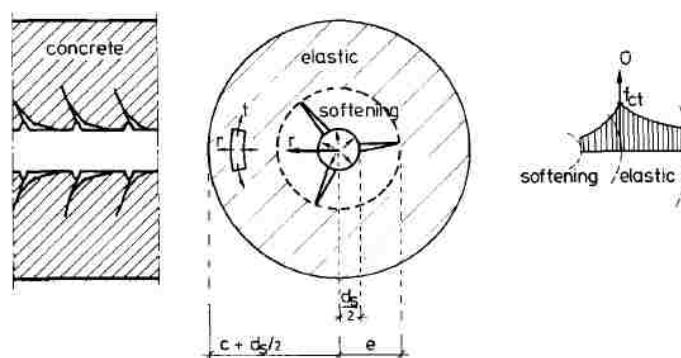
Figure 6.7 Softening Behavior of Internal Cracks (Van der Veen 1990)

At the interface between the cracked and uncracked portions, depth *e*, no cracks exist. In a one-dimensional approach (ignoring Poisson's effect) total tangential deformations reduce to Equation 6.19. Van der Veen showed that by using this one-dimensional approach, only 10% of the strain is neglected assuming perfect linear elastic behavior.

$$\varepsilon_t 2\pi e \approx \frac{f_t}{E_c} 2\pi e \qquad \text{(Eq. 6.19)}$$

Thus, at the depth e, the total tangential deformation is:

$$\delta_{total} = \frac{f_t}{E_c} 2\pi e = \varepsilon_{cr} 2\pi e \qquad \text{(Eq. 6.20)}$$

Where the concrete has reached its tensile strength, $\varepsilon_{cr} = f_t/E_c$. Van der Veen showed that for the tangential stress at the depth e to be sufficient to close the crack opening, or gap, Equations 6.18 and 6.20 must be equal, thus:

$$\varepsilon_t 2\pi r + n\delta_o \left(1 - \frac{\sigma}{f_t}\right)^{\frac{1}{k}} = \varepsilon_{cr} 2\pi e \qquad \text{(Eq. 6.21)}$$

Equation 6.21 can be rearranged to give a tangential stress equation at the uncracked portion equal to:

$$\sigma_t(r) = f_t \left[1 - \left\{\frac{2\pi}{n\delta_o}(e\varepsilon_{cr} - r\varepsilon_t)\right\}^k\right] \qquad \text{(Eq. 6.22)}$$

Van der Veen assumed that for $r \leq e$, $\varepsilon_t = \varepsilon_{cr}$. This is an overestimation for the tangential strain for radial locations within the cracked portion. However, since his derivation ignores tangential expansion due to radial compressive stress, he assumed there is only a small difference between the assumed and real tangential strain. Substituting $\varepsilon_t = \varepsilon_{cr}$ into equation 6.22 gives:

$$\sigma_t(r) = f_t \left[1 - \left\{\frac{2\pi\varepsilon_{cr}}{n\delta_o}(e - r)\right\}^k\right] \qquad \text{(Eq. 6.23)}$$

Taking the integral of stress over the cracked depth to obtain the force developed in the cracked zone, or the softening effect, yields:

$$\int_{\frac{d_s}{2}}^{e} \sigma_t(r)dr = f_t \int_{\frac{d_s}{2}}^{e} dr - \left(\frac{2\pi\varepsilon_{cr}}{n\delta_o}\right)^k f_t \int_{\frac{d_s}{2}}^{e} (e - r)^k dr$$

$$\int_{\frac{d_s}{2}}^{e} \sigma_t(r)dr = f_t\left(e - \frac{d_s}{2}\right)\left[1 - \left\{\left(\frac{2\pi\varepsilon_{cr}}{n\delta_o}\right)\left(e - \frac{d_s}{2}\right)\right\}^k \frac{1}{k+1}\right] \qquad \text{(Eq. 6.24)}$$

The cracking resistance developed by the softening then is:

$$\tau\tan\alpha = \frac{2f_t}{d_s}\left(e - \frac{d_s}{2}\right)\left[1 - \left\{\left(\frac{2\pi\varepsilon_{cr}}{n\delta_o}\right)\left(e - \frac{d_s}{2}\right)\right\}^k \frac{1}{k+1}\right] \qquad \text{(Eq. 6.25)}$$

$$2\pi\varepsilon_{cr}\left(e - \frac{d_s}{2}\right) \leq n\delta_o \qquad \text{(Eq. 6.26)}$$

The solution in Equation 6.25 is true when the stress is transferred across the entire crack depth. This assumption is true when Equation 6.26 is satisfied. If not, the lower boundary for integration must be adjusted to x:

$$2\pi\varepsilon_{cr}(e - x) = n\delta_o \qquad \text{(Eq. 6.27)}$$

The total cracking resistance is a combination of the elastic part, given by Tepfer's solution in Equation 6.10, and the softening part, given by Van der Veen's solution in Equation 6.25:

$$\tau\tan\alpha = \frac{f_t 2e}{d_s}\frac{\left(c_y + \frac{d_s}{2}\right)^2 - e^2}{\left(c_y + \frac{d_s}{2}\right)^2 + e^2} + \frac{2f_t}{d_s}\left(e - \frac{d_s}{2}\right)\left[1 - \left\{\left(\frac{2\pi\varepsilon_{cr}}{n\delta_o}\right)\left(e - \frac{d_s}{2}\right)\right\}^k \frac{1}{k+1}\right] \text{(Eq. 6.28)}$$

As seen in Equation 6.25, the cracking resistance is dependent on the number of cracks. It can be shown that as the number of cracks increases to infinity, taking lim n→∞, the resistance becomes the plastic stage as described by Tepfers in Equation 6.7:

$$\lim_{n\to\infty} \frac{2f_t}{d_s}\left(e - \frac{d_s}{2}\right)\left[1 - \left(\frac{2\pi\varepsilon_{cr}}{n\delta_o}\right)^k \left(e - \frac{d_s}{2}\right)^k \frac{1}{k+1}\right] = \frac{2f_t}{d_s}\left(e - \frac{d_s}{2}\right)$$

$$\tau\tan\alpha = \frac{2f_t}{d_s}\left(e - \frac{d_s}{2}\right) = \frac{2f_t c_y}{d_s}$$

This feature can be explained by considering the physical limitations of multiple versus single crack openings. If numerous cracks form, they will not be allowed to open as wide as a single crack. Thus, more stress is transferred across numerous smaller crack openings than a single larger opening. The minimum crack resistance can be obtained by considering only one crack. This is the most conservative case.

6.4 COMPARISON OF ANALYTICAL SOLUTIONS TO EXPERIMENTAL DATA

The experimental data from the splitting failures in the spliced beam specimens were compared to Van der Veen's softening model and Tepfer's three stages of bond behavior. To achieve the lowest cracking resistance, the softening model was plotted assuming only one crack forms around the bonded reinforcing bar. Since this model is a function of the concrete properties, the 0% RCA control mix design properties for tensile strength and modulus of elasticity were used. Typical values of $k = 0.248$ and $\delta_o = 0.00787$ in. (0.2 mm) were used as recommended by Van der Veen for normal strength concrete. The following equation was used to approximate the optimum crack depth:

$$e = \beta \left(c_y + \frac{d_s}{2} \right)$$
(Eq. 6.29)

When considering only one crack, Van der Veen calculated the β values for optimum crack depth. These β values are shown in Table 6.1 as a function of concrete cover. The data obtained in this study utilized #6 (No. 19) reinforcing bars, where $d_s = 19.0$ mm. To plot this model, β was assumed to be 0.69.

Table 6.1 β Values for Optimum Crack Depths with n=1

d_s (mm)	c/d_s			
	1.5	2.5	3.5	4.5
10	0.73	0.70	0.68	0.67
20	0.69	0.67	0.65	0.63
40	0.66	0.63	0.61	0.59

As shown in Figure 6.8, the softening model plots between the fully plastic and partially cracked elastic stages as predicted. The data obtained in the study were from beams with #6 (No. 19) reinforcing bars and a minimum cover of 1.0 in. (25.4 mm). The ratio of concrete cover to bar diameter was 1.33. The data points for all nine spliced beam specimens are also plotted in Figure 6.8. It should be noted that the interaction of the contact lap splice and the adjacent bars was neglected in this comparison. As anticipated, the experimental values fall between the plastic and partially cracked elastic stages. Also shown in Figure 6.8, Van der Veen's model closely predicts the experimental results. This result indicates that the primary mode of failure in the spliced beam specimens was by splitting through the concrete cover. The comparison also indicates that bond strength can be closely predicted using existing analytical softening models for concretes with up to 100% RCA replacement of coarse aggregate.
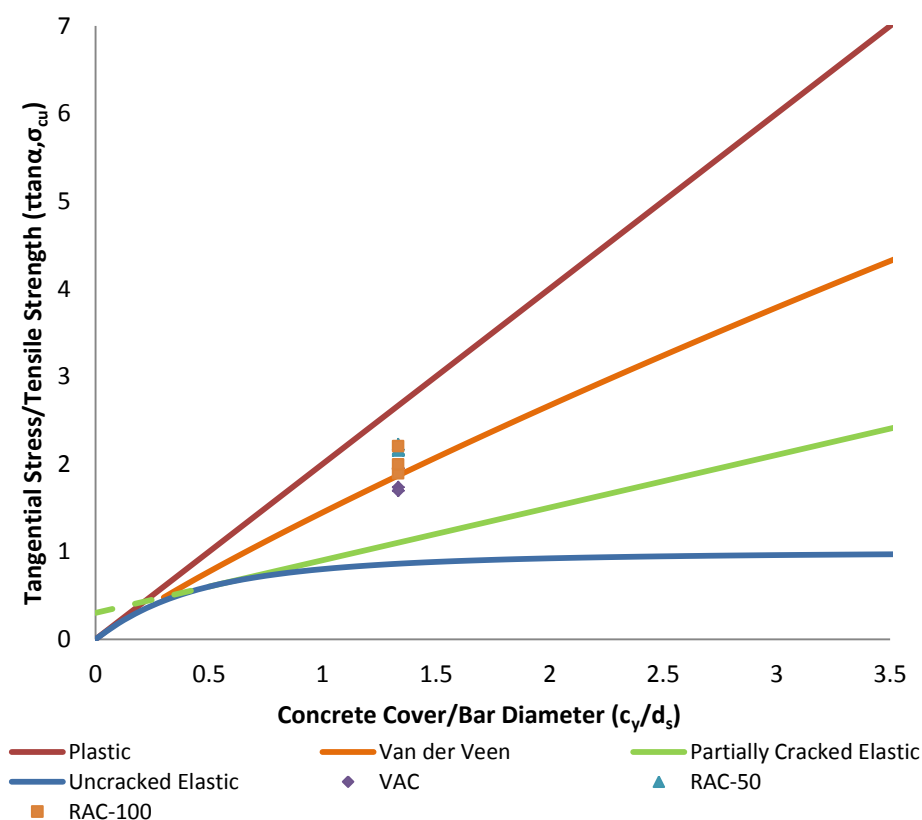

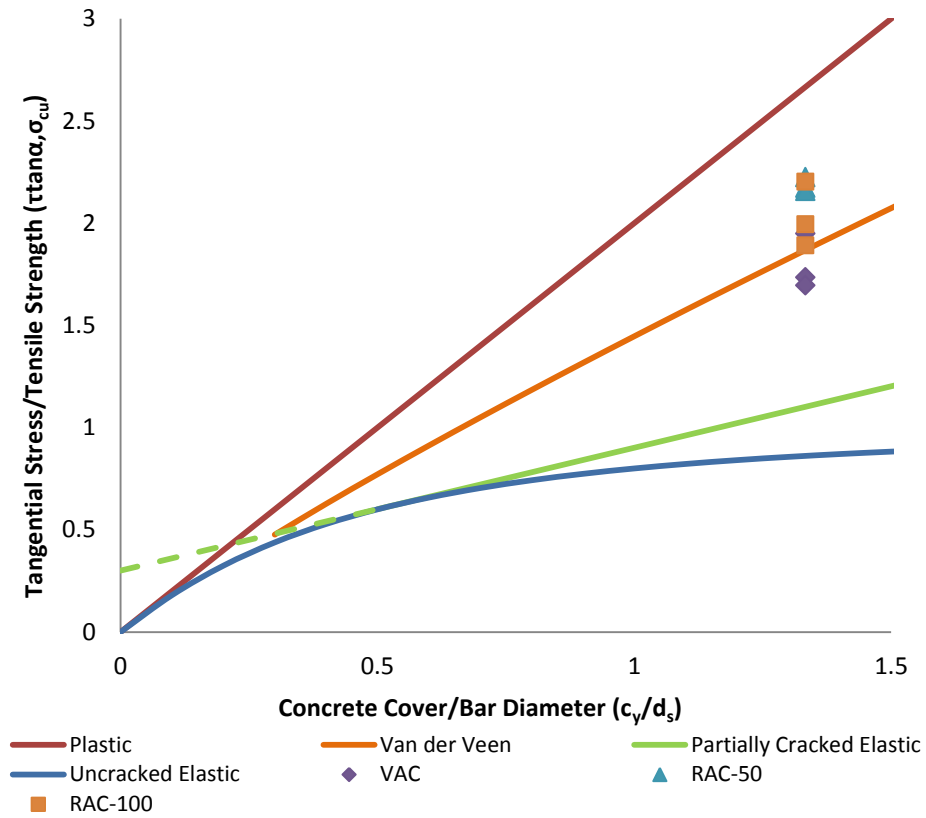**Figure 6.8 Comparison of Experimental Data to Analytical Models**

Figure 6.8 Comparison of Experimental Data to Analytical Models (cont'd.)

7. FINDINGS, CONCLUSIONS, AND RECOMMENDATIONS

7.1 INTRODUCTION

The objective of this study was to determine the effect of replacing coarse natural aggregates with RCA on the bond strength between deformed steel bars and surrounding concrete. The following section presents the findings, conclusions, and recommendations of this study. The testing program compared mix designs at three different RCA replacement levels, 0%, 50%, and 100%. A standard Missouri Department of Transportation (MoDOT) Class B mix design was used as a baseline mix throughout the study. Two test methods were used to evaluate bond performance. The first method was the direct pull-out test based on the RILEM 7-II-128 *RC6: Bond test for reinforcing steel* (RILEM, 1994). The second method was a full-scale spliced beam tested under third point loading. While the direct pull-out test is a widely used test method for comparing bond performance, the full-scale beam splice specimens are regarded as the most realistic stress state response in evaluating bond performance.

7.2 FINDINGS

7.2.1 Material Properties Testing. All concrete material properties were negatively impacted with increasing replacement of coarse natural aggregates with RCA. The most drastic decreases were seen in splitting tensile strength and fracture energy. The splitting tensile strength decreased 12% and 29% for 50% RCA replacement and 100% RCA replacement, respectively. The fracture energy decreased 14% and 22% for 50% RCA replacement and 100% RCA replacement, respectively.

7.2.2 Direct Pull-Out Testing. A total of 18 direct pull-out specimens were constructed and tested in this study. For each RCA replacement level, three specimens were constructed with a #4 (No. 13) deformed bar and three specimens were constructed with a #6 (No. 19) deformed bar. Comparing average square root normalized data for the #4 (No.13) specimens indicates that there was essentially no difference in peak bond stress between the VAC and RAC-50 specimens and a slight increase of 6.0% in the RAC-100 over the VAC specimens. A comparison of the average square root normalized data for the #6 (No.19) specimens indicates that there was a 1% decrease in peak bond

stress in the RAC-50 specimens over the controls and essentially no difference in peak bond stress between the RAC-100 specimens and the VAC specimens.

Comparing the fourth root normalized data for the #4 (No.13) specimens, there was a slight increase in peak bond stress between the control and both RCA replacement levels. The bond stress increased 7.9% in RAC-50 specimens and 12.9% in the RAC-100 specimens. Likewise, comparing the fourth root normalized data for the #6 (No. 19) specimens, there was a slight increase in peak bond stress between the control and both RCA replacement levels. In both RAC-50 and RAC-100 specimens, the average peak bond stress was 7.1% higher than the control.

In all RCA replacement levels, the #6 (No. 19) specimens exhibited higher bond stresses than the #4 specimens. However, as RCA replacement increases, the percent difference between decreased. The percent difference between #4 (No. 13) and #6 (No. 19) was 8.6%, 7.8%, and 3.1% for the VAC, RAC-50, and RAC-100, respectively.

7.2.3 Beam Splice Testing. Three beam splice specimens were constructed and tested for each RCA replacement level. Deformed #6 (No. 19) steel bars were used as longitudinal reinforcement and no confinement was provided in the spliced region. All beams were cast with longitudinal reinforcement in the bottom of the beam. A comparison of the square root normalized results indicates that 50% RCA beams had a slight increase in developed stress in the steel of 5.9% over the VCA control. However, the 100% RCA beams had a decrease in stress of 16.9% over the VCA control. A comparison of the fourth root normalized results shows that generally, both RCA beam sets had a lower stress in the steel. The 50% RCA beams decreased by 5.0%, and the 100% RCA beams decreased by 19.5%.

The experimental data from the full-scale beam tests were compared with Tepfers' (1977) plastic, partially cracked elastic, and elastic models for concrete bond failures. The plastic model overestimated the experimental bond strength and the partially cracked elastic model underestimated the experimental bond strength. The full-scale beam data were also compared to Van der Veen's (1990) concrete softening model. This model was in good agreement with the experimental data for all RCA replacement levels tested.

7.3 CONCLUSIONS

7.3.1   Direct Pull-Out Testing. Analysis of the direct pull-out data indicates that both 50% and 100% RCA mixes preformed comparably or had a slight improvement in bond capacity over the controls. However, a statistical analysis indicates that all mixes performed comparably when normalized by the square root of concrete compressive strength for both #4 (No. 13) and #6 (No. 19) specimens. When normalized by the fourth root of concrete compressive strength, #4 (No. 13) specimens performed comparably across all three mixes, and #6 (No. 19) specimens were comparable between the 50% RCA and control mixes. Only the #6 (No. 19) specimens had a statistically significant difference between the 100% RCA and control mixes, with the 100% RCA showing a 7.1% increase in bond strength. The inability to draw definitive conclusions from this data set is largely due to the high variability in the data compared to the largest percent difference in strength. The coefficient of variance for these pull-out tests ranged from 1.2% to 7.3% making any change in bond stress difficult to detect. Testing more specimens would help potentially help reduce the noise in this data.

7.3.2   Beam Splice Testing. Analysis of the beam splice data indicates that both 50% and 100% RCA specimens exhibited diminished bond strength over the control specimens. A statistical analysis indicates that when normalized by either the square root or fourth root of concrete compressive strength, the 50% RCA specimens performed comparably to the control specimens. However, the 100% RCA specimens exhibited a statistically significant decrease in bond strength from the control specimens, 16.9% based on the square root normalization and 19.5% based on the fourth root normalization. This decrease in bond strength parallels the decrease in splitting tensile strength, 29%, and fracture energy, 22%, both of which are related to the tensile response of the concrete, which governs bond failures where splitting cracks control. This reduction in tensile response and thereby bond strength is likely due to the two-phase, pre-cracked natural of RCA. As a two-phase material, there exist two interfacial transition zones within concrete containing RCA. Furthermore, RCA is demolition and pre-crushed material. These characteristics result in more planes of weakness between the coarse aggregate and mortar in recycled aggregate concrete.

These findings indicate that replacing more than 50% of the coarse natural aggregates with RCA may require some modification to the bond and development length to achieve sufficient bond strength between deformed steel reinforcing bars and the surrounding concrete.

From the theoretical analysis, it was shown that the bond splitting failure was closely predicted using Van der Veen's (1990) concrete softening model for concretes with up to 100% RCA replacement of coarse aggregate.

7.4 RECOMMENDATIONS

Due to the limited number of studies into the bond behavior of RCA, further research is needed to make comparisons and conclusions across a larger database. To better understand the influence of RCA replacement on the bond behavior of reinforced concrete, additional variables important to design must also be investigated. A list of the testable variables relating to the structural characteristics and bar properties of the reinforced member is given below:

- Perform tests with wider variation in bar sizes to investigate bar size effect
- Perform tests with smooth bars and deformed bars with different rib heights to develop relationship between rib height and bond strength
- Perform tests with different surface deterioration and cleanliness
- Perform tests with epoxy or zinc coated bars
- Perform studies with transverse reinforcement provided in the spliced region to investigate effect of confinement
- Perform studies with splice region cast with more than 12 in. (30.5 cm) of concrete below to investigate "top bar" effect
- Perform tests with noncontact lap splices to evaluate performance with contact lap splices

Testable variables relating to the RCA material itself are listed below:

- Perform studies on RCA from different source structures (pavements, building structures, bridge structures, etc.)

- Perform studies on RCA from different source locations (different geographical regions of the United States)
- Perform studies on RCA from different parent rock material
- Perform studies with varied amounts of chloride contamination
- Perform studies with varied amounts of organic impurities
- Perform studies with varied amounts of fine RCA

APPENDIX A
DIRECT PULL-OUT TEST DATA PLOTS
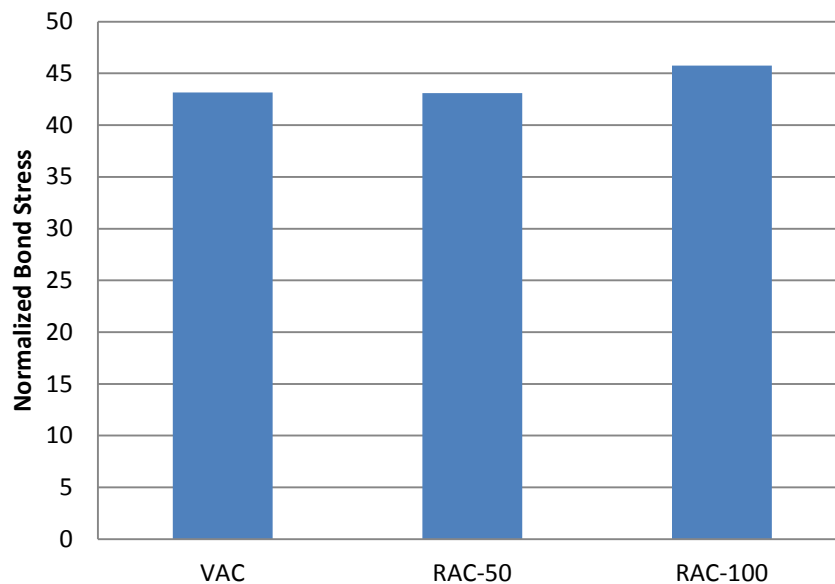
Figure A.1 Bond stresses for #4 pull-out specimens, square root normalization
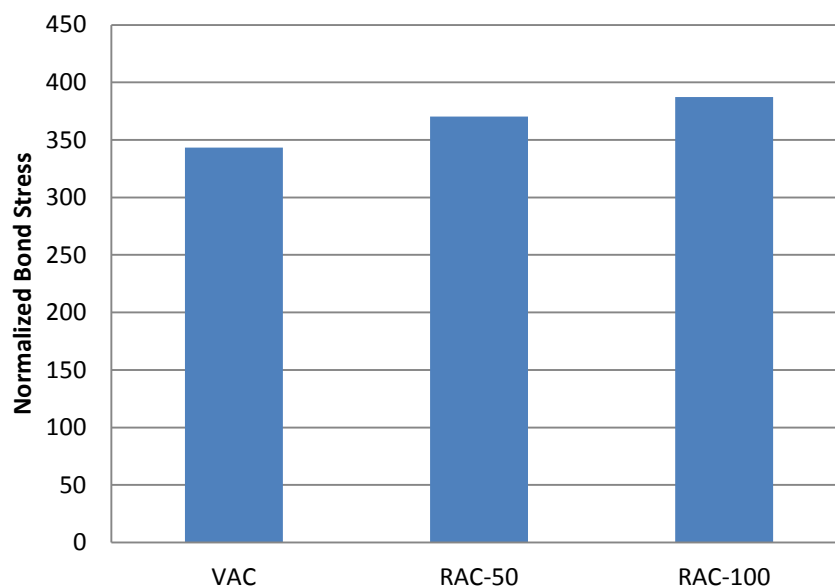
Figure A.2 Bond stresses for #4 pull-out specimens, fourth root normalization
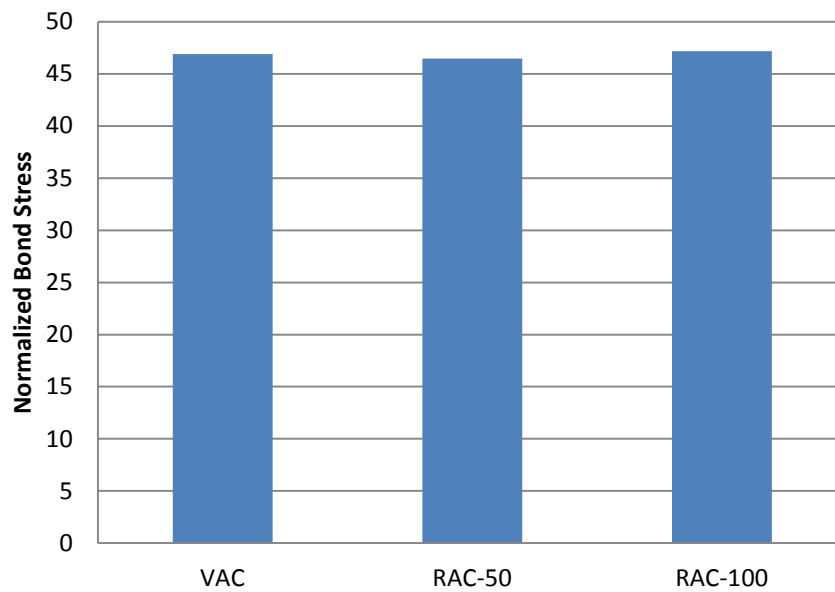
Figure A.3 Bond stresses for #6 pull-out specimens, square root normalization
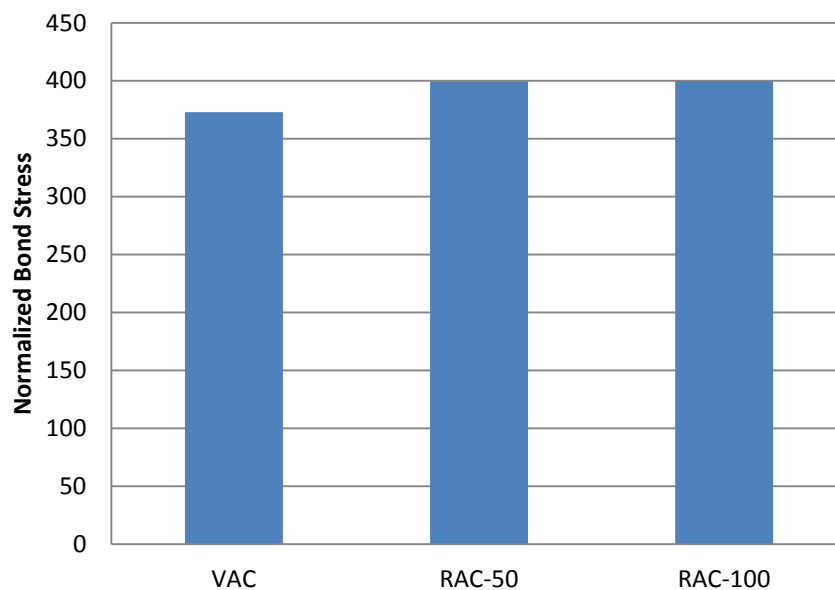
Figure A.4 Bond stresses for #6 pull-out specimens, fourth root normalization
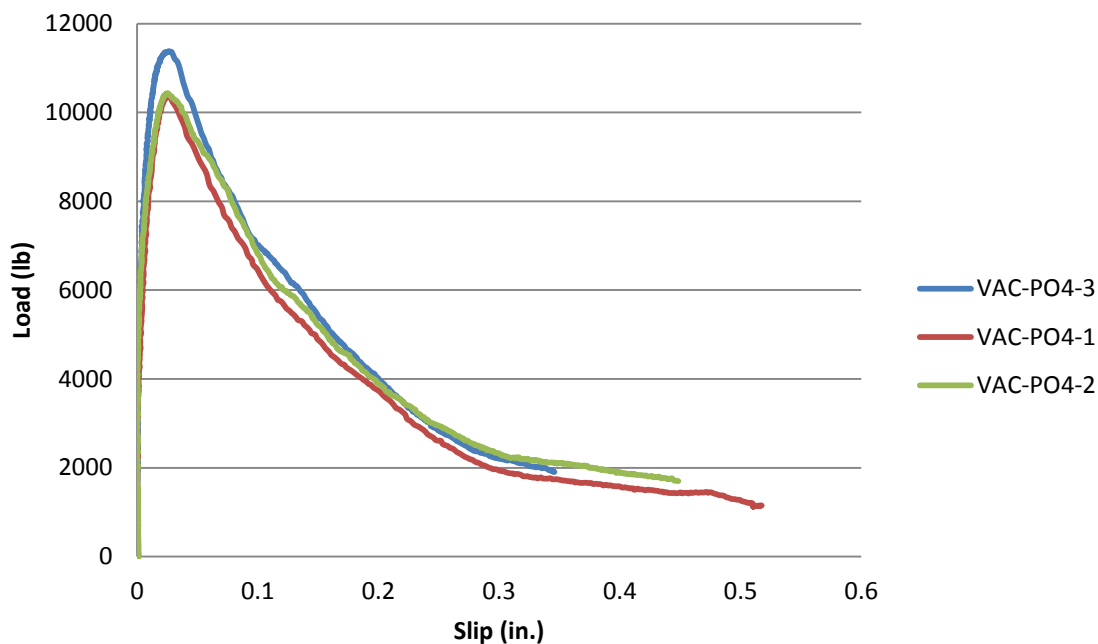
Figure A.5 Applied load vs. slip plot for #4 (No. 13) VAC-PO4
Conversion: 1 in. = 25.4 mm
1 lb. = 4.45 N
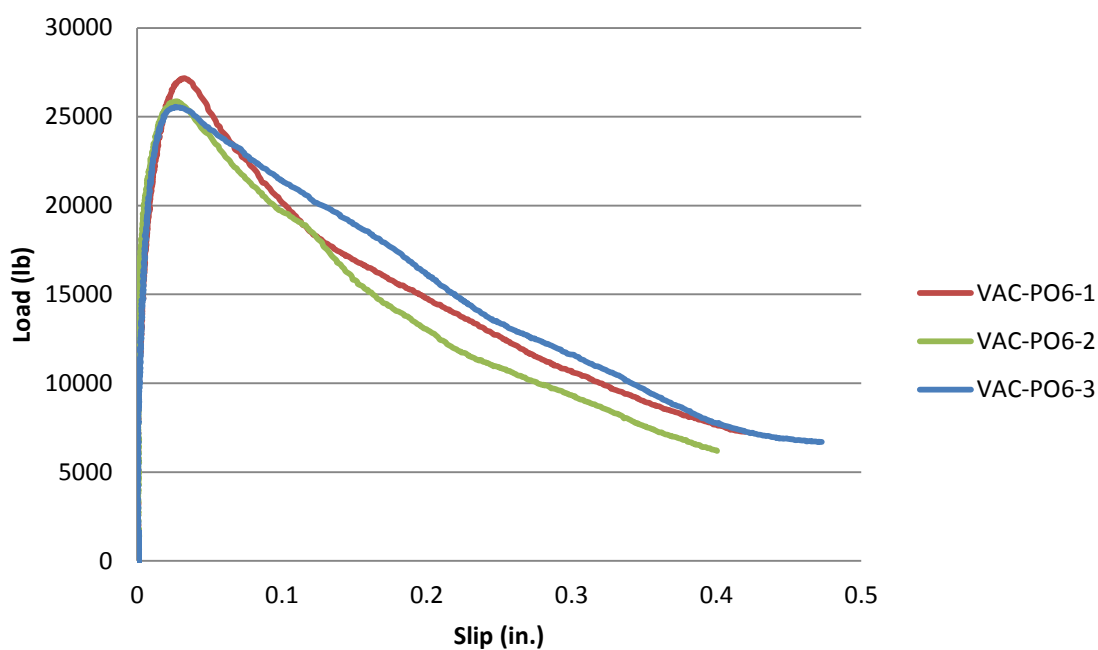
Figure A.6 Applied load vs. slip plot for #6 (No. 19) VAC-PO6
Conversion: 1 in. = 25.4 mm
1 lb. = 4.45 N
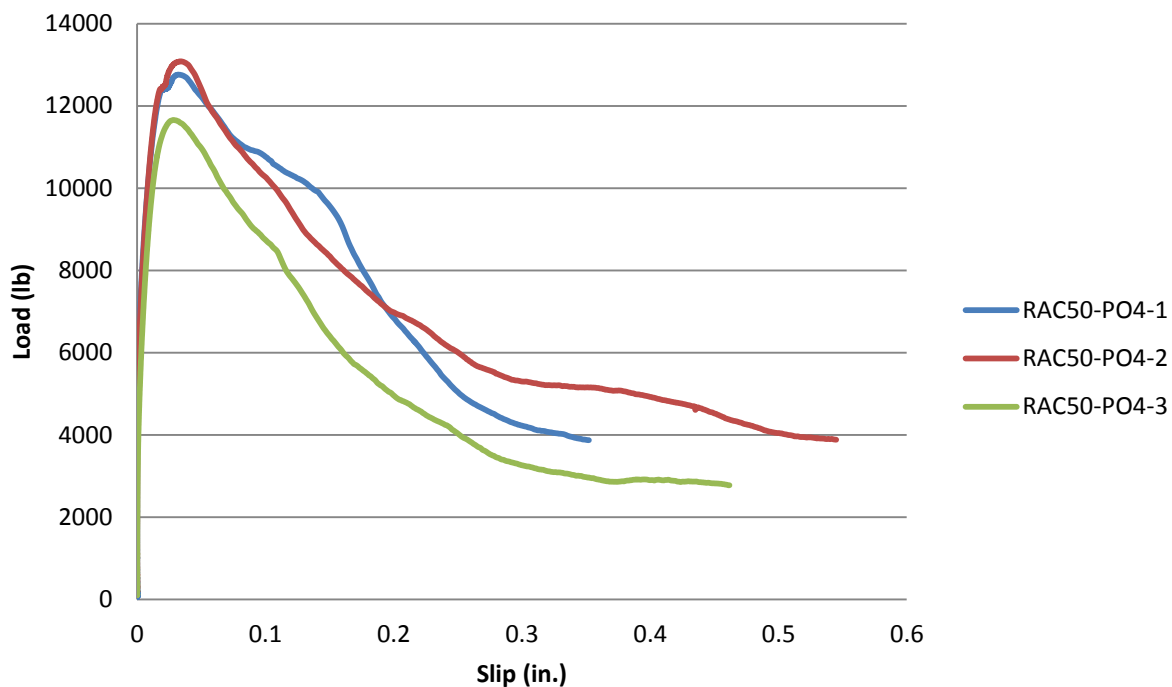
Figure A.7 Applied load vs. slip plot for #4 (No. 13) RCA50-PO4
Conversion: 1 in. = 25.4 mm
1 lb. = 4.45 N
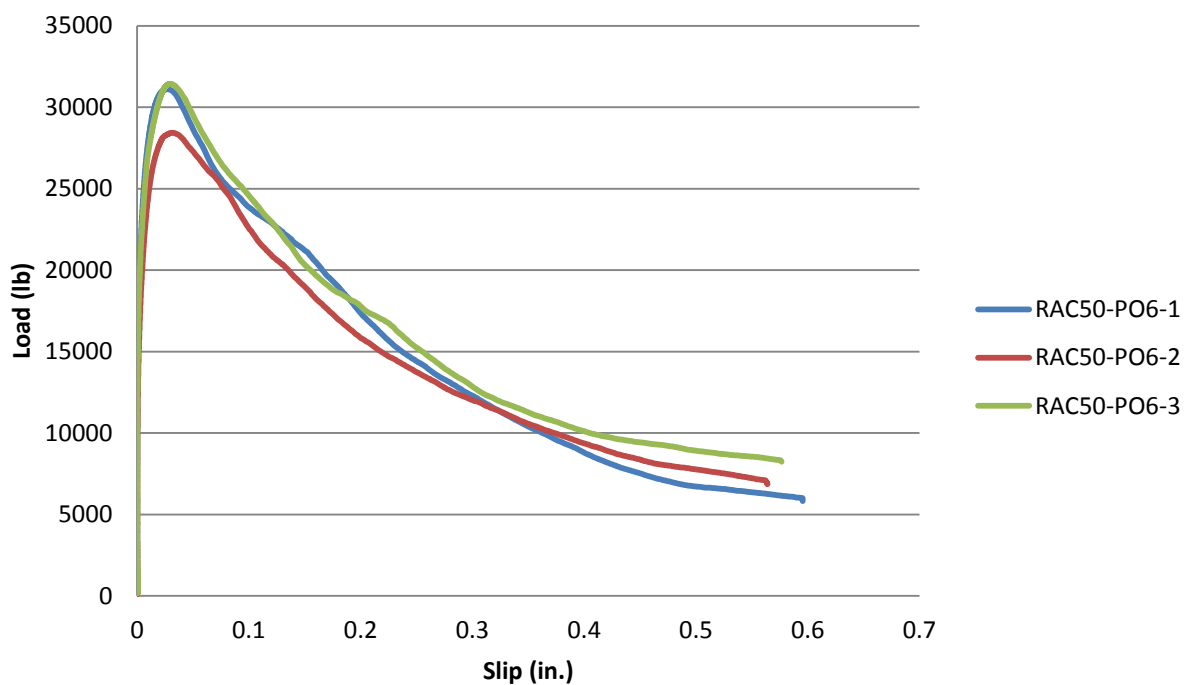
Figure A.8 Applied load vs. slip plot for #6 (No. 19) RCA50-PO6
Conversion: 1 in. = 25.4 mm
1 lb. = 4.45 N
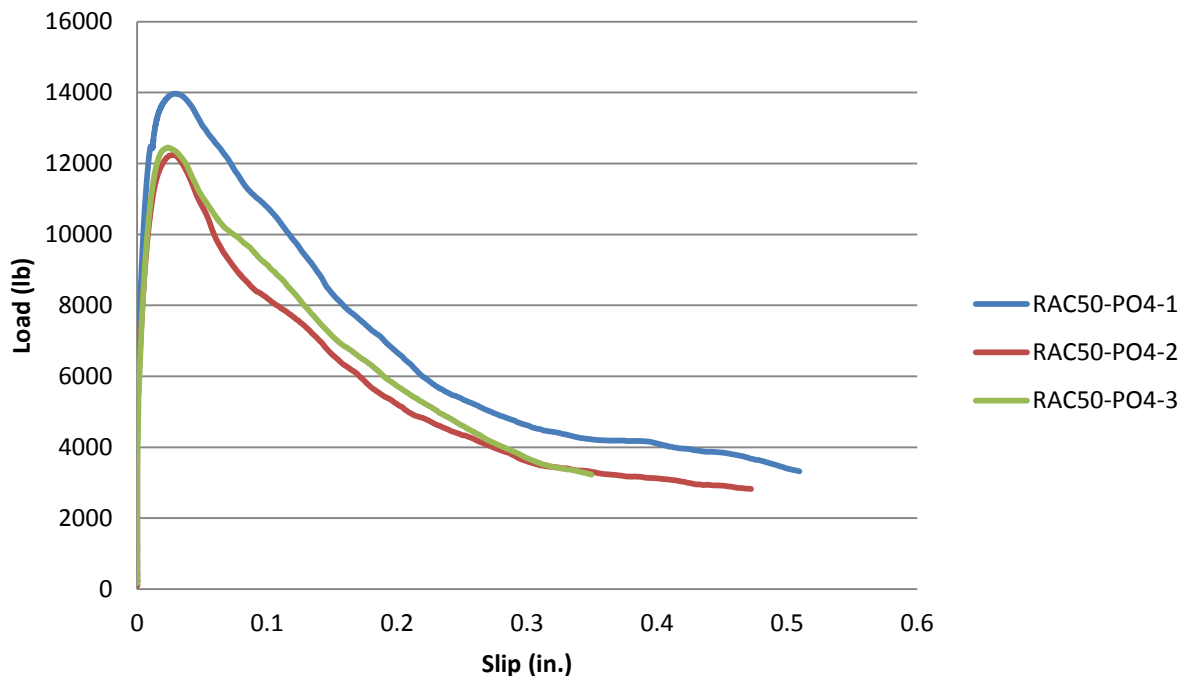
Figure A.9 Applied load vs. slip plot for #4 (No. 13) RCA100-PO4
Conversion: 1 in. = 25.4 mm
1 lb. = 4.45 N
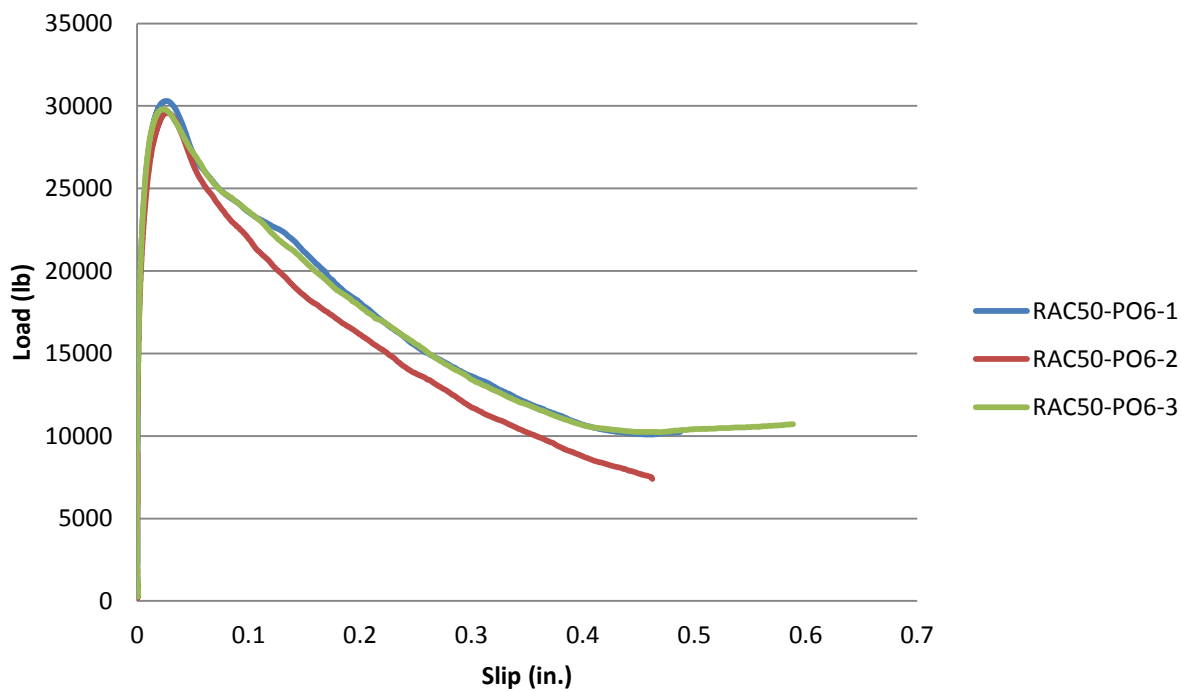
Figure A.10 Applied load vs. slip plot for #6 (No. 19) RCA100-PO6
Conversion: 1 in. = 25.4 mm
1 lb. = 4.45 N

APPENDIX B
BEAM SPLICE TEST DATA PLOTS
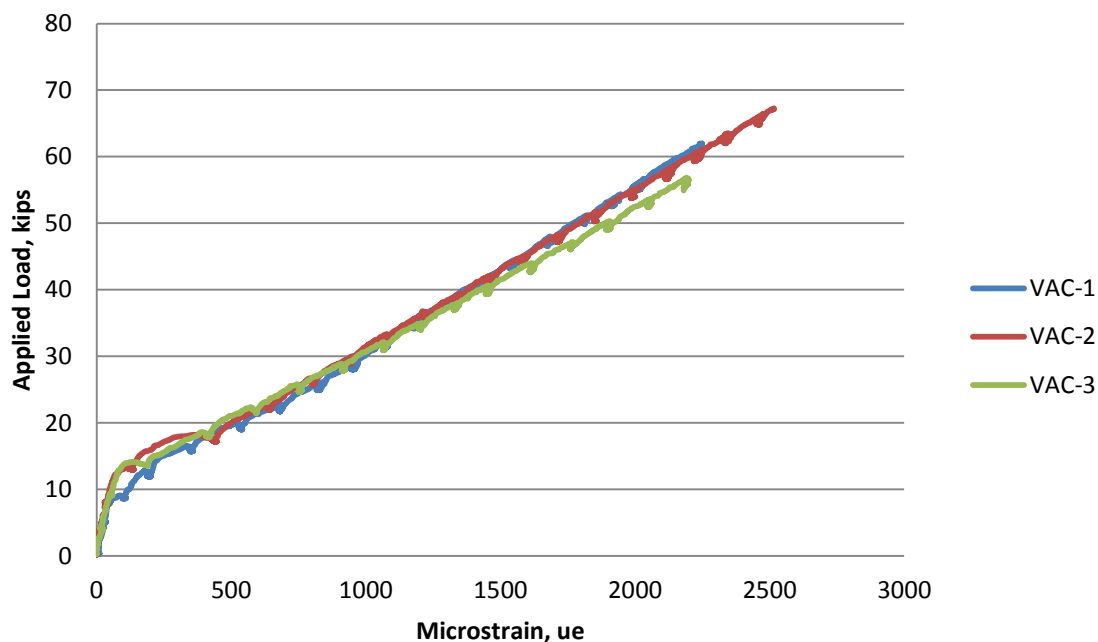
Figure B.1 Applied load vs. strain (average of all gauges per specimen) for VAC
Conversion: 1 kip = 4.45 kN
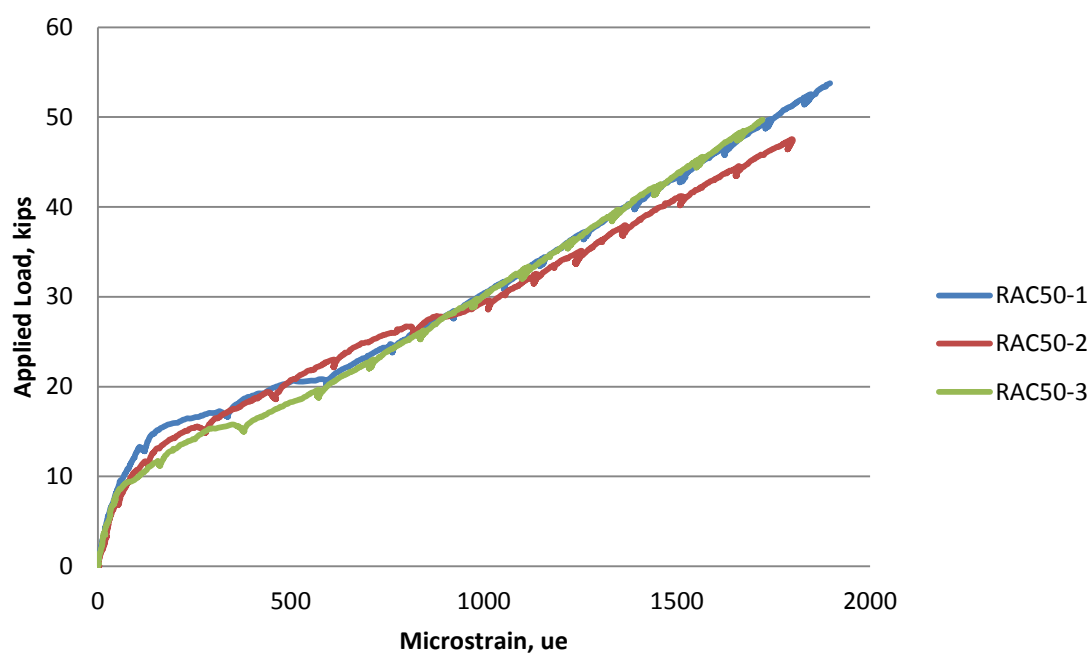
Figure B.2 Applied load vs. strain (average of all gauges per specimen) for RAC50
Conversion: 1 kip = 4.45 kN
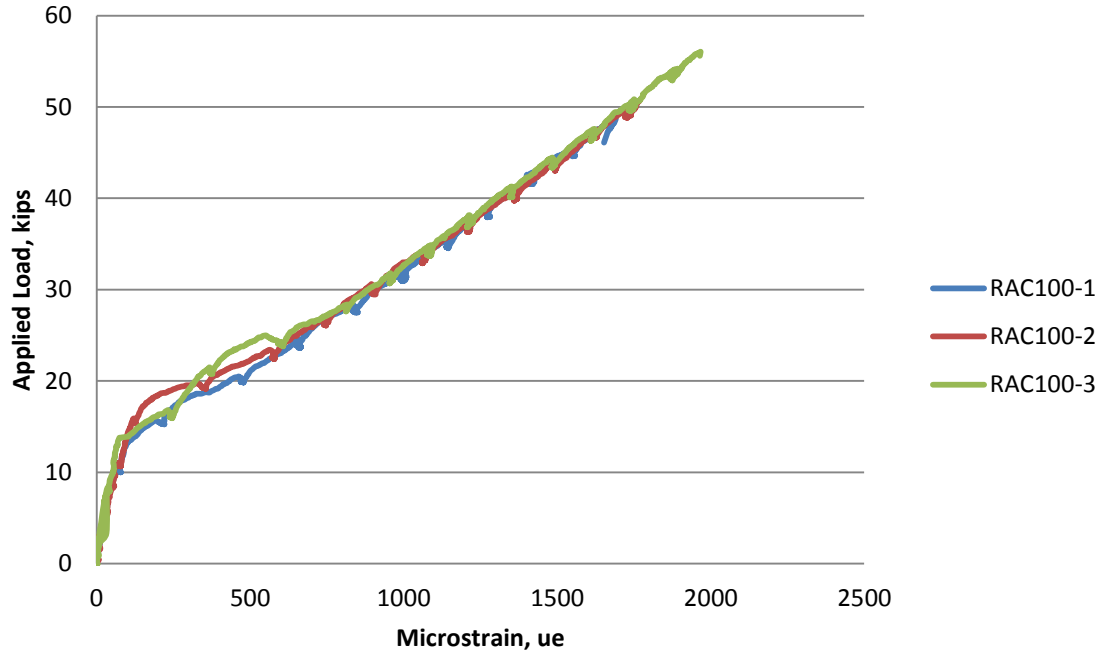
Figure B.3 Applied load vs. strain (average of all gauges per specimen) for RAC100
Conversion: 1 kip = 4.45 kN
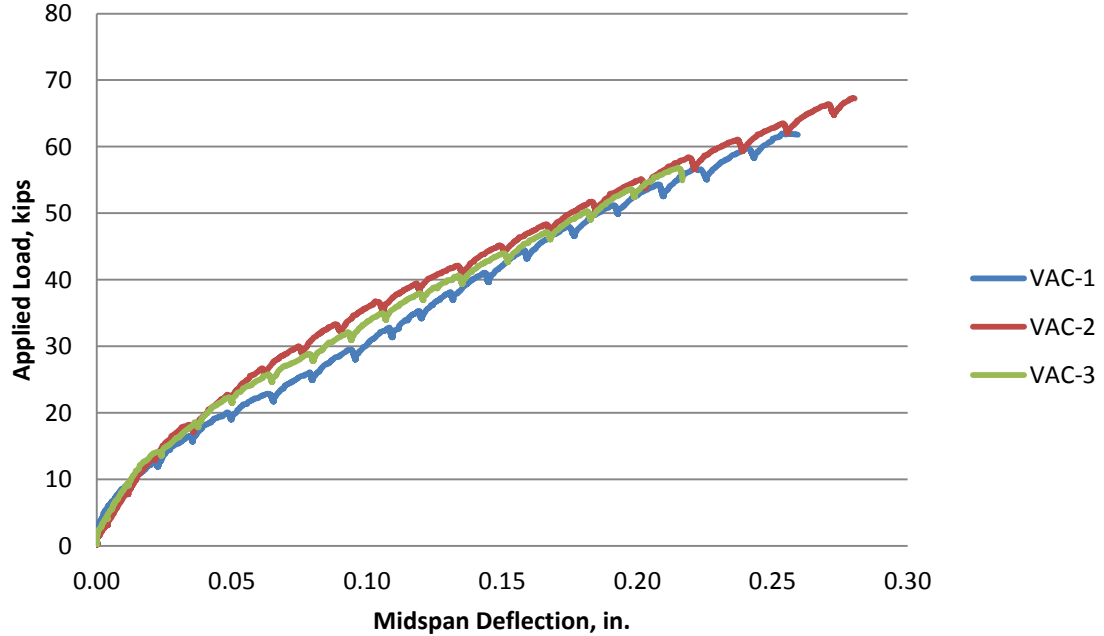
Figure B.4 Applied load vs. Midspan Deflection for VAC
Conversion: 1 in. = 25.4 mm
1 kip. = 4.45 kN
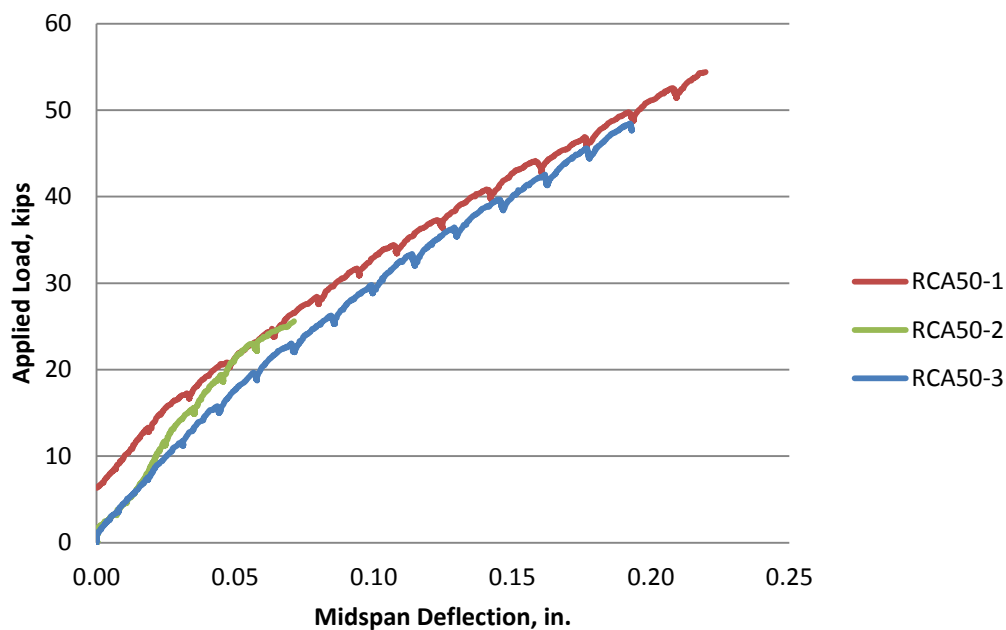
Figure B.5 Applied load vs. Midspan Deflection for RAC50
Conversion: 1 in. = 25.4 mm
1 kip. = 4.45 kN
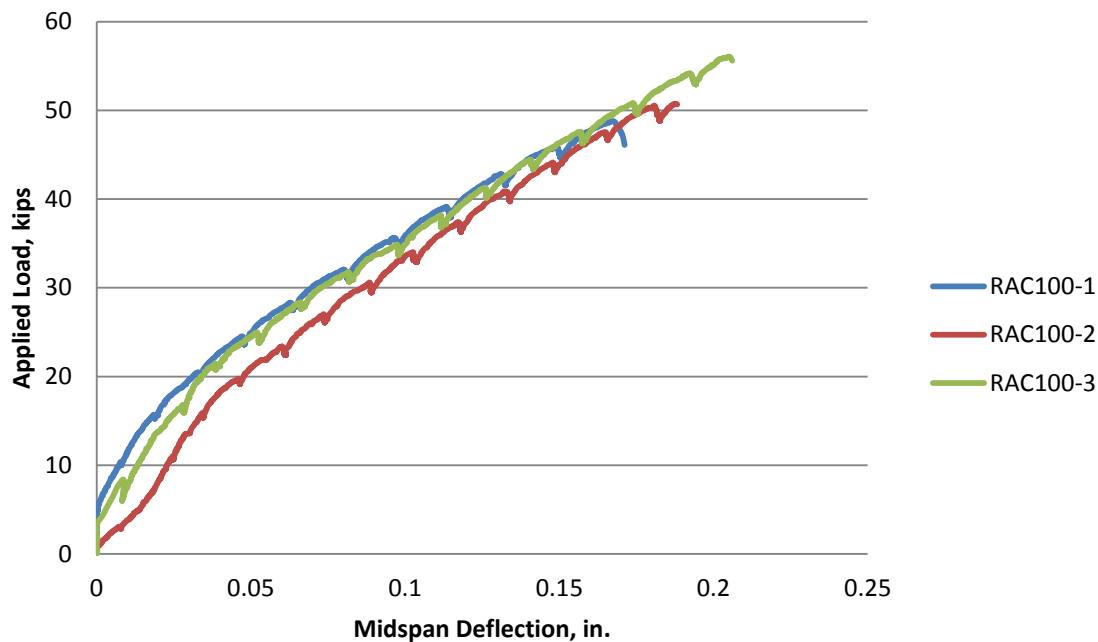
Figure B.6 Applied load vs. Midspan Deflection for RAC100
Conversion: 1 in. = 25.4 mm
1 kip. = 4.45 kN

APPENDIX C

PHOTOGRAPHS OF BEAM SPLICE FAILURES

Figure C.1 Side View of VAC-1

Figure C.2 Bottom View of VAC-1

Figure C.3 Side View of VAC-2

Figure C.4 Bottom View of VAC-2

Figure C.5 Side View of VAC-3

Figure C.6 Bottom View of VAC-3

Figure C.7 Side View of RCA50-1

Figure C.8 Bottom View of RCA50-1
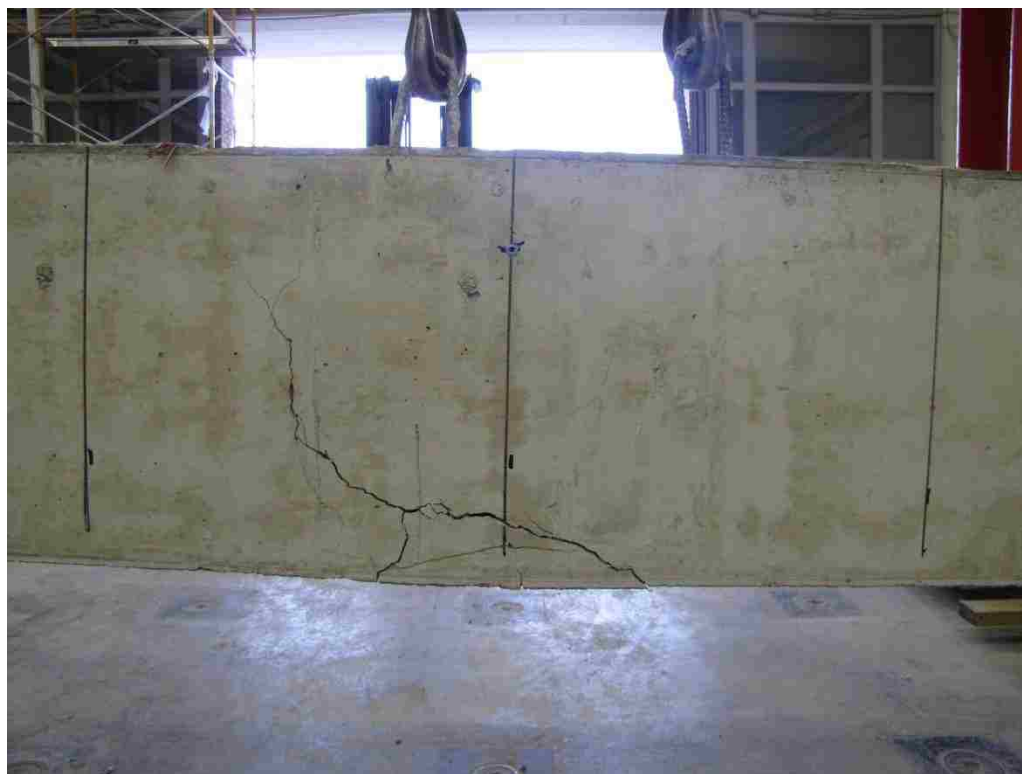
Figure C.9 Side View of RCA50-2

Figure C.10 Bottom View of RCA50-2

Figure C.11 Side View of RCA50-3

Figure C.12 Bottom View of RCA50-3

Figure C.13 Side View of RCA100-1
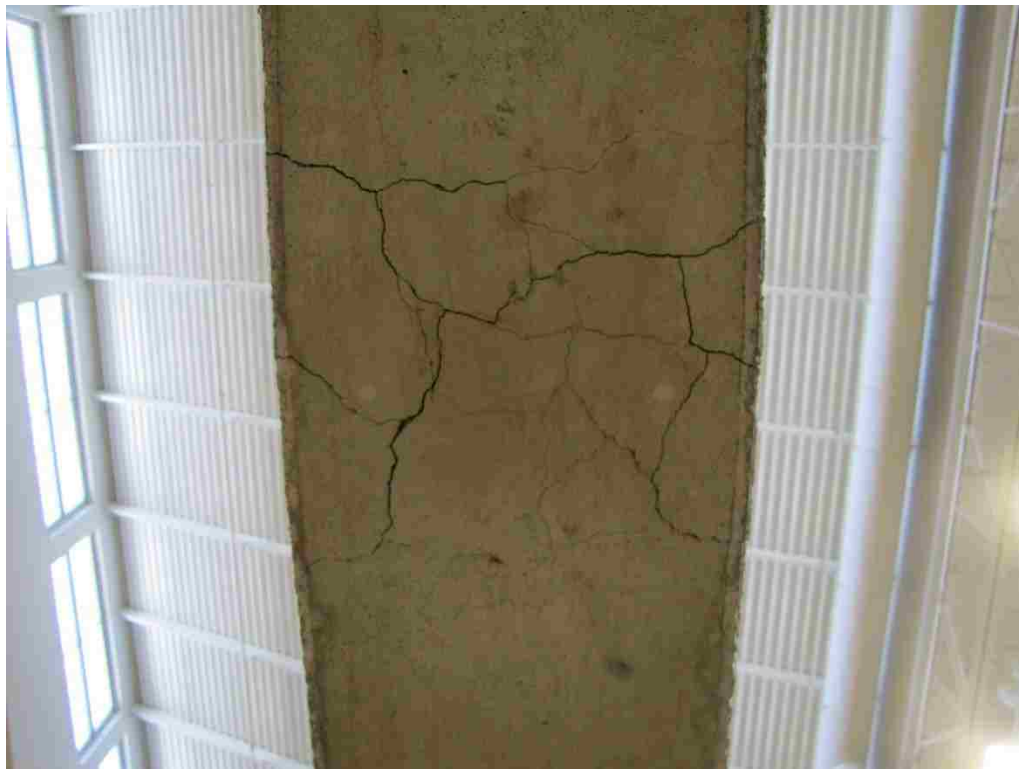
Figure C.14 Bottom View of RCA100-1

Figure C.15 Side View of RCA100-2

Figure C.16 Bottom View of RCA100-2

Figure C.17 Side View of RCA100-3

Figure C.18 Bottom View of RCA100-3

APPENDIX D
STATISTICAL ANALYSIS OF RESULTS

Table D.1 Parametric Analysis of #4 (No.13) Pull-Out Results with Square Root Normalization between VAC and RCA-50

t-Test: Two-Sample Assuming Unequal Variances

	VAC	RAC-50
Mean	43.15965	43.07783
Variance	5.324474	6.639769
Observations	3	3
Hypothesized Mean Difference	0	
df	4	
t Stat	0.040971	
P(T<=t) one-tail	0.484641	
t Critical one-tail	2.131847	
P(T<=t) two-tail	0.969283	
t Critical two-tail	2.776445	

Table D.2 Non-parametric Analysis of #4 (No.13) Pull-Out Results with Square Root Normalization between VAC and RCA-50

```
Mann-Whitney Test and CI: VAC, RAC-50


      N  Median
VAC    3  42.015
RAC-50  3  43.974




Point estimate for ETA1-ETA2 is 0.729
91.9 Percent CI for ETA1-ETA2 is (-3.438,5.645)
W = 11.0
Test of ETA1 = ETA2 vs ETA1 not = ETA2 is significant at 1.0000
```

Table D.3 Parametric Analysis of #4 (No.13) Pull-Out Results with Square Root Normalization between VAC and RCA-100

t-Test: Two-Sample Assuming Unequal Variances

	VAC	RAC-100
Mean	43.15965	45.73487
Variance	5.324474	11.22826
Observations	3	3
Hypothesized Mean Difference	0	
df	4	
t Stat	-1.09633	
P(T<=t) one-tail	0.167254	
t Critical one-tail	2.131847	
P(T<=t) two-tail	0.334509	
t Critical two-tail	2.776445	

Table D.4 Non-parametric Analysis of #4 (No.13) Pull-Out Results with Square Root Normalization between VAC and RCA-100

```
Mann-Whitney Test and CI: VAC, RAC-100


       N  Median
VAC    3  42.015
RAC-100  3  44.194



Point estimate for ETA1-ETA2 is -2.180
91.9 Percent CI for ETA1-ETA2 is (-7.932,2.384)
W = 8.0
Test of ETA1 = ETA2 vs ETA1 not = ETA2 is significant at 0.3827
```

Table D.5 Parametric Analysis of #6 (No.19) Pull-Out Results with Square Root Normalization between VAC and RCA-50

t-Test: Two-Sample Assuming Unequal Variances

	VAC	RAC-50
Mean	46.88684	46.44951
Variance	2.337816	6.39148
Observations	3	3
Hypothesized Mean Difference	0	
df	3	
t Stat	0.256377	
P(T<=t) one-tail	0.407118	
t Critical one-tail	2.353363	
P(T<=t) two-tail	0.814236	
t Critical two-tail	3.182446	

Table D.6 Non-Parametric Analysis of #6 (No.19) Pull-Out Results with Square Root Normalization between VAC and RCA-50

```
Mann-Whitney Test and CI: VAC, RAC-50


      N  Median
VAC    3  46.292
RAC-50  3  47.648



Point estimate for ETA1-ETA2 is 0.469
91.9 Percent CI for ETA1-ETA2 is (-2.410,5.080)
W = 11.0
Test of ETA1 = ETA2 vs ETA1 not = ETA2 is significant at 1.0000
```

Table D.7 Parametric Analysis of #6 (No.19) Pull-Out Results with Square Root Normalization between VAC and RCA-100

t-Test: Two-Sample Assuming Unequal Variances

	VAC	RAC-100
Mean	46.88684	47.17004
Variance	2.337816	0.32679
Observations	3	3
Hypothesized Mean Difference	0	
df	3	
t Stat	-0.30049	
P(T<=t) one-tail	0.391712	
t Critical one-tail	2.353363	
P(T<=t) two-tail	0.783424	
t Critical two-tail	3.182446	

Table D.8 Non-Parametric Analysis of #6 (No.19) Pull-Out Results with Square Root Normalization between VAC and RCA-100

```
Mann-Whitney Test and CI: VAC, RAC-100


      N  Median
VAC    3  46.292
RAC-100  3  47.017



Point estimate for ETA1-ETA2 is -0.725
91.9 Percent CI for ETA1-ETA2 is (-2.057,1.933)
W = 9.0
Test of ETA1 = ETA2 vs ETA1 not = ETA2 is significant at 0.6625
```

Table D.9 Parametric Analysis of #4 (No.13) Pull-Out Results with Fourth Root Normalization between VAC and RCA-50

t-Test: Two-Sample Assuming Unequal Variances

	VAC	RAC-50
Mean	343.236	370.2985
Variance	336.7493	490.6246
Observations	3	3
Hypothesized Mean Difference	0	
df	4	
t Stat	-1.62959	
P(T<=t) one-tail	0.089261	
t Critical one-tail	2.131847	
P(T<=t) two-tail	0.178522	
t Critical two-tail	2.776445	

Table D.10 Non-parametric Analysis of #4 (No.13) Pull-Out Results with Fourth Root Normalization between VAC and RCA-50

```
Mann-Whitney Test and CI: VAC, RAC-50


     N  Median
VAC    3  334.13
RAC-50  3  378.00



Point estimate for ETA1-ETA2 is -23.21
91.9 Percent CI for ETA1-ETA2 is (-56.36,19.04)
W = 7.0
Test of ETA1 = ETA2 vs ETA1 not = ETA2 is significant at 0.1904
```

Table D.11 Parametric Analysis of #4 (No.13) Pull-Out Results with Fourth Root Normalization between VAC and RCA-100

t-Test: Two-Sample Assuming Unequal Variances

	VAC	RAC-100
Mean	343.236	387.3789
Variance	336.7493	805.5445
Observations	3	3
Hypothesized Mean Difference	0	
df	3	
t Stat	-2.26221	
P(T<=t) one-tail	0.054352	
t Critical one-tail	2.353363	
P(T<=t) two-tail	0.108704	
t Critical two-tail	3.182446	

Table D.12 Non-parametric Analysis of #4 (No.13) Pull-Out Results with Fourth Root Normalization between VAC and RCA-100

```
Mann-Whitney Test and CI: VAC, RAC-100


         N  Median
VAC      3  334.13
RAC-100  3  374.33



Point estimate for ETA1-ETA2 is -40.20
91.9 Percent CI for ETA1-ETA2 is (-88.70,-3.51)
W = 6.0
Test of ETA1 = ETA2 vs ETA1 not = ETA2 is significant at 0.0809
```

Table D.13 Parametric Analysis of #6 (No.19) Pull-Out Results with Fourth Root Normalization between VAC and RCA-50

t-Test: Two-Sample Assuming Unequal Variances

	VAC	*RAC-50*
Mean	372.8773	399.2816
Variance	147.8565	472.2781
Observations	3	3
Hypothesized Mean Difference	0	
df	3	
t Stat	-1.83651	
P(T<=t) one-tail	0.081803	
t Critical one-tail	2.353363	
P(T<=t) two-tail	0.163606	
t Critical two-tail	3.182446	

Table D.14 Non-Parametric Analysis of #6 (No.19) Pull-Out Results with Fourth Root Normalization between VAC and RCA-50

```
Mann-Whitney Test and CI: VAC, RAC-50


     N  Median
VAC    3  368.15
RAC-50  3  409.59



Point estimate for ETA1-ETA2 is -27.25
91.9 Percent CI for ETA1-ETA2 is (-50.14,12.37)
W = 7.0
Test of ETA1 = ETA2 vs ETA1 not = ETA2 is significant at 0.1904
```

Table D.15 Parametric Analysis of #6 (No.19) Pull-Out Results with Fourth Root Normalization between VAC and RCA-100

t-Test: Two-Sample Assuming Unequal Variances

	VAC	RAC-100
Mean	372.8773	399.5349
Variance	147.8565	23.44476
Observations	3	3
Hypothesized Mean Difference	0	
df	3	
t Stat	-3.52778	
P(T<=t) one-tail	0.01935	
t Critical one-tail	2.353363	
P(T<=t) two-tail	0.038701	
t Critical two-tail	3.182446	

Table D.16 Non-Parametric Analysis of #6 (No.19) Pull-Out Results with Fourth Root Normalization between VAC and RCA-100

```
Mann-Whitney Test and CI: VAC, RAC-100


      N  Median
VAC     3  368.15
RAC-100  3  398.24



Point estimate for ETA1-ETA2 is -30.09
91.9 Percent CI for ETA1-ETA2 is (-41.10,-8.79)
W = 6.0
Test of ETA1 = ETA2 vs ETA1 not = ETA2 is significant at 0.0809
```

Table D.17 Parametric Analysis of Beam Splice Results with Square Root Normalization between VAC and RCA-50

t-Test: Two-Sample Assuming Unequal Variances

	VAC	RAC-50
Mean	65.12762	68.98221
Variance	24.56742	1.342879
Observations	3	3
Hypothesized Mean Difference	0	
df	2	
t Stat	-1.3116	
P(T<=t) one-tail	0.159997	
t Critical one-tail	2.919986	
P(T<=t) two-tail	0.319993	
t Critical two-tail	4.302653	

Table D.18 Non-Parametric Analysis of Beam Splice Results with Square Root Normalization between VAC and RCA-50

```
Mann-Whitney Test and CI: VAC, RAC-50


      N  Median
VAC   3  63.010
RAC-50  3  68.611



Point estimate for ETA1-ETA2 is -5.602
91.9 Percent CI for ETA1-ETA2 is (-8.700,2.736)
W = 9.0
Test of ETA1 = ETA2 vs ETA1 not = ETA2 is significant at 0.6625
```

Table D.19 Parametric Analysis of Beam Splice Results with Square Root Normalization between VAC and RCA-100

t-Test: Two-Sample Assuming Unequal Variances

	VAC	RAC-100
Mean	65.12762	54.09878
Variance	24.56742	17.64037
Observations	3	3
Hypothesized Mean Difference	0	
df	4	
t Stat	2.940316	
P(T<=t) one-tail	0.021188	
t Critical one-tail	2.131847	
P(T<=t) two-tail	0.042376	
t Critical two-tail	2.776445	

Table D.20 Non-Parametric Analysis of Beam Splice Results with Square Root Normalization between VAC and RCA-100

Mann-Whitney Test and CI: VAC, RAC-100

      N Median
VAC   3   63.01
RAC-100 3   53.14

Point estimate for ETA1-ETA2 is 11.12
91.9 Percent CI for ETA1-ETA2 is (2.89,20.33)
W = 15.0
Test of ETA1 = ETA2 vs ETA1 not = ETA2 is significant at 0.0809

Table D.21 Parametric Analysis of Beam Splice Results with Fourth Root Normalization between VAC and RCA-50

t-Test: Two-Sample Assuming Unequal Variances

	VAC	RAC-50
Mean	65.12762	61.8741
Variance	24.56742	1.08039
Observations	3	3
Hypothesized Mean Difference	0	
df	2	
t Stat	1.112727	
P(T<=t) one-tail	0.190821	
t Critical one-tail	2.919986	
P(T<=t) two-tail	0.381643	
t Critical two-tail	4.302653	

Table D.22 Non-Parametric Analysis of Beam Splice Results with Fourth Root Normalization between VAC and RCA-50

```
Mann-Whitney Test and CI: VAC, RAC-50


     N  Median
VAC    3  63.010
RAC-50  3  61.541



Point estimate for ETA1-ETA2 is 1.468
91.9 Percent CI for ETA1-ETA2 is (-1.459,9.748)
W = 13.0
Test of ETA1 = ETA2 vs ETA1 not = ETA2 is significant at 0.3827
```

Table D.23 Parametric Analysis of Beam Splice Results with Fourth Root Normalization between VAC and RCA-100

t-Test: Two-Sample Assuming Unequal Variances

	VAC	RAC-100
Mean	65.12762	52.39721
Variance	24.56742	16.54813
Observations	3	3
Hypothesized Mean Difference	0	
df	4	
t Stat	3.438744	
P(T<=t) one-tail	0.013162	
t Critical one-tail	2.131847	
P(T<=t) two-tail	0.026324	
t Critical two-tail	2.776445	

Table D.24 Non-Parametric Analysis of Beam Splice Results with Fourth Root Normalization between VAC and RCA-100

Mann-Whitney Test and CI: VAC, RAC-100

     N Median

VAC   3 63.01

RAC-100 3 51.47

Point estimate for ETA1-ETA2 is 12.71

91.9 Percent CI for ETA1-ETA2 is (4.73,21.92)

W = 15.0

Test of ETA1 = ETA2 vs ETA1 not = ETA2 is significant at 0.0809

BIBLIOGRAPHY

AASHTO (2007). *AASHTO LRFD Bridge Design Specification*. Fourth Edition, Washington, D.C.

Abbas, A., Fathifazl, G., Isgor, O.B., Razaqpur, A.G., Fournier, B., Foo, S. (2008). "Proposed Method for Determining the Residual Mortar Content of Recycled Concrete Aggregates," *Journal of ASTM International*, Vol. 5, Issue 1, pp. JAI101087.

ACI 408R (2003). Bond and Development of Straight Reinforcing Bars in Tension. American Concrete Institute, Farmington Hills, MI.

ACI 318 (2011). Building Code Requirement for Structural Concrete, Farmington Hills, MI.

ASTM C 29 (2009). Standard Test Method for Bulk Density (Unit Weight) and Voids in Aggregate. *American Society for Testing and Materials*. West Conshohocken, PA.

ASTM C 39 (2011). Standard Test Method for Compressive Strength of Cylindrical Concrete Specimens. *American Society for Testing and Materials*. West Conshohocken, PA.

ASTM C 78 (2010). Standard Test Method for Flexural Strength of Concrete (Using Simple Beam with Third-Point Loading). *American Society for Testing and Materials*. West Conshohocken, PA.

ASTM C 127 (2012). Standard Test Method for Density, Relative Density (Specific Gravity), and Absorption of Coarse Aggregate. *American Society for Testing and Materials*. West Conshohocken, PA.

ASTM C 136 (2006). Standard Test Method for Sieve Analysis of Fine and Coarse Aggregates. *American Society for Testing and Materials*. West Conshohocken, PA.

ASTM C 138 (2010). Standard Test Method for Density (Unit Weight), Yield, and Air Content (Gravimetric) of Concrete. *American Society for Testing and Materials*. West Conshohocken, PA.

ASTM C 143 (2010). Standard Test Methods for Slump of Hydraulic Cement Concrete. *American Society for Testing and Materials*. West Conshohocken, PA.

ASTM C 231 (2010). Standard Test Method for Air Content of Freshly Mixed Concrete by the Pressure Method. *American Society for Testing and Materials*. West Conshohocken, PA.

ASTM C 469 (2010). Standard Test Method for Static Modulus of Elasticity and Poisson's Ratio of Concrete in Compression. *American Society for Testing and Materials*. West Conshohocken, PA.

ASTM C 496 (2011). Standard Test Method for Splitting Tensile Strength of Cylindrical Concrete Specimens. *American Society for Testing and Materials*. West Conshohocken, PA.

ASTM E8 (2009). Standard Test Methods for Tension Testing of Metallic Materials. *American Society for Testing and Materials*. West Conshohocken, PA.

Bentz, E., Collins, M. (2000). Response-2000 Reinforced Concrete Sectional Analysis. Version 1.0.5. Toronto, Canada.

Butler, L., West, J.S., Tighe, S.L. (2011). "The effect of recycled concrete aggregate properties on the bond strength between RCA concrete and steel reinforcement," *Cement and Concrete Research*, Vol. 41, Issue 10, pp. 1037-1049.

CEB-FIP Model Code for Concrete Structures (1990). "Evaluation of the Time Dependent Behaviour of Concrete," Bulletin d'Information No. 199, Comite European du Béton/Fédération Internationale de la Precontrainte, Lausanne, 1991, pp. 201

Fathifazl, G. (2008). "Structural performance of steel reinforced recycled concrete members." Ph.D. Dissertation, Department of Civil and Environmental Engineering, Carleton University, Ottawa, Ontario, Canada.

Federal Highway Administration. (2012). *Transportation Application of Recycled Concrete Aggregate: Federal Highway Administration State of Practice National Review*, <http://www.fhwa.dot.gov/pavement/recycling/applications.pdf> Accessed 3 February 2014.

Kim, S.W. (2012). "Influence of recycled coarse aggregates on the bond behavior of deformed bars in concrete," *Engineering Structures*, Vol. 48, pp. 133.

Looney, T. (2012). "Bond Behavior of High-Volume Fly Ash and Self-Consolidation Concrete." M.S. Thesis, Missouri University of Science and Technology, Rolla, MO.

Lutz, L.A., Gergeley, P. (1967). "Mechanics of Bond and Slip of Deformed Bars in Concrete," *ACI-Journal*. pp. 711-721.

Reinhardt, H.W. (1984). "Fracture mechanics of an elastic softening material like concrete," Heron, 29, pp. 42.

RILEM 7-II-28. (1994). "Bond Test for Reinforcing Steel. 2. Pull-out test." E & FN Spon, London.

RILEM, TC 50-FMC, (1985). Fracture Mechanics of Concrete, "Determination of the Fracture Energy of Mortar and Concrete by Means of Three-Point Bend Tests on

Notched Beams," RILEM Recommendation, Materials and Structures, V. 18, No. 16, pp. 287-290.

Shayan, A., and Xu, A. (2003). "Performance and Properties of Structural Concrete Made with Recycled Concrete Aggregate," *ACI Mater. J.*, Vol. 100, No. 5, pp. 371–380.

Shi-Cong Kou, Chi-Sun Poon , Hui-Wen Wan (2012). "Properties of concrete prepared with low-grade recycled aggregates," *Construction and Building Materials,* Vol. 36, pp. 881–889.

Tepfers, R. (1977). "A Theory of Bond Applied to Overlapped Tensile Reinforcement Splices for Deformed Bars." Ph.D. Dissertation, Department of Civil Engineering, Chalmers University of Technology, Göteborg, Sweden.

Veen, C. van der. (1990). "Cryogenic Bond Stress-Slip Relationship." Ph.D. Dissertation, Department of Civil Engineering, Delft University of Technology, Stevinweg, Netherlands.

Wolfe, M. (2011). "Bond Strength of High-Volume Fly Ash Concrete." M.S. Thesis, Missouri University of Science and Technology, Rolla, MO.

Zuo, J., and Darwin, D. (2000). "Splice Strength of Conventional and High Relative Rib Area Bars in Normal and High Strength Concrete," *ACI Structural Journal*, V. 97, No.4, July-Aug., pp.630-641.

VITA

Amanda Renee Steele is from St. Joseph, Missouri. She received her Bachelors of Science in Civil Engineering from Missouri University of Science & Technology in May 2012. During her time as an undergraduate, Amanda interned with APAC Kansas Inc. and Union Pacific Railroad. In August 2012, Amanda enrolled in the Civil Engineering Master's program at the Missouri University of Science & Technology. During her time as a Master's student she held positions of graduate research assistant and graduate teaching assistant in the Department of Civil, Architectural, and Environmental Engineering. Amanda completed her Masters of Science in Civil Engineering with a Structural emphasis in May 2014.